UNIVERSITY OF CALIFORNIA,
IRVINE

Generation and application of a chimeric model to examine human microglia responses to amyloid pathology

DISSERTATION

Submitted in partial satisfaction of the requirements for the degree of

DOCTOR OF PHILOSOPHY

In Biological Sciences

By

Jonathan Hasselmann

Dissertation Committee:
Associate Professor Mathew Blurton-Jones, Chair
Associate Professor Kim Green
Professor Brian Cummings

2021

DEDICATION

To Nikki and Isla:

During this journey, I have been fortunate enough to have the love and support of two of the strongest ladies I have ever met. I can say without a doubt that I would not have made it here without the two of you standing behind me. I love you both with all my heart and this achievement belongs to the two of you just as much as it belongs to me. Thank you for always having my back.

TABLE OF CONTENTS

LIST OF FIGURES ..... **v**

LIST OF TABLES ..... **vii**

ACKNOWLEDGEMENTS ..... **viii**

CURRICULUM VITAE ..... **xi**

ABSTRACT OF THE DISSERTATION ..... **xiv**

INTRODUCTION **1**

A. MICROGLIA AND THEIR ROLES IN ALZHEIMER'S DISEASE 3

History of Microglia 3

Microglia in Alzheimer's Disease 5

B. CURRENT METHODS OF STUDYING MICROGLIA 8

Mouse Microglia 8

Primary Human Microglia 9

iPSC-derived Human Microglia 11

Organoid Microglia 14

C. PITFALLS ASSOCIATED WITH THE CURRENT MODELS 16

D. MICROGLIA XENOTRANSPLANTATION INTO THE MOUSE BRAIN 19

CHAPTER 1: TRANSPLANTATION OF HUMAN IPSC-DERIVED MICROGLIA INTO THE MOUSE BRAIN INDUCES APPROPRIATE TRANSCRIPTOMIC PROGRAMMING AND REVEALS HUMAN SPECIFIC AMYLOID RESPONSES **21**

INTRODUCTION 21

MATERIALS AND METHODS 23

RESULTS 40

DISCUSSION 69

CHAPTER 2: THE ALZHEIMER'S DISEASE-ASSOCIATED TREM2 R47H GENETIC POLYMORPHISM DRIVES TRANSCRIPTOMIC AND FUNCTIONAL ALTERATIONS IN XENOTRANSPLANTED MICROGLIA **71**

INTRODUCTION 71

MATERIALS AND METHODS 72

RESULTS 79

DISCUSSION 85

CHAPTER 3: ALTERATIONS TO CHROMATIN STRUCTURE AND TRANSCRIPTOMIC PROGRAMMING UNDERLIE THE MICROGLIA RESPONSE TO AMYLOID PATHOLOGY **87**

INTRODUCTION 87

MATERIALS AND METHODS 88
RESULTS 94
DISCUSSION 101
CONCLUSIONS AND FUTURE DIRECTIONS 105
REFERENCES 111

LIST OF FIGURES

INTRODUCTION

FIGURE 1: Homology between human and mouse proteins associated with Alzheimer's disease risk 1

FIGURE 2: In vivo and in vitro microglia ontogeny 12

CHAPTER 1

FIGURE 1.1: iPSC-derived human HPCs differentiate into microglia and display robust engraftment within the forebrain of MITRG mice 41

FIGURE 1.2: Xenotransplanted human cells express microglia markers 43

FIGURE 1.3: Chimeric distribution of human xMG is influenced by age of transplantation and hCSF1 expression level 44

FIGURE 1.4: Transplanted iHPCs adapt to diverse niches within the brain and differentiate into the four CNS macrophage subtypes in a context-dependent manner 45

FIGURE 1.5: Methods of tissue dissociation and validation of the human microglia flow cytometry paradigm 48

FIGURE 1.6: Transplantation of human iHPCs into the murine brain recapitulates an in vivo human transcriptome 49

FIGURE 1.7: xMG cluster closely with brain-derived human microglia 52

FIGURE 1.8: xMG survey their surroundings, rapidly respond to laser ablation, and interact with neuronal components after trauma 55

FIGURE 1.9: Differential responses of xMG and iMG to LPS administration 57

FIGURE 1.10: LPS treatment upregulates numerous inflammatory pathways and induces a transcriptomic profile resembling disease-affected microglia 59

FIGURE 1.11: xMG gene expression profiles are indicative of known microglial activation signatures 61

FIGURE 1.12: xMG down-regulate homeostatic markers and upregulate activation markers around Aβ plaques 63

FIGURE 1.13: Single-cell sequencing of xMG from MITRG and MITRG-5X mice reveals altered population distributions and human-specific genetic responses 65

FIGURE 1.14: Analysis of scRNA-seq by individual sex or genes reveals additional aspects of xMG transcriptomics 67

CHAPTER 2

FIGURE 2.1: Deletion of *TREM2* suppresses the development of Disease-Associated Microglia in vivo 80

FIGURE 2.2: CRISPR/Cas9 editing to create a homozygous *TREM2* R47H mutant human iPSC line 81

FIGURE 2.3: xMG response to Aβ plaques is altered by the *TREM2* R47H mutation.....82

FIGURE 2.4: The *TREM2* R47H mutation alters the population-level response to amyloid in xMG 83

CHAPTER 3

FIGURE 3.1: Cluster identification and FACS sorting of xMG subpopulations.....95

FIGURE 3.2: Bulk RNA-seq differential gene expression analysis between clusters reveals genetic characteristics of each population.....98

FIGURE 3.3: ATAC-seq motif analysis reveals population-specific chromatin alterations ...100

LIST OF TABLES

CHAPTER 2

TABLE 2.1: Genes significantly dysregulated by the *TREM2* R47H mutation and the overlap with the DAM and IFN cluster signatures 83

CHAPTER 3

TABLE 3.1: Differential gene expression results for selected subpopulation cell surface marker genes 96

ACKNOWLEDGEMENTS

I would like to thank my mentor, Dr. Mathew Blurton-Jones, for always giving me the opportunity to run with my ideas and continuing to believe in me even when a number of those ideas didn't fully pan out. Our conversations where we would pour over every crazy experiment that would come to mind until we found something that made sense are some of my fondest memories of this journey. You have also always possessed a practicality that has balanced out my impeccable ability to overcomplicate things, a trait of yours that I have always been grateful for. You have been a wonderful mentor, an incredible friend, and I look forward to our continued work together.

To everyone in the Blurton-Jones lab, I can honestly say that my projects would not have been nearly as successful without your support and the hard work that you have all put in. In particular, I would like to thank Dr. Hayk Davtyan for keeping the lab together and handling all of the minor details (and not so minor details like the INSANE amount of mouse breeding) so I could focus on the bigger picture in my experiments. Your friendship and selflessness have been critical to my success. Thank you, my friend. Morgan Coburn also deserves a special thank you for her significant contributions to the development of the xMG model and for her friendship over the years. I can honestly say that this project would not have been as successful without your hard work, ingenuity, and all the laughs we had along the way. Thank you.

I would also like to thank my committee members, both past and present (Drs. Andrea Tenner, Sunil Gandhi, Brian Cummings, and Kim Green). I am both honored and humbled by the fact that you all took time out of your busy schedules to assess my work and help me grow as a researcher. Thank you for all your feedback and mentorship and for helping me reach this milestone.

A special thank you also goes out to another key mentor in my grad school journey, Manuella Yassa. Your passion for teaching and giving back has inspired me to be a better person and the opportunities you have given me to grow as a leader have given me the tools that I need to accomplish many of my future goals. There isn't enough space here to describe the immense amount of respect I have for you as a person, a parent, a scientist, and a friend, so I will just have to capitalize this THANK YOU to try and get the point across.

It is also very important to acknowledge that I did not complete this journey alone. To my fellow Moist Boi Jesse Holt, our adventures kept me sane and your strength and perseverance in so many aspects of your life served as a reminder that I could always dig deeper. I am honored to say that you are a part of my family. I love you, brother. To my girlfriend Nikki and daughter Isla who had to put up with all the stress of grad school without the benefit of getting a PhD at the end of it. I can't count the number of times that I would have fallen apart if it weren't for the support of both of you incredible women. Words can't express how much I love you both and how grateful I am that you supported me all these years. I could not have done it without you.

Thank you to Elsevier Inc. and Wiley Periodicals Inc. for granting permission to include copyrighted material and figures in my dissertation.

This work was supported by NIH grants AG048099, AG055524, AG016573, AG056303 (MBJ), AG061895 (HD), Brain Initiative R01 DA048813 (MBJ), NIA T32 AG00096 (JH), CIRM RT3-07893 (MBJ), the Women's Alzheimer's Movement: UCI MIND/WAM 01-2018 (MBJ).

CURRICULUM VITAE

Jonathan Hasselmann

Education

2016-2021 **University of California, Irvine**
Department of Neurobiology and Behavior
PhD, Biological Science

2019 MS, Biological Science

2012-2014 **University of California, San Diego**
BS, Physiology & Neuroscience

2009-2012 **San Diego Mesa College**

Research Experience

2016-2021 **University of California, Irvine**
Graduate Researcher
PI: Dr. Mathew Blurton-Jones, PhD
Department of Neurobiology and Behavior

2014-2016 **University of California, Riverside**
Staff Research Associate I
PI: Dr. Seema Tiwari-Woodruff, PhD
Department of Biomedical Sciences

2013-2014 **University of California, San Diego**
Lab Assistant III
PI: Dr. Quyen Nguyen, MD/PhD
Department of Surgery

2012-2014 **University of California, San Diego**
Lab Assistant III
PI: Dr. Lesley Ellies, PhD
Department of Pathology

Grants & Awards

2019-2020 **DTEI Pedagogical Fellowship**
University of California, Irvine

2020 **DTEI Summer Graduate Fellowship**
University of California, Irvine

2020 **James L. McGaugh Award for Excellence in Research**
UCI Neurobiology and Behavior

2020 **Edward Steinhaus Teaching Award**
UCI School of Biological Science

2020 **Lauds and Laurels Outstanding Graduate Student Award**
UCI Alumni Association

2020 **Dr. William F. Holcomb Scholarship**
UCI School of Biological Science

Grants & Awards Continued

2018-2020	**T32 AG00096-34: Neurobiology of Aging** National Institute on Aging
2019	**Roger W. Russell Award in the Neurobiology of Learning and Memory** UCI Center for the Neurobiology of Learning and Memory
2019	**Fine Science Tools Graduate Travel Award in Neurobiology** UCI School of Biological Science
2018	**NSF Graduate Research Fellowship Program** *Honorable Mention* National Science Foundation
2016	**Francisco J. Ayala Graduate Fellowship** University of California, Irvine
2012-2014	**Revelle College Provost Honors** University of California, San Diego
2013	**CALIT2 Summer Undergraduate Research Scholar** University of California, San Diego
2012-2013	**Community College Math and Science Scholarship** The San Diego Foundation
2012	**Reuben H. Fleet Memorial Scholarship** The San Diego Foundation
2009-2012	**Dean's List for Academic Excellence** San Diego Mesa College

Conference Presentations

2020	**REMIND 11th Annual Emerging Scientists Symposium** Irvine, CA Poster Presentation
2019	**Sanford Burnham Prebys 40th Annual Symposium** La Jolla, CA Poster Presentation
2019	**International Conference on Alzheimer's and Parkinson's Diseases (AD/PD)** Lisbon, Portugal Oral Presentation
2019	**REMIND 10th Annual Emerging Scientists Symposium** Irvine, CA Oral Presentation
2018	**Keystone Symposia: New Frontiers in Neuroinflammation** Keystone, CO Poster Presentation

Conference Presentations Continued

2018	**International Conference on Learning and Memory** Huntington Beach, CA Oral Presentation
2016	**American Society for Neurochemistry Annual Meeting** Denver, CO Poster Presentation
2014	**27th Annual Undergraduate Research Conference** San Diego, CA Oral Presentation
2013	**CALIT2 Summer Undergraduate Research Conference** San Diego, CA Oral Presentation

Teaching Experience

Instructor of Record

Fall 2020	**NEUROBIO 399 (University Teaching)**

Guest Lecturer

Summer 2019	**BIO SCI 93 (Introductory Biology)**
Summer 2018	**BIO SCI 93 (Introductory Biology)**

Pedagogical Fellow

Fall 2020	**TA Professional Development Program (TAPDP)** *Department of Molecular Biology and Biochemistry* *Department of Developmental and Cell Biology*
Summer 2020	**TA Professional Development Program (TAPDP)** *Department of Developmental and Cell Biology*

Teaching Assistant

Fall 2020	**BIO SCI 93 (From DNA to Organisms)** *Head Teaching Assistant*
Summer 2020	**BIO SCI 99 (Molecular Biology)**
Spring 2019	**BIO SCI N113L (Neurobiology Lab)**
Winter 2019	**BIO SCI N113L (Neurobiology Lab)**
Fall 2019	**BIO SCI 93 (From DNA to Organisms)** *Head Teaching Assistant*
Summer 2019	**BIO SCI 93 (From DNA to Organisms)**
Winter 2018	**NEUROBIO 207L (Cellular Neuroscience Lab)** *Graduate-level course*
Fall 2018	**BIO SCI 93 (From DNA to Organisms)** *Head Teaching Assistant*
Summer 2018	**BIO SCI 93 (From DNA to Organisms**

Service

2019-2021	**CNLM Brain Explorer Academy** *Program Co-Chair*
2017-2021	**CNLM Ambassador Program** *Science Ambassador*
Fall 2020	**TA Professional Development Program (TAPDP)** *Department of Molecular Biology and Biochemistry* *Department of Developmental and Cell Biology*
Summer 2020	**TA Professional Development Program (TAPDP)** *Department of Developmental and Cell Biology*
Summer 2019	**UCI Brain Camp** *Mentor*
Fall 2018	**TA Professional Development Program** *Pedagogical Liaison*

Certifications

2020	**Certificate in Remote Instruction** *University of California, Irvine* *Division of Teaching Excellence and Innovation*
2018	**Center for the Integration of Research, Teaching and Learning** *Associate Level*
2018	**Certificate in Course Design** *University of California, Irvine* *Division of Teaching Excellence and Innovation*

Review Articles

Hasselmann J, Blurton-Jones M. (2020) *Human iPSC-derived microglia: A growing toolset to study the brain's innate immune cells.* GLIA. 68(4):721-739.

Hasselmann J*, Khalaj AJ*, Augello CJ, Moore SM, Tiwari-Woodruff SK. (2016) *Nudging Oligodendrocyte Intrinsic Signaling to Remyelinate and Repair: Estrogen receptor ligand effects*. J Steroid Biochem Mol Bio, 160, 43-52

Peer-Reviewed Publications

McQuade A, Kang YJ, **Hasselmann J**, Jairaman A, Sotelo A, Kiani Shabestari S, Coburn M, Chadarevian JP, Fote G, Tu CH, Danhash E, Silva J, Martinez E, Cotman C, Prieto GA, Thompson LM, Steffan JS, Smith I, Davtyan H, Cahalan M, Cho H, Blurton-Jones M (2020) *Transcriptomic and functional deficits in human TREM2 knockout microglia cause an impaired response to Alzheimer's disease pathology in vivo.* Nature Comm. 11(1):5370.

Hasselmann J*, Coburn M*, England W, Figueroa-Velez D, Kiani Shabestari S, Tu CH, McQuade A, Kolahdouzan M, Echeverria K, Claes C, Nakayama T, Azevedo R, Coufal N, Han CZ, Cummings BJ, Davtyan H, Glass CK, Healy L, Gandhi S, Spitale R, Blurton-Jones M (2019) *Development of a chimeric model to study and manipulate human microglia in vivo.* Neuron. 103(6):1016-1033.

Peer-Reviewed Publications Continued

Atkinson KC, Lee JB, **Hasselmann JPC**, Kim SH, Drew A, Soto J, Katzenellenbogen JA, Harris NG, Obenaus A, Tiwari-Woodruff SK. (2019) *Diffusion tensor imaging identifies aspects of therapeutic estrogen receptor β ligand-induced remyelination in a mouse model of multiple sclerosis.* Neurobiol. Dis. 130:104501.

McQuade A, Coburn M, Tu CH, **Hasselmann J**, Blurton-Jones M (2018) *Development and validation of a simplified method to generate human microglia from pluripotent stem cells*. Mol. Neurodegener. 13(1):67.

Hingorani DV, Lippert CN, Crisp JL, Savariar EN, **Hasselmann JPC**, Kuo C, Nguyen QT, Tsien RY, Whitney MA, Ellies LG. (2018) *Impact of MMP-2 and MMP-9 enzyme activity on wound healing, tumor, growth and RACPP cleavage.* PLoS One. 13(9):e0198464.

Gold EM, Vasilevko V, **Hasselmann J**, Tiefenthaler C, Hoa D, Ranawaka K, Cribbs DH, Cummings BJ. (2018) *Repeated mild closed head injuries induce long-term white matter pathology and neuronal loss that are correlated with behavioral deficits*. ASN Neuro. 10:1759091418781921.

Hasselmann JPC*, Karim H*, Khlaj AJ, Tiwari-Woodruff SK. (2017) *Consistent induction of chronic experimental autoimmune encephalomyelitis in C57BL/6J mice for the longitudinal study of pathology and repair.* J Neurosci Methods. 284:71-84.

Lapato A*, Szu J*, **Hasselmann JPC**, Khalaj AJ, Binder DK, Tiwari-Woodruff SK. (2017) *Chronic demyelination induced seizures*. Neuroscience. 346:409-22.

Hussain T, Nguyen LT, Whitney M, **Hasselmann J**, Nguyen QT. (2016*) Improved facial nerve identification during parotidectomy with fluorescently labeled peptide*. Laryngoscope. 126(12):2711-2717.

Hauff SJ, Raju SC, Orosco RK, Gross AM, Diaz-Perez JA, Savariar E, Nashi N, Hasselman J, Whitney M, Myers JN, Lippman SM, Tsien RY, Ideker T, Nguyen QT. (2014) *Matrix-metalloproteinases in head and neck carcinoma-cancer genome atlas analysis and fluorescence imaging in mice*. Otolaryngol Head Neck Surg, 151(4), 612-8

* Authors contributed equally

ABSTRACT OF THE DISSERTATION

Generation and application of a chimeric model to examine human microglia responses to amyloid pathology

By

Jonathan Hasselmann

Doctor of Philosophy in Biological Sciences

University of California, Irvine, 2021

Associate Professor Mathew Blurton-Jones, Chair

Microglia are the primary cell type comprising the brain's immune system and, as such, inflammatory responses in these cells have been implicated in essentially all diseases of the central nervous system. Historically, directly studying human microglia has been experimentally challenging, so much of what we understand has been inferred from the study of animal models despite species-specific genetic variation that underlies the inability of rodent microglia to fully recapitulate the human condition. However, recent advancements in the use of human induced pluripotent stem cells (iPSCs) to generate human microglia surrogates has ushered in a new era of microglia research. While the initial *in vitro* studies utilizing these iPSC-derived microglia (iMG) were revolutionary, subsequent work has demonstrated that these cells are highly sensitive to their environment and exhibit robust transcriptomic deficiencies when kept in isolation from the brain.

Therefore, the development of a model that would allow for the examination of these cells within a surrogate brain environment was necessary for the continued development of our understanding of the roles of microglia in health and disease. By transplanting iPSC-derived hematopoietic progenitor cells into the postnatal brain of humanized, immune-deficient mice, transplanted cells were shown to undergo context-dependent differentiation into microglia and

other CNS macrophages. Transcriptomic analyses showed that the resulting cells acquired an *ex vivo* human microglial gene signature and appropriately responded to acute and chronic inflammatory insults. Most notably, transplanted microglia exhibited robust transcriptional responses to Aβ plaques that only partially overlapped with that of murine microglia, revealing multiple human-specific Aβ-response genes.

Further expansion of this model in conjunction with CRISPR gene editing technology has allowed for the direct interrogation of the Alzheimer's disease (AD)-related triggering receptor expressed in myeloid cells 2 (TREM2) R47H genetic polymorphism. This study demonstrated that a key effect of the R47H mutation is an alteration in the distribution of microglia subpopulations and a reduction in plaque associated microglia. Furthermore, cells with the R47H mutation exhibit an inflammatory signature that is not present in WT cells, suggesting that their lack of responsiveness is also paired with inappropriate inflammation. Importantly, these results have highlighted aspects of the R47H mutation that have not previously been observed in mouse models.

Finally, as disruption of activation states in response to amyloid pathology appeared to be a primary result of genetic mutation in xMG, further understanding the complex genetic interactions driving these states was a question of critical importance. Analysis of the epigenomic and transcriptomic landscapes of the individual xMG subpopulations that arise in response to amyloid pathology has provided insight into the chromatin structure and gene expression alterations that underlie the microglia response to Aβ plaques. What these data have begun to demonstrate is that the amyloid-responsive population of microglia appear to rely on chromatin modifications that allow transcription factors in the MiTF/TFE family to upregulate the expression of genes related to phagocytosis and lysosomal function. While there are still aspects of these

results that have not been fully elucidated, future studies are underway that will determine the nature of these changes and their ability to drive microglial responses in AD.

Taken as a whole, the development of the xMG model and application to the study of the early amyloid response has yielded important new insight into Alzheimer's disease. While these experiments are only the first steps in what will hopefully become a much broader body of human microglia research, my dissertation work has demonstrated that the xMG model is a powerful tool for the future study of microglial homeostasis and disease-associated inflammatory responses.

INTRODUCTION

As scientists have sought to understand the genetic underpinnings of Alzheimer's disease (AD), genome-wide association studies (GWAS) have begun to identify a multitude of single nucleotide polymorphisms (SNPs) that are associated with altered risk of developing AD (Efthymiou & Goate, 2017; Guerreiro, Wojtas, et al., 2013; Huang et al., 2017; Jansen et al., 2019; Jonsson et al., 2013; Karch, Cruchaga, & Goate, 2014; Kunkle et al., 2019; Lambert et al., 2009; Sims et al., 2017). Of the over three dozen loci identified by GWAS, many are associated with genes that are either highly or uniquely expressed in microglia (Hansen, Hanson, & Sheng, 2018), suggesting that these cells play a significant role in driving the observed alterations in AD risk (**Figure 1**). However, our ability to study the effects of the implicated genes has been hindered by the fact that obtaining human microglia from AD patients is a non-trivial task and the rodent versions of these risk genes often exhibit poor homology to their human counterparts. However, in recent years, multiple protocols have been developed that enable the differentiation of microglia from human induced pluripotent stem cell (iPSC) lines, providing a high-throughput method of

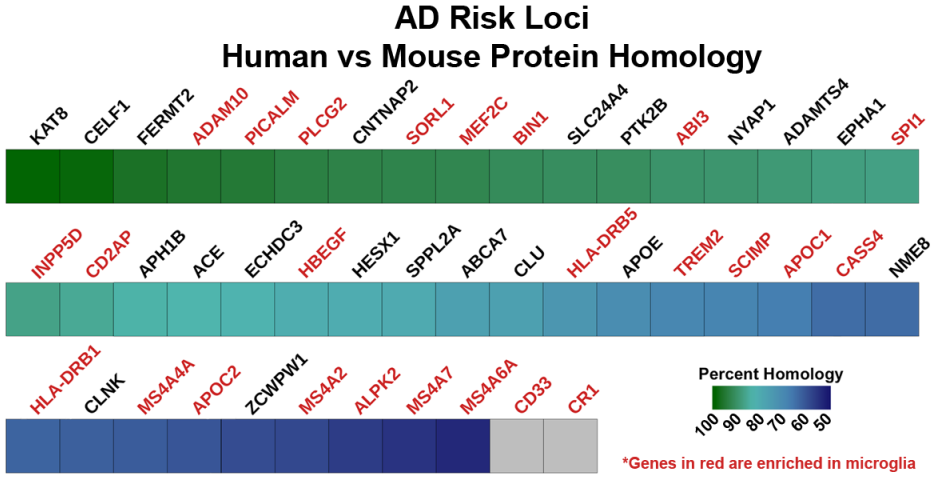

Figure 1. Homology between human and mouse proteins associated with Alzheimer's disease risk. Human amino acid sequences for genes associated with Alzheimer's disease GWAS-identified risk loci were compared to the homologous mouse proteins using NCBI's Homologene database. Genes in red are either highly or specifically expressed in microglia and gray boxes denote genes with no reliable orthologues in the mouse (i.e. <50% homology with any possible murine orthologue).

generating microglia from healthy or disease-affected patients (Abud et al., 2017; Douvaras et al., 2017; Haenseler et al., 2017; Muffat et al., 2016; Pandya et al., 2017; Takata et al., 2017).

While *in vitro* studies utilizing iPSC-derived microglia (iMG) to examine AD-related processes have begun to yield interesting results (Claes et al., 2019; Lin et al., 2018; Xiang et al., 2018), concerns have recently been raised over the transcriptomic validity of such *in vitro* models (Bohlen et al., 2017; Gosselin et al., 2017), suggesting that the most reliable method of studying mature microglia is in an *in vivo* setting. Indeed, recent *in vivo* studies into the roles of microglia in AD have provided novel insights into the transcriptomic responses of microglia to amyloid pathology (Keren-Shaul et al., 2017; Krasemann et al., 2017). However, these findings have relied on mouse models designed upon genetic mutations that mimic early-onset AD (EOAD) and, as such, do not contain microglia that possess any of the microglial SNPs that have been implicated in late-onset AD (LOAD). And while some mouse models have begun to incorporate mutations in risk genes such as the triggering receptor expressed on myeloid cells 2 (*TREM2*), the lipid-sensing receptor critical for the disease associated microglia (DAM) response to amyloid (Keren-Shaul et al., 2017), many of the murine versions of these genes share limited homology with the human gene (**Figure 1**), leaving considerable doubt as to whether they are functionally equivalent (Liao et al., 2015; Song et al., 2018; Xiang et al., 2018).

While many current attempts to remedy these deficiencies are focused on developing more complex, humanized transgenic mice, generating enough mouse lines to accurately recapitulate the highly variable genetic backgrounds associated with LOAD patients is both unrealistically time consuming and costly. However, iPSCs offer a readily available pool of material that can either be derived from patients possessing the desired genetic profiles or paired with gene editing technology to efficiently introduce relevant genetic mutations (Deltcheva et al., 2011; Jinek et al.,

2012; Mali et al., 2013). Furthermore, differentiating these cell lines into microglia and pairing them with xenotransplantation-compatible mouse models of disease would provide researchers with the ability to study a wide-variety of genetic mutations related to AD or any other disease that microglia have been implicated in. Furthermore, these xenotransplanted microglia (xMG) would exist in an environment that supports the maintenance of *in vivo* microglia morphology, function, and gene expression, likely resulting in a more accurate recapitulation of the human condition.

Therefore, the primary goal of my dissertation is to build upon the recently developed iMG protocols to create a robust *in vivo* model that more accurately captures the microglia states underlying the human response to neurological diseases, such as AD. In pursuit of this goal, my dissertation will put forth evidence that I have developed and validated a xenotransplantation model that allows for the accurate examination of microglia in the healthy brain as well as elucidation of the *in vivo* human microglia response to amyloid pathology. By utilizing this model along with CRISPR gene editing, I will also demonstrate that this model is suitable for examining the effects of disease-relevant genetic mutations on microglia response to pathology. By generating isogenic iPSC lines engineered to contain the AD-related *TREM2* R47H SNP, I will show that this mutation drives a multitude of transcriptomic alterations and disrupts the population distribution of xMG in response to amyloid pathology. Finally, I will develop a method of isolating individual xMG subpopulations in order to perform a robust analysis of the epigenomic and transcriptomic alterations underlying activation states that occur in the microglia response to amyloid pathology.

A. MICROGLIA AND THEIR ROLES IN ALZHEIMER'S DISEASE

History of Microglia

Microglia, the primary tissue macrophage of the central nervous system (CNS), were first described by multiple researchers in the late 1800's to early 1900's, including Gluge, Nissl,

Achúcarro, Merzbacher, and Cajal (Tremblay, Lecours, Samson, Sanchez-Zafra, & Sierra, 2015). While many of these initial descriptions noted the phagocytic capacity of these cells, there was little agreement on what to call them or the exact lineage of the "third element," as Cajal initially referred to them. Fortunately, the precise and in-depth descriptions by Pio del Rio-Hortega in 1919 clearly delineated these cells from the other "neuroglia" and officially designated them microglia, greatly expanding our understanding of these elusive cells (Río-Hortega, 1919a, 1919b, 1919c, 1919d, 1939). Yet despite Rio-Hortega's clear descriptions of these cells' mesodermal lineage, propensity to alter their morphology in response to neuronal damage, and their appetite for lipids and cellular debris, little progress was made in furthering our understanding of these cells during the six decades that followed his initial studies.

Fortunately, the past thirty years have seen a rapid acceleration in our understanding of microglia, and it is now known that these cells play critical roles in sculpting the brain during development, modulating neural plasticity, and maintaining brain homeostasis (Salter & Stevens, 2017; Stevens et al., 2007; Wolf, Boddeke, & Kettenmann, 2017; Wu, Dissing-Olesen, MacVicar, & Stevens, 2015). In addition to these critical functions, microglia have also been shown to be highly responsive to a variety of local injuries, neuroinflammation, and a multiplicity of brain pathologies (Davalos et al., 2005; Nimmerjahn, Kirchhoff, & Helmchen, 2005; Perry & Holmes, 2014). Recent genetic studies have begun to further highlight the importance of these cells in disease, with the discovery of many risk loci and polymorphisms that are linked to microglial-enriched genes that are associated with a variety of neurological disorders including Alzheimer's disease, frontotemporal dementia, amyotrophic lateral sclerosis, autism, and schizophrenia (Karch et al., 2014; Salter & Stevens, 2017).

Microglia in Alzheimer's Disease

It has long been known that microglia associate with beta-amyloid (Aβ) plaques in the brains of AD patients. In fact, in Alois Alzheimer's initial descriptions of the disease in 1907, he noted the presence of glia cells associated with plaques and a reanalysis of these histological sections has confirmed his descriptions (Alzheimer, Stelzmann, Schnitzlein, & Murtagh, 1995; Graeber et al., 1997). Over time, these glial cells came to be identified as microglia and various studies began to describe their associations with Aβ plaques in AD patients (Akiyama & McGeer, 1990; Mackenzie, Hao, & Munoz, 1995; Rozemuller, Eikelenboom, Pals, & Stam, 1989). In addition to these studies directly linking microglia to amyloid pathology, epidemiological studies examining the long-term use of non-steroidal anti-inflammatory drugs (NSAIDs) began to report a reduction in risk of developing AD (Imbimbo, Solfrizzi, & Panza, 2010; Stewart, Kawas, Corrada, & Metter, 1997), adding indirect support for the idea that brain inflammation could somehow be contributing to the development of disease. As microglia are the resident immune cells of the brain, these reports inspired more research into the roles of microglia in AD. Interestingly, while multiple clinical trials, including the recent INTREPAD trial ("INTREPAD: A randomized trial of naproxen to slow progress of presymptomatic Alzheimer disease," 2019), have now demonstrated that long-term NSAID use leads to a plethora of adverse side effects without significantly reducing AD risk, the links between microglia and AD had already taken hold.

One such avenue of research was focused on the phagocytic capacity of microglia as researchers began to question why these phagocytic cells were apparently unable to clear the amyloid plaques that they were seen to be associated with. Various studies have demonstrated that microglia are capable of taking up both soluble and fibrillar Aβ (Koenigsknecht & Landreth, 2004;

Mandrekar et al., 2009). However, it has also been reported that they fail to efficiently degrade the aggregates which leads to the cells being overwhelmed with increasing amounts of pathological material (Paresce, Chung, & Maxfield, 1997). This observation has led some researchers to further investigate the role of microglial lysosomal function in the degradation of Aβ, leading to interesting results. In one study by Majumdar et al., it was demonstrated that microglia *in vitro* maintain their lysosomes at pH ~6 which is too basic for many lysosomal enzymes to function optimally (Majumdar et al., 2007). However, upon activation with macrophage colony stimulating factor (MCSF), microglia increased the acidity of their lysosomes to pH ~5, closer to that of peripheral monocytes which readily degrade amyloid, and this facilitated the efficient degradation of Aβ (Majumdar et al., 2007). This finding suggests that not all microglia are prepared to phagocytose and degrade proteins like Aβ and the involvement of outside factors is necessary to drive certain populations of microglia towards this phenotype.

In this vein, additional studies have been aimed at examining the effects of complement system proteins on AD and microglia phagocytosis. Numerous studies have identified increased levels of complement proteins C3 and C1q as being associated with fibrillar amyloid plaques in AD brains (Eikelenboom & Stam, 1982; Fu et al., 2012; Jiang, Burdick, Glabe, Cotman, & Tenner, 1994; Loeffler, Camp, & Bennett, 2008). Furthermore, the amount of complement associated with plaques appears to increase along with disease severity (Zanjani et al., 2005). Additionally, it has been demonstrated that microglia uptake of amyloid fibrils is increased when the fibrils are associated with the complement protein C1q (Brazil, Chung, & Maxfield, 2000), suggesting that the plaque-associated complement in patients is a protective mechanism aimed at increasing microglia phagocytosis of pathological amyloid. However, a similar study at the time showed that C1q binding to $A\beta_{1-42}$ actually reduced the microglial uptake of amyloid by cultured microglia (S.

D. Webster et al., 2000). These conflicting findings suggest that the effect of complement on microglial phagocytosis may be dependent not only on the complement proteins involved, but also on the preparation and the *in vitro* experimental conditions.

A more recent study shifted away from examining the *in vitro* role of complement proteins bound to Aβ and instead identified a population of plaque-associated microglia expressing CD11c (*ITGAX*), a component of the complement receptor CR4, in the mouse brain (Kamphuis, Kooijman, Schetters, Orre, & Hol, 2016). In addition to being directly associated with amyloid plaques in the brains of APP/PS1 mice, these microglia were found to exhibit significantly increased expression of various genes that have been linked to lysosomal function, suggesting that this population of microglia were more phagocytic than their $CD11c^-$ counterparts. As the Kamphuis study stopped short of directly detailing the interactions of complement cascade proteins with the CR4 receptor on this microglia population, the exact nature of these interactions is still an open question.

However, in hindsight, it appears that the Kamphuis study was one of the first to describe the microglia subpopulation that is now commonly referred to as Disease Associated Microglia or DAM. While it had long been known that microglia were directly interacting with amyloid plaques in the brains of AD patients and mouse models, single-cell RNA sequencing (scRNA-seq) of microglia from the brains of wildtype and 5X-fAD mice revealed a subset of microglia that were only present in brains containing amyloid pathology (Keren-Shaul et al., 2017). In this study, it was demonstrated that in response to the buildup of amyloid plaques, microglia began to shift away from a homeostatic immune surveillance state and towards an amyloid responsive state. This transition involved the upregulation of pathways associated with lipid metabolism and, as described by Kamphuis et al., increased phagocytic capacity and CD11c expression. However, the

Keren-Shaul study went a step further and described a dependence of this population on the gene *TREM2*. Genetic knockout of *TREM2* effectively halted the microglial transition to the DAM phenotype, a finding that dovetailed nicely with various studies suggesting that loss of function mutations in *TREM2* are significantly associated with altered levels AD risk (Guerreiro, Bilgic, et al., 2013; Guerreiro, Wojtas, et al., 2013; Jonsson et al., 2013).

Overall, there is a long-standing history of microglia involvement in the progression maintenance of AD pathology. However, the previously referenced studies have been carried out in a wide array of experimental models, some of which were more relevant to the human condition than others. While variations in the experimental models are not a valid reason to disregard any specific finding, better understanding the current methodologies used in the study of microglia is critical to being able to appropriately interpret this substantial body of research.

B. CURRENT METHODS FOR STUDYING MICROGLIA

Mouse microglia

Studies of murine microglia have been fundamental in developing our understanding of microglia physiology and function. For instance, in the context of LOAD, such models have been critical in clarifying the roles of *TREM2* in microglial response to Aβ plaques. While initial GWAS findings utilized human data to associate *TREM2* gene variants with AD risk (Guerreiro, Wojtas, et al., 2013; Jonsson et al., 2013), the resulting dysfunctions, such as decreased migration and barrier formation in response to Aβ plaques, were first identified in multiple mouse models of AD (Jay et al., 2015; Ulrich et al., 2014; Y. Wang et al., 2015). These findings were then confirmed in human patients, demonstrating that this phenotype was relevant to AD while lending support to the validity of the murine models (Yuan et al., 2016b). Together, these results demonstrated the potential benefits of utilizing murine microglia as surrogates for the human condition.

However, while mouse models have provided invaluable tools for elucidating the roles of microglia in health and disease, rodents cannot easily recapitulate the growing complement of human genetic variability implicated in polygenic diseases such as AD (Dawson, Golde, & Lagier-Tourenne, 2018; Friedman et al., 2018; Ueda, Gullipalli, & Song, 2016). Although a recent study utilized the 5XfAD model of amyloidosis to accurately describe a population of microglia that respond to increased amyloid in the brain (Keren-Shaul et al., 2017), the genetic background of the microglia that were being studied better modeled EOAD rather than the more complex LOAD background. While this observation by no means invalidates the results put forth by Keren-Shaul and colleagues, it does raise questions as to how this response may be altered in the presence of a variety of LOAD risk mutations and whether the lack of homology between some mouse and human AD risk genes may affect microglia function. While a few models have introduced individual human risk genes into the 5XfAD model, such as the *TREM2* R47H polymorphism (Song et al., 2018; Xiang et al., 2018), generating a novel mouse line each time a new gene is to be investigated is neither cost-effective nor efficient, especially when researchers wish to study the interactions between multiple human risk genes. Because of this, modeling the complex genetic backgrounds that appear to drive LOAD pathogenesis is becoming a task that may be more streamlined by utilizing models that can readily incorporate differing levels of genetic variability.

Primary human microglia

One approach that allows researchers to model relevant genetic backgrounds involves collecting microglia directly from human patients and maintaining them in an *in vitro* environment. Indeed, the use of primary human microglia has aided in elucidating some human-specific features of these cells, including their decreased propensity to produce the inflammatory molecule nitric oxide compared to murine microglia (Janabi, 2002), although increased production appears to be

linked to APOE variant status, with APOE ε4 carrier microglia exhibiting increased production (Colton et al., 2004). Studies into primary human microglia have also demonstrated differences in responsiveness to pharmacological agents, such as valproic acid and propentofylline, when compared to animal models (Gibbons et al., 2011; Landry, Jacobs, Romero-Sandoval, & DeLeo, 2012). The human-specific responses highlighted in the latter studies have shed light on why these drugs may have failed in clinical trials aimed at altering microglia function. Overall, these data suggest that validation of findings based on mouse models in human microglia may be a necessary step before further translating results into clinical trials.

Despite the benefits of directly studying human microglia, this method also comes with caveats of its own. One such drawback is that these microglia must be collected from residual tissue obtained from the margins of surgeries such as brain tumor or epileptic tissue resections. As there are currently no studies that have been able to thoroughly examine whether microglia isolated from these types of disease-associated tissues are phenotypically normal, or if they possess aberrant behaviors and gene expression due to their environmental origins, it is not possible to say with confidence that this model can be readily applied to other unrelated disorders such as AD.

However, microglia can also be isolated from postmortem tissue, bypassing the concerns of having to use microglia from cancerous and epileptic tissue. This approach is also especially relevant if cells can be collected directly from patients diagnosed with AD or another disease of interest. Nevertheless, this raises another concern, which is that it has recently been revealed that microglia rapidly change their gene expression patterns upon being removed from the brain and placed in a cell culture environment (Bohlen et al., 2017; Gosselin et al., 2017). These changes include reductions in many homeostatic genes, such as *P2RY12, TMEM119,* and *SALL1*, along with increases in multiple inflammatory genes including *SPP1, ITGAX,* and *APOE*. As these

changes have been shown to occur in as little as six hours (Gosselin et al., 2017), it is possible that even microglia that were carefully isolated from patients diagnosed with a relevant disease may not present the researcher with an accurate portrayal of *in vivo* microglia function.

It is important to note that these technical difficulties in no way invalidate the history of microglia data that has been amassed as collecting primary microglia from human tissue samples has been and will continue to be one of the most direct methods of examining human microglia function. However, the ability to generate large amounts of human microglia, without having to rely on limited amounts of left-over brain tissue, would greatly streamline the process of designing well controlled experiments for examining microglia biology.

iPSC-derived human microglia

Fortunately, the ability to generate iPSCs from patients, and then differentiate these iPSCs into defined cell subtypes, has generated exciting opportunities to examine the relationships between complex genetic backgrounds and disease-associated phenotypes. As the development of methods capable of deriving large numbers of microglia from human iPSCs became a priority, the field gained six protocols to accomplish this between the years 2016 and 2017 (Abud et al., 2017; Douvaras et al., 2017; Haenseler et al., 2017; Muffat et al., 2016; Pandya et al., 2017; Takata et al., 2017). While each protocol was unique regarding their specific details, each method was based on the concept that, in order to generate accurate microglial surrogates *in vitro*, one needed to try to mimic the cues that naturally drive microglia differentiation *in vivo.* Whereas early attempts at *in vitro* microglia generation tried to produce microglia by pushing embryonic stem cells through a neuroectodermal lineage (Beutner, Roy, Linnartz, Napoli, & Neumann, 2010; Tsuchiya et al., 2005), this new generation of protocols was highly informed by an elegant set of developmental ontogeny studies that traced the lineage of microglia from mesodermal primitive yolk sac

progenitors, to erythromyeloid progenitors (EMPs), and finally to microglia within the brain (Ginhoux et al., 2010; Kierdorf et al., 2013; Schulz et al., 2012). With this guidance, these new protocols were able to produce cells that transitioned from iPSCs through a range of lineage states resembling primitive hematopoietic precursor cells (HPCs), EMPs, and, ultimately, microglia (**Figure 2**), as confirmed in each study by transcriptomic and protein-level analysis of canonical microglia markers.

In addition to genetic validation, each of these studies sought to functionally validate their iMG to demonstrate that these *in vitro* systems could recapitulate a range of traditional microglia behaviors. For example, the characteristic ability of microglia to respond to inflammatory cues was tested via stimulation with lipopolysaccharide (LPS), phorbol myristate acetate, IFNγ, or IL1β, and confirmed by measurement of reactive oxygen species or a variety of inflammatory cytokines (Abud et al., 2017; Haenseler et al., 2017; Pandya et al., 2017). The propensity of iMG to migrate towards sites of damage was also tested by employing a laser induced injury to a 3D culture system, similar to *in vivo* studies (Davalos et al., 2005), or through the addition of ADP, which is typically released by damaged neurons. In all cases, iMG exhibited rapid responses by

Figure 2. *In vivo* and *in vitro* microglia ontogeny. (Top) Lineage-tracing studies in mice have shown that microglia follow a distinct developmental pathway *in vivo.* Pluripotent embryonic stem cells (ESCs) within the inner cell mass of the blastocyst give rise to hypoblasts which in turn produce the extraembryonic endoderm of the yolk-sac. Hemogenic endothelium within the yolk-sac then gives rise to primitive hematopoietic progenitor cells (HPCs) that can further differentiate into erythromyeloid progenitors (EMPs). These cells then infiltrate into the developing central nervous system (CNS) where maturation under homeostatic conditions results in neatly tiled microglia that develop complex ramifications. In contrast, pathological conditions, such as the development of amyloid plaques in a murine model of Alzheimer's disease (AD), induces robust migratory and morphological alterations. (Bottom) iPSC-derived microglia protocols seek to mimic *in vivo* ontogeny in order to generate cells that appropriately recapitulate endogenous human microglia. This is accomplished by obtaining either human ESCs (hESCs) or reprogramming human fibroblasts (or other cells) into induced pluripotent stem cells (hiPSC). These pluripotent stem cells can then be further differentiated into $CD43^{+}$ microglial progenitors that resemble *in vivo* HPCs/EMPs. By providing additional key microglial growth factors and signaling molecules including CSF-1, IL34, and TGFβ, that mimic the homeostatic brain environment, researchers can promote the further differentiation and maturation of large numbers of iPSC-derived microglia (iMG). Subsequent xenotransplantation of these microglia into the murine brain induces similar morphology and tiling patterns as endogenous murine microglia while retaining the ability to respond to AD pathology. Upregulated (green arrows) and downregulated (red arrows) genes are relevant to the human cellular identity at each differentiation step.

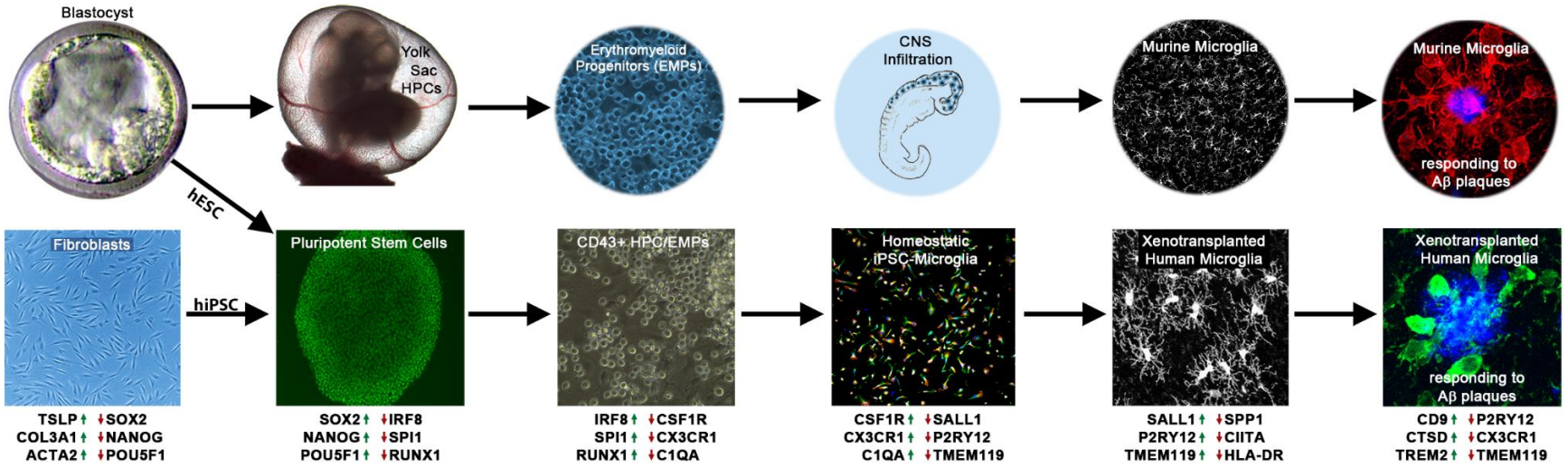
Blastocyst
Yolk Sac HPCs
Erythromyeloid Progenitors (EMPs)
CNS Infiltration
Murine Microglia
Murine Microglia
responding to Aβ plaques
hESC
Fibroblasts
hiPSC
Pluripotent Stem Cells
CD43+ HPC/EMPs
Homeostatic iPSC-Microglia
Xenotransplanted Human Microglia
Xenotransplanted Human Microglia
responding to Aβ plaques
TSLP↑ ↓SOX2
COL3A1↑ ↓NANOG
ACTA2↑ ↓POU5F1
SOX2↑ ↓IRF8
NANOG↑ ↓SPI1
POU5F1↑ ↓RUNX1
IRF8↑ ↓CSF1R
SPI1↑ ↓CX3CR1
RUNX1↑ ↓C1QA
CSF1R↑ ↓SALL1
CX3CR1↑ ↓P2RY12
C1QA↑ ↓TMEM119
SALL1↑ ↓SPP1
P2RY12↑ ↓CIITA
TMEM119↑ ↓HLA-DR
CD9↑ ↓P2RY12
CTSD↑ ↓CX3CR1
TREM2↑ ↓TMEM119

extending process towards the perceived site of damage and/or relocating their cell bodies (Abud et al., 2017; Douvaras et al., 2017; Muffat et al., 2016). Finally, the phagocytic capacity of these cells was determined by utilizing a variety of substrates, ranging from zymosan-coated microbeads, *E. coli* particles, or more physiological substrates such as synaptosomes, fibrillar beta-amyloid, and brain-derived Tau oligomers (Abud et al., 2017; Douvaras et al., 2017; Pandya et al., 2017; Takata et al., 2017). While the overall level of uptake varied by assay and substrate, each study demonstrated the genesis of phagocitically functional cells. As a whole, these results demonstrated a plethora of microglia-related activities that can be modeled *in vitro*, supporting the use of these cells in a variety of experimental contexts.

Organoid microglia

The advent of iPSC-derived brain organoids (BORGs) (Lancaster et al., 2013) provided researchers with the opportunity to study the unique, 3D characteristics of brain tissue in the medium to high throughput manner that is afforded by *in vitro* work. However, original descriptions of these "mini brains" pointed out that they were lacking microglia due to the ectodermal lineage of the neuroepithelium used to generate them, whereas microglia arise from mesoderm. So, in an attempt to rectify this, Abud and colleagues, demonstrated that iMG migrate to and engraft within BORGs when the two were maintained in a co-culture system (Abud et al., 2017). Following engraftment, the iMG took on a more ramified morphology and responded to cerebral damage, in the form of a blunt force puncture injury induced by a needle. Following these injuries, the engrafted iMG adopted an ameboid morphology, reminiscent of the "activated" microglia response typically observed in injured brain tissue (Karperien, Ahammer, & Jelinek, 2013). However, the dual-differentiation approach that is required to generate this model is both

technically complex and expensive, and a single technique that would innately develop microglia within brain organoids would likely be preferable.

Fortunately, a recent study demonstrated that the original Lancaster protocol was perhaps capable of doing this all along (Ormel et al., 2018). In this report, organoid-grown microglia (oMG) were shown to innately develop within BORGs, with only limited alterations from the original protocol published by Lancaster (2013). This finding was predicated on a scRNA-seq study that demonstrated BORGs contained a cell population defined by markers of mesodermal lineage (Quadrato et al., 2017), strongly suggesting that the presence or absence of this population likely influences the development of microglia within the organoid. Ormel and colleagues were able to demonstrate that their BORGs inherently developed cells that, when analyzed by immunohistochemistry, expressed the myeloid transcription factor PU.1, the lysosomal marker CD68, and the macrophage/microglia marker IBA1. Furthermore, the transcriptomic signature of oMG was shown to resemble that of *ex vivo* human microglia (Gosselin et al., 2017), in comparison to iPSCs and fibroblasts, although a higher resolution comparison to iMG and/or primary cultured microglia was not performed, making it difficult to determine whether oMG necessarily exhibit a more 'in vivo-like' microglial signature than other *in vitro* iMG models.

Comparable to the *in* vitro studies before them, Ormel et al. went on to functionally validate their oMG. As BORGs have been shown to develop functional synapses, complete with neurotransmitter release and recordable electrical activity (Pasca et al., 2015), determining whether oMG interacted with synapses in a manner consistent with previously described *in vivo* reports was critical (Schafer et al., 2012). Therefore, super resolution microscopy was employed and showed, what appeared to be, interactions between IBA1 and PSD95 puncta. While the authors stopped short of clearly demonstrating synaptic phagocytosis, which has been the subject of recent

debate (Weinhard et al., 2018), the data presented appears similar to what has been observed with *in vivo* microglia during development (Schafer et al., 2012). Additionally, oMG were isolated from BORGs, via CD11b magnetic sorting, and subjected to further functional analyses. To test the inflammatory response capabilities of oMG, isolated cells were exposed to LPS for up to 72 hours and significant increases in IL6 and TNFα were observed. Phagocytic capacity in the isolated cells, via the C3-dependent complement pathway, was also assessed by incubating the oMG with iC3b-coated microbeads for up to 1 hour, demonstrating a rate of complement-dependent phagocytosis similar to that of primary human microglia.

Overall, the ability to generate a surrogate human brain environment in a dish that is populated with human iMG, either endogenously or through co-culture, is an exciting prospect. Ongoing studies aimed at producing BORGs that show more consistent ratios of the different cell types across both individual organoids (Quadrato et al., 2017; Velasco et al., 2019), experiments, and labs, may well prove to be a fertile avenue for discovery.

C. PITFALLS ASSOCIATED WITH THE CURRENT MODELS

While generating microglia from iPSCs produces and exponential increase in cell number when compared to the traditional method of isolating microglia from human brain tissue, this method does not come without drawbacks of its own, the most notable being the transcriptional deficiencies that occur in cultured microglia. While the results published by Gosselin et al. (Gosselin et al., 2017) were focused primarily on the transcriptional deficits induced in primary human microglia upon maintenance outside of the brain environment, many of these deficits can also be observed in iMG. While many of these transcriptional deficiencies can be corrected upon transplantation into the murine brain (Hasselmann et al., 2019b), suggesting that iMG possess the same transcriptomic potential as primary human microglia, the downstream effects of these

deficiencies are not fully understood, meaning that, whenever possible, *in vitro* results should be validated in an *in vivo* model.

Another obvious limitation of standard iMG monoculture experiments is the absence of other important CNS cell types. Many of the currently published studies that developed or utilized iMG methods, employed monocultures to examine microglial functions such as migration, phagocytosis, and inflammatory responses. While these represent straightforward experiments that are easy to interpret, they neglect the reality of the brain environment in which microglia interact with neurons, astrocytes, oligodendrocytes, endothelial cells or infiltrating immune cells. Growing evidence demonstrates the considerable interplay between microglial and astrocyte signaling (Liddelow et al., 2017) and likewise the neuronal regulation of microglial activation state is well-established (Marinelli, Basilico, Marrone, & Ragozzino, 2019; Sheridan & Murphy, 2013). More recently, interactions between vascular endothelial cells and microglia have been implicated in aging, AD, and stroke (Dudvarski Stankovic, Teodorczyk, Ploen, Zipp, & Schmidt, 2016; Merlini et al., 2019; Yousef et al., 2019). Thus, monoculture experiments likely provide only an initial, albeit highly quantitative, assessment of microglial function. The additional application of co-culture methods that combine iMG with iPSC-neurons, astrocytes, endothelial cells, or other cell types will thus likely provide important additional information.

As an *in vitro* model, oMG afford the experimenter similar benefits to iMG in that experiments can be designed that are medium throughput and offer a substantial amount of experimental control. However, one of the greatest benefits of oMG is the fact that one can model the complex interactions between microglia and all the other cell types of the CNS within a 3-dimensional environment. To add to this, oMG and the cells making up the organoid contain the same human genetic background, which is a benefit that is currently unique to this research model.

This allows for increased control over some of the extrinsic factors that may have an effect on microglial function.

However, certain considerations need to be taken into account before deciding to use oMG. First, it has been noted that BORGs express a transcriptome more closely resembling that of the fetal brain (Camp et al., 2015), which presents a bit of a double-edged sword. While this makes the model well suited for the study of neurodevelopmental disorders, such as autism (Mariani et al., 2015; P. Wang et al., 2017), schizophrenia (Ye et al., 2017), or the transmission of Zika virus (Muffat et al., 2018), it also presents problems when attempting to utilize BORGs in the study of diseases that require a more developed brain environment, such as PD or AD. This does not mean that BORGs are entirely inappropriate for studying diseases of the developed brain, as it has been shown that the transcriptome may begin to mature as BORGs are aged (Pasca et al., 2015; Quadrato et al., 2017), but the development of transplant-compatible mouse models may cause oMG to become a less-attractive model for studying disorders of the fully developed CNS.

There is also a significant concern regarding the quantitative nature of BORG-based experiments. As the generation of BORGs is typically performed in a self-organizing manner, without the aid of external patterning cues, BORGs tend to lack a consistent structure and cellular makeup (Kadoshima et al., 2013; Lancaster et al., 2013; Quadrato et al., 2017). Furthermore, while BORGs from the same bioreactor appear transcriptionally similar, significant batch effects are introduced when comparing BORGs across bioreactors, even if they were generated during the same initial differentiation (Quadrato et al., 2017). Recent modifications to the protocol and application of bioengineering techniques have been shown to ameliorate this to an extent (Velasco et al., 2019), although this requires additional expertise and the presence of endogenous microglia has not yet been investigated in these newer models.

D. MICROGLIA XENOTRANSPLANTATION INTO THE MOUSE BRAIN

One possible approach to remedy the limited cell availability and transcriptomic deficiencies that are associated with *in vitro* and *in situ* microglia models could involve pairing iMG techniques with xenotransplant-compatible mouse models. Indeed, a preliminary demonstration of this concept was performed by Abud et al. which showed that the murine brain could provide a habitable environment for human microglia (Abud et al., 2017). By delivering iMG into the cortex and hippocampus of adult MITRG mice (Rongvaux et al., 2014), which are deficient in T cells, B cells, and NK cells, but also humanized for CSF1, CSF2, and thrombopoietin, engraftment of ramified human microglia could be observed in the regions directly surrounding the injection sites (Abud et al., 2017). It is important to note, however, that immune deficiency alone is not sufficient for the engraftment and survival of human microglia, and little to no human microglia survive beyond 1-2 weeks when transplanted into traditional immune deficient mice that lack expression of human versions of either CSF1 or IL34, the two ligands for the CSF1 receptor (Hasselmann et al., 2019b; Mathews et al., 2019). This finding is highly consistent with prior studies that show the importance of CSF1 signaling for microglia development and survival and that human monocytes fail to respond appropriately to murine CSF1 (Elmore et al., 2014; Erblich, Zhu, Etgen, Dobrenis, & Pollard, 2011; Rathinam et al., 2011; Sieff, 1987; Y. Wang et al., 2012).

Recently, the concept of microglia xenotransplantation has also been adapted to utilize more traditional sources of hematopoietic cells, such as $CD34^+$ cord blood cells, to try to induce microglial-like differentiation with some success (Capotondo et al., 2017; Mathews et al., 2019). However, cord blood cells include definitive hematopoietic stem cells and their downstream progenitors which differ from the yolk sac-derived primitive progenitors that give rise to microglia

during development. Thus, these cord blood-derived cells likely only partially recapitulate a microglia phenotype, perhaps better mimicking brain-infiltrating blood monocytes. Unfortunately, a transcriptomic analysis of transplanted cord blood cells that could resolve this lingering question was not reported in these publications. Another group transplanted human fetal brain macrophages and postnatal microglia into hCSF1 expressing, immune-deficient mice, demonstrating convincing evidence of microglial-like morphology and marker expression (F. C. Bennett et al., 2018). However, this study also identified important differences in the expression of specific genes between transplanted microglia and transplanted blood-derived cells. Therefore, taken together, these studies clearly demonstrate that while peripherally-derived monocytes can adopt the expression of many microglial markers, the ontogeny of the transplanted cells likely continues to influence the expression of many key genes, regardless of transplantation into the brain.

While these initial reports have opened the door to xenotransplantation as a promising new approach to study human microglia *in vivo*, many questions remain. For example, does transplantation of human iMG into the mouse brain induce the expression of an *in vivo*-like human transcriptome and the adoption of typical *in vivo* microglial behavior? Also, is it possible that transplanting more primitive hematopoietic progenitor cells into the developing CNS will result in more widespread engraftment, since this better mimics natural microglia differentiation than HSC transplants or iMG transplants into adult mice? Evaluation of a model aimed at answering these questions will set the stage for subsequent experiments that can begin to directly assess the effects of the ever-growing list of AD risk genes on microglia function and AD pathogenesis.

CHAPTER 1

TRANSPLANTATION OF HUMAN IPSC-DERIVED MICROGLIA INTO THE MOUSE BRAIN INDUCES APPROPRIATE TRANSCRIPTOMIC PROGRAMMING AND REVEALS HUMAN SPECIFIC AMYLOID RESPONSES

INTRODUCTION

Microglia play critical roles in sculpting brain development, modulating neural plasticity, and maintaining homeostasis (Salter & Stevens, 2017; Stevens et al., 2007; Wu et al., 2015). As the primary immune cell of the central nervous system (CNS), microglia are highly responsive, reacting rapidly to local injury, neuroinflammation, and a multiplicity of brain pathologies (Nimmerjahn et al., 2005; Perry & Holmes, 2014). Recent genetic studies have further highlighted the importance of these cells in disease, with the discovery of many polymorphisms in microglial-enriched genes that are associated with a variety of neurological disorders including Alzheimer's disease (AD), frontotemporal dementia, amyotrophic lateral sclerosis, autism, and schizophrenia (Karch et al., 2014; Salter & Stevens, 2017). However, despite these important findings, experimental platforms that enable systematic analyses of human microglia *in vivo*, and the effects of genetic variability on microglia function within the brain, have yet to be realized.

While transgenic mouse models have provided invaluable tools for examining the role of microglia in these disorders, rodents cannot fully recapitulate the growing complement of human genetic variability implicated in these polygenic diseases (Dawson et al., 2018; Friedman et al., 2018; Ueda et al., 2016). Fortunately, the ability to generate induced pluripotent stem cells (iPSCs) from patients, and then differentiate iPSCs into defined cell subtypes, has generated exciting opportunities to examine the relationships between complex genetic backgrounds and disease-associated phenotypes. The recent development of methods to differentiate iPSCs into microglia

has further allowed researchers to begin unraveling the contribution of microglial risk genes to human disease (Pocock & Piers, 2018). Yet, while these protocols have provided researchers with the ability to generate an abundance of human microglia *in vitro*, a recent study has highlighted that microglia, as highly plastic cells, undergo dramatic alterations when maintained outside of the brain environment, exhibiting numerous changes in gene expression within hours to days of transfer to culture conditions (Gosselin et al., 2017). Unfortunately, many of these *in vitro*-related transcriptional programs are mirrored in iPSC-derived microglia (iMG), demonstrating an important limitation to the modeling of microglial biology in a cell culture environment. Overall, this suggests that experiments utilizing *in vitro* microglia to model disease states may present an incomplete picture of their genetic state or how they respond to stimuli, presenting a major roadblock to a deeper and more complete understanding of *in vivo* microglial biology.

To begin to address this challenge, we and others performed initial experiments to determine the feasibility of transplanting human microglia or hematopoietic stem cells (HSCs) into the brains of immunodeficient mice (Abud et al., 2017; F. C. Bennett et al., 2018; Capotondo et al., 2017; McQuade et al., 2018). Yet, to date no studies have thoroughly examined and validated the phenotype, transcriptional profile, and functional responses of engrafted human microglia to injury or disease-associated pathology, steps that are critical for determining the suitability of this approach for studying *in vivo* microglia biology. Toward this goal, we present the development and validation of a chimeric model system that allows researchers to examine iPSC-derived human microglia in the context of the living mammalian brain.

MATERIALS AND METHODS

Animals

All animal procedures were conducted in accordance with the guidelines set forth by the National Institutes of Health and the University of California, Irvine Institutional Animal Care and Use Committee. The MITRG mouse was purchased from Jackson Laboratories (stock #017711); this BALB/c/129 model includes two knockouts alleles, $Rag2^{-}$ ($Rag2^{tm1.1Flv}$), γc^{-} ($Il2rg^{tm1.1Flv}$), and three humanized knock-in alleles, M-CSFh ($Csf1^{tm1(CSF1)Flv}$), IL-3/GM-CSFh ($Csf2/Il3^{tm1.1(CSF2,IL3)Flv}$), TPOh ($Thpo^{tm1.1(TPO)Flv}$). The related and parental M-CSFh mouse line was also purchased form Jackson Laboratories (stock # 017708) and contains Rag2 and Il2rg deletions and humanized M-CSFh. The 5xFAD-MITRG model was created by backcrossing the MITRG mouse with 5xFAD mice which overexpress co-integrated transgenes for Familial Alzheimer's Disease (FAD) mutant APP (Swedish, Florida, and London) and mutant FAD PS1 (M146L and L286V). Progeny of these pairings were then genotyped and backcrossed with MITRG mice to return the 5 MITRG genes to homozygosity and maintain the APP/PS1 transgenic loci in the hemizygous state, resulting in the MITRG5x ($Rag2^{-}$; γc^{-}; $M\text{-}CSF^{h}$; $IL\text{-}3/GM\text{-}CSF^{h}$; TPO^{h}; Tg(APPSwFlLon,PSEN1*M146L*L286V)6799Vas). To generate mice that lacked M-CSFh but included GM-CSFh and TPOh, MITRG mice were crossed with M-CSFh mice and then F1 progeny were crossed and genotyped to select mice that lacked either both or one copy of M-CSFh. For 2 photon living-imaging of mouse microglia, the CX3CR1-GFP (B6.129P2(Cg)-*Cx3cr1*^{tm1Litt}/J; stock # 005582) mouse was used. All mice were age and sex matched and group housed on a 12h/12h light/dark cycle with food and water *ad libitum*.

Acquisition and maintenance of iPSC lines

iPSC lines were purchased from Coriell and the European Bank for induced pluripotent Stem Cells. The GFP cell line (Coriell, AICS-0036) was generated by CRISPR modification of the line WTC11 to insert a monoallelic mEGFP into the AAVS1 safe harbor locus (chromosomal location 19q13.4-qter) under the control of a CAG promoter. Maintenance of all iPSC lines involved culturing in feeder-free conditions in complete mTeSR E8 medium (Stemcell Technologies), in a humidified incubator (5% CO2, 37°C), with medium changed daily. Passaging was performed every 7-8 days using ReLeaSR (Stemcell Technologies) and cells were plated onto 6-well plates (Corning), coated with growth factor-reduced Matrigel (1 mg/mL; BD Biosciences), in mTeSR E8 medium, supplemented with 0.5uM Thiazovivin (Stemcell Technologies) for the first 24 hours post-passage. All cell lines were tested for mycoplasma on a monthly basis, and confirmed to be negative, and cell line karyotyping was performed every ten passages.

Differentiation of Hematopoietic Progenitor Cells and *in vitro* Microglia from iPSCs

iHPCs and iPS-microglia were differentiated according to the protocol published by McQuade et al. (McQuade et al., 2018). To begin iHPC differentiation, iPSCs were passaged in mTeSR-E8 to achieve a density of 80 colonies of 100 cells each per 35mm well. On day 0, cells were transferred to Medium A from the STEMdiff™ Hematopoietic Kit (Stem Cell Technologies). On day 3, flattened endothelial cell colonies were exposed to Medium B and cells remained in medium B for 7 additional days while iHPCs began to lift off the colonies. On day 10, non-adherent CD43+ iHPCs were collected by removing medium and cells with a serological pipette. At this point, d10-d11 iHPCs can be frozen in Bambanker (Wako). Cells used for early-postnatal iHPC transplantation were thawed in iPS-Microglia medium (DMEM/F12, 2X insulin-transferrin-selenite, 2X B27, 0.5X N2, 1X glutamax, 1X non-essential amino acids, 400μM monothioglycerol,

and 5 μg/mL human insulin freshly supplemented with 100 ng/mL IL-34, 50 ng/mL TGFβ1, and 25 ng/mL M-CSF (Peprotech)) and allowed to recover for 24 hours, then resuspended at 62,500 cells/uL in 1X DPBS (low Ca^{2+}, low Mg^{2+}). Cells utilized for *in vitro* experiments continued microglial differentiation for 28 days. During the last 3 days in culture, 100 ng/mL CD200 (Novoprotein) and 100 ng/mL CX3CL1 (Peprotech) were added to mature microglia in a brain-like environment.

Early Postnatal Intracerebroventricular Transplantation of iHPCs

P0 to P1 MITRG mice were placed in a clean cage over a heating pad with a nestlet from the home cage to maintain the mother's scent. Pups were then placed on ice for 2-3 minutes to induce hypothermic anesthesia. Free-hand transplantation was performed using a 30-gauge needle affixed to a 10μL Hamilton syringe, mice received 1μL of iHPCs suspended in sterile 1X DPBS at 62.5K cells/μL at each injection site (8 sites) totaling 500K cells/pup. Bilateral injections were performed at $2/5^{th}$ of the distance from the lambda suture to each eye, injecting into the lateral ventricles at 3mm and into the overlying anterior cortex at 1 mm, and into the posterior cortex in line with the forebrain injection sites, and perpendicular to lambda at a 45° angle. Transplanted pups were then returned to their home cages and weaned at P21.

Adult intracranial transplants

All mouse surgeries and use were performed in strict accordance with approved NIH and AALAC-certified institutional guidelines. Direct bilateral intracranial injections of WT iMG into the cortex and hippocampus were performed on adult MITRG mice. Briefly, adult mice (3 months old) were anesthetized under continuous isoflurane and secured to a stereotaxic frame (Kopf), and local anesthetic (Lidocaine 2%) was applied to the head before exposing the skull. Using a 30-guage needle affixed to a 10μL Hamilton syringe, mice received 2 μL of mature iMG suspended

in sterile 1X DPBS at 50,000 cells/μL at each injection site. Transplantation was conducted bilaterally in the cortex and hippocampus at the following coordinates relative to bregma: anteroposterior, -2.06 mm; dorsoventral, -1.75 mm (hippocampus), -0.95 mm; mediolateral, ±1.75 mm. Cells were injected at a rate of 50,000/ 30s with 4min in between injections. The needle was cleaned with consecutive washes of PBS, 70% (vol/vol) ethanol, and PBS in between hemispheres and animals. Animals were allowed to recover on heating pads before being placed in their home cages and received 2 mg/mL Acetaminophen (Mapap) diluted in water for five days. Animals were perfused 2 months following surgery with 1X PBS followed by 4% paraformaldehyde, entire brains were removed for immunohistochemistry.

Immunohistochemistry and Confocal Microscopy

Animals were administered Euthasol and monitored for loss of consciousness. Once animals no longer responded to toe pinch, mice were intracardially perfused with ice cold 1X DPBS. If xMG were being isolated from ½ brains, the remaining half brain was drop fixed in 4% (w/v) PFA for 48 hours, otherwise, the mice were intracardially perfused with 4% PFA and post-fixed for 24 hours. Samples were then cryoprotected in 30% (w/v) sucrose until the tissue sank in the solution. Brains were then cut either coronally or sagittally at a section thickness of 40um on a sliding microtome cooled to -79°C. Tissue sections were collected as free-floating sections in PBS with and 0.05% sodium azide. For staining, tissue was blocked for 1 hour in 1X PBS, 0.2% Triton X-100, and 10% goat or donkey serum. Immediately following blocking, sections were placed in primary antibodies diluted in 1X PBS and 1% goat or donkey serum and incubated overnight on a shaker at 4°C. Sections were then incubated in conjugated secondary antibodies for 1 hour, before washing and mounting on microscope slides. Immunofluorescent sections were then visualized and captured using an Olympus FX1200 confocal microscope. In some cases, brightness

and contrast settings of confocal images were slightly adjusted to reveal fine structures and morphology. Importantly, no such changes were made to any images used for quantification.

Quantification Percent xMG Engraftment

For analysis of xMG engraftment and its reproducibility, two separate preparations of iHPCs (HPCs #1; n=4 & HPC #2; n=4) were transplanted as described above, on separate days, and perfused at 2 months. Brains were sectioned sagittally and stained with Ku80 (human nuclear marker) and PU.1 (myeloid nuclear marker). The Allen Brain Atlas was used to identify regions where, 4, 40x images per region were captured (Somatosensory Cortex: CTX; Hippocampus: HIP; and Striatum: STR), all images were acquired using identical settings with an Olympus FV1200 scanning laser confocal microscope. Using the "Spots" function in IMARIS software (Bitplane) total Ku80+ and PU.1+ spots were quantified separately. Then total human cells (all Ku80+ spots) and total mouse cells (all PU.1 positive spots minus total number of Ku80+ spots) were determined. Total percentage of human cells was then found by dividing total human cells by mouse cells and multiplying by 100. To determine any significant interactions between transplantation preparation and brain region a 2-way ANOVA was run using Prism 7.

Antibody Immunoreactivity after Systemic LPS Treatment

For analysis of antibody immunoreactivity all images for a given antibody were acquired using identical settings with an Olympus FV1200 scanning laser confocal microscope, then analyzed using the image processing package FIJI, a distribution of NIH Image J software. Images were first split into single channels (GFP and P2RY12) and thresholded to create a mask around cells. The resulting mask was then overlaid onto the original images and mean intensity values were measured within the ROI. For normalization, human cells were hand counted in the GFP channel and mean intensity was divided by total cell counts, then divided by the saline mean

values. For analysis of CD45 immunoreactivity, IMARIS "Surfaces" function was used to detect CD45 immunoreactivity, then mean intensity values within CD45+ surfaces were measured. For normalization, intensity values for each animal were divided by the saline mean values. Normalized intensity values for all antibodies were tested for statistical significance ($p<0.05$) though unpaired t test using Prism 7 (n=5 LPS; 4 Saline).

Tissue dissociation for bulk RNA-seq

Following perfusion with ice cold PBS, whole or half brains were dissected, and the cerebellum was removed. Tissue was stored briefly in 1X HBSS until subsequent perfusions were completed. Tissue dissociation was then performed utilizing the Adult Brain Dissociation Kit (Miltenyi) and the gentleMACS Octo Dissociator with Heaters (Miltenyi) according to manufacturer guidelines with modifications. Briefly, tissue was cut into ~1mm^3 pieces and placed into the C-tubes with the kit's enzymes and samples were dissociated using the preprogrammed protocol. Following enzymatic digestion, samples were strained through a 70um filter and pelleted by centrifugation. Myelin and debris were removed by resuspending the pellet in 6mL 23% Percoll, overlaid with 2mL of 1X DPBS, and spinning at 400xg for 25 minutes at 4°C, with acceleration and brake set to 0. The supernatant was discarded, and the cell pellet was processed for flow cytometry.

Fluorescence activated cell sorting of xMG

For sorting of xMG expressing endogenous GFP, dissociated cell pellets were resuspended in 400uL of FACS buffer (2% BSA in 1X DPBS) containing either Zombie Violet (Biolegend, 1:100) or Propidium Iodide (PI) (Biolegend, 1:400) as a viability marker. For animals transplanted with non-fluorescent cell lines, cell pellets were resuspended in 100uL of FACS buffer containing 5ug of mouse and human Fc block (BD) and incubated for 5 minutes on ice. 100uL of FACS buffer

including the following antibodies was then added to the sample for a final staining volume of 200uL: Rat anti-HLA-ABC-PE clone YTH862.2 (Novus, 1:100) and mouse anti-human CD11b clone ICRF44 (Biolegend, 1:200). Samples were then spun down and resuspended in 400uL of FACS buffer containing either Zombie Violet (Biolegend, 1:100) or PI (Biolegend, 1:400) as a viability marker. Samples were then sorted on a FACSARIA Fusion II (BD Biosciences) directly into 900uL of Trizol (Thermo Fisher), immediately vortexed to ensure rapid lysis, and placed on dry ice.

Bulk RNA Isolation from xMG

FACS sorted xMG, ranging from 40,000-172,000 cells, were stored at -80°C until RNA isolation. Samples were then thawed on ice and RNA was isolated by adding 140uL of TET (10mM Tris 8.0/0.01mM EDTA/0.05% Tween20) followed by 140uL Chloroform:Isolamyl alcohol 24:1 (Sigma). Samples were centrifuged at 15,000xg for 10 min. at 4°C and the aqueous phase was collected and added to 1.5uL of GlycolBlue (Thermo Fisher). 55uL (~1/10 supernatant volume) of 3M sodium acetate and 550uL (~1 supernatant volume) of isopropanol (Sigma) were added and the samples were mixed by inverting then stored at -20°C overnight. Samples were then spun at 15,000xg for 30 min. at 4°C, supernatants were removed from pellets, and 500uL of 75% ethanol was added to the pellet. Samples were then spun at 15,000xg for 30 min. at 4°C, and supernatants were removed from pellets. RNA pellets were dried at RT to remove any residual ethanol, resuspended in 14uL of RNase-free H_2O, and used immediately or aliquoted and stored at -80°C for downstream analysis.

Isolation of microglia from human tissue

Human microglia were isolated from adult, normal appearing cortical tissue resected from non-malignant cases of temporal lobe epilepsy. Tissue was mechanically dissociated followed by

gentle enzymatic digestion, using DNase and trypsin, to generate a single cell suspension. Cells were then passed through a nylon mesh filter and separated from debris via ultracentrifugation. Pelleted cells were resuspended in PBS (0.4% BSA), counted, stained with cell surface markers, and purified by flow cytometry (BD Biosciences FACs ARIA Fusion). Microglia were defined as live (Zombie Aqua Fixable Viability stain, Biolegend), $CD11b^{+}$ (Anti-human PE, Biolegend) $CD45^{low}$ (Anti-human APC/Cy7, Biolegend), $CX3CR1^{high}$ (Anti-human FITC, Biolegend) single cells. ExVivo samples were immediately pelleted, resuspended in Trizol LS (Thermo Fisher Scientific), and stored at -80°C until subsequent RNA isolation.

InVitro samples were pelleted, resuspended, counted, and plated at $2x10^6$ cells/mL in MEM supplemented with heat-inactivated FBS (5%), P/S (0.1% v/v) and glutamine (0.1% v/v.). Microglia were grown for 3 days, collected and plated at $1x10^5$ cells/mL, and maintained in culture for 6 days during which time cells received two treatments of TGFb (20 ng/mL) on days 3 and 5. Human fetal brain tissue was obtained from the Fetal Tissue Repository (Albert Einstein College of Medicine, Bronx, NY). Total RNA was isolated using standard Trizol LS (Thermo Fisher Scientific) protocols and stored at -80°C.

RNA analysis, Library Construction and Bulk RNA-seq

RNA integrity (RIN) values were determined using an Agilent Bioanalyzer 2100 series and RNA concentrations were assayed by Qubit and the average RIN value for RNA samples used in sequencing was 9.4. 10ng of RNA was used for library construction using ClonTech SMART-seq V4 Ultra Low Input kit (Takara Bio) which utilized poly-A selection to enrich for mRNAs. The quality of the DNA libraries was assayed using the Agilent 2100 bioanalyzer high sensitivity DNA assay and the DNA high sensitivity Qubit. The libraries were quantified by Kapa qPCR,

normalized to 2nM and then multiplexed for sequencing on the Illumina HiSeq 4000 platform with single read 100 base chemistry.

Tissue dissociation for scRNA-seq

Following perfusion with ice cold PBS containing 5 ug/ml actinomycin D (act D), half brains were dissected, and the cerebellum was removed. Tissue was stored briefly in RPMI 1640 containing 5 ug/mL act D, 10uM triptolide, and 27.1 ug/mL anisomycin until subsequent perfusions were completed. Tissue dissociation was then performed utilizing the Tumor Dissociation kit, human (Miltenyi) and the gentleMACS OctoDissociator with Heaters (Miltenyi) according to manufacturer guidelines with modifications. Briefly, tissue was cut into ~1mm^3 pieces and placed into the C-tubes with the kit's enzymes, 5 ug/mL act D, 10uM triptolide, and 27.1 ug/mL anisomycin and samples were dissociated using the preprogrammed protocol. Following enzymatic digestion, samples were strained through a 70um filter and pelleted by centrifugation. Myelin and debris were removed by resuspending the pellet in 8mL 23% Percoll, overlaid with 2mL of 1X DPBS, spinning at 400xg for 25 minutes at 4°C, with acceleration and brake set to 0, and discarding the myelin band and supernatant.

Magnetic Isolation of xMG for scRNA-seq

Dissociated cell pellets were resuspended in 160uL FACS buffer (0.5% BSA in 1X DPBS) + 40uL Mouse cell removal beads (Miltenyi) and incubated at 4°C for 15 minutes. Samples were then separated using LS columns and the MidiMACs separator (Miltenyi) and the human cells were collected in the flow through. Cells were pelleted via centrifugation (10 minutes, 400xg) and resuspended to ~1,000 cells per microliter in FACS buffer, according to counts performed on a hemocytometer.

Single-cell sequencing via 10X

Following magnetic isolation, the scRNA-seq library preparation was performed according to the Chromium Single Cell 3' Reagents kit v2 user guide. Briefly, a volume of single cells to target a capture of 10,000 cells was used in the generation of GEMS (gel bead in emulsions). The workflow was followed according to the 10X protocol and sequenced on an Illumina HiSeq 4000. All samples were multiplexed and sequenced to a depth of 60-100K reads per cell.

Intraperitoneal LPS injections

A neuroinflammatory state was induced via systemic LPS treatment. Animals received i.p. injections of either 2mg/kg LPS (eBioscience) (n=5 mice) or PBS (n=4 mice) once every 24 hours over a 72-hour period (3 injections total). 12-hours after the final LPS treatment, animals were euthanized, perfused with PBS, and half brains were collected for either IHC or transcriptomic analyses, as described above.

In vitro iMG LPS Stimulation

Day 38 iMG were plated at 200,000 cells/well on a Matrigel-coated (1mg/well) 24-well-plate containing 2mL of microglia medium (McQuade et al., 2018). Cells were treated with either LPS (100 ng/mL; eBioscience) or DPBS (Ca^{2+} and Mg^{2+} free) and allowed to incubate for 24 hours at 37°C before immediate lysis for RNA isolation (n=3 wells per treatment group).

Cranial Window Implantation

Mice were anesthetized with isoflurane (Patterson Veterinary) in O_2 (2% for induction, 1-1.5% for maintenance). To provide perioperative analgesia, minimize inflammation, and prevent cerebral edema, Carprofen (10 mg/kg, s.c., Zoetis) and Dexamethasone (4.8mg/kg, s.c. Phoenix) were administered immediately following induction. Ringer's lactate solution (0.2mL/20g/hr, s.c, Hospira) was given to replace fluid loss. Sterile eye ointment (Rugby) was used to prevent corneal

drying. Surgical tools were sterilized using a hot glass bead sterilizer (Germinator 500). Following hair removal, Povidone-iodine (Phoenix) and Lidocaine Hydrochloride Jelly (2%, Akorn) was used to disinfect and numb the scalp, respectively. The scalp and underlying connective tissue were removed to expose the parietal and interparietal bone. Lidocaine hydrochloride injectable (2%, Phoenix) was used for muscle analgesia and the right temporal muscle detached from the superior temporal line. The skull was dried using ethanol (70% in DI water) and a thin layer of Vetbond Tissue Adhesive (3M) applied. Custom-printed ABS headplates were attached using Contemporary Ortho-Jet liquid and powder (LANG) at an angle parallel to the skull. A small craniotomy (3mm diameter) was performed over the right hemisphere 2.5mm anterior and 3mm lateral lambda. Hemostatic gelfoam sponges (Pfizer) pre-soaked in sterile saline (CareFusion AirLife Modudose) were used to absorb dural bleeding. Surgery was terminated if dural tears or parenchymal hemorrhage was observed. A 4mm glass coverslip (World Precision Instruments) was placed over the exposed brain and its edges attached to the skull first with a thin layer of Vetbond and second with dental acrylic. Following surgery, mice recovered in their home cage over a warm heating pad until normal behavior resumed (~15-30 minutes). Postoperative care consisted of daily Carprofen injections (10mg/kg, s.c.) for one week.

Two-Photon Imaging and Laser Ablation

Fluorescence was gathered with a resonant two-photon microscope (Neurolabware, Los Angeles, CA) with 900 nm excitation light (Mai Tai HP, Spectra-Physics, Santa Clara, CA). A 16x Nikon water immersion lens (0.8 NA) or a 20x water immersion lens (Olympus, 1.0 NA) was used. Emissions were filtered using a 510/84nm and 607/70 nm BrightLine bandpass filter (Semrock, Rochester, NY). Image stacks (2.89μm step size) were gathered every 30-300s using Scanbox acquisition software (Scanbox, Los Angeles, CA) at a depth of 150-250μm below the

meninges, corresponding to cortical layer 2/3. Laser ablation consisted of scanning over a small region (70x10μm, 1.2-1.5W) at magnification 25 for 1 minute.

Homeostatic and Response to Laser-Induced Ablation Analysis

All image stacks were processed and analyzed using the image processing package FIJI. Images were temporally binned down to 5 min. intervals and the resulting z stack used to analyze homeostatic activity and response to laser-induced ablation. To measure extension and retraction rates, the first 100 notable changes in process length was measured manually for each mouse. To discriminate ablation-specific motility from homeostatic extension/retraction, we restricted our measurements to long process extensions (>20μm) growing toward the laser ablation site. The increase in microglia processes toward the laser-ablated site is reflected by an increase in the amount of GFP fluorescence. Therefore, we measured the local microglial response to laser-induced ablation by taking the average intensity of GFP within a circle (r = 50μm) centered at the epicenter of damage. These values were compared to the average intensity of GFP within a circle (r = 50μm) centered 100μm away from the epicenter of damage. The intensity at any timepoint (t_x) was normalized using the intensity at t_5 min.

Repeat Mild Closed Head Injury (rmCHI)

2 month old, EGFP iHPC transplanted MITRG mice underwent repeat mild closed head injury (rmCHI) as described by Gold et al. (Gold et al., 2018). Briefly, transplanted MITRG mice were randomly assigned to either sham or hit groups Sham animals received 5 days of Isoflorane anesthesia only, with no injury, 5-Hit animals received 5 days of Isoflorane anesthesia with 1 injury each day. Injuries were performed using a controlled cortical impact device (TBI-0310 Head Impactor, Precision Systems and Instrumentation, LLC, Fairfax Station, VA) Injury

parameters are as follows: speed: 5 m/s; depth: 1mm; dwell time: 50ms. Following injury, animals rested until euthanized for histology 8 weeks later.

Bulk RNA-seq Data Analysis

FASTQ files were preprocessed using BBDuk (Bushnell, 2018) to filter out ribosomal RNA and PhiX reads, trim Illumina adapters, and to quality trim any base pairs below a PHRED score of 10. FASTQC (Andrews, 2014) was then performed to verify the quality of the sequencing files and all files were determined to be of sufficient quality for downstream processing. Reads were then pseudoaligned to the human GRCh38.p12 transcriptome (Ensembl release 94) (Schneider et al., 2017; Zerbino et al., 2018) using Kallisto (Bray, Pimentel, Melsted, & Pachter, 2016), transcripts were summarized to the gene level via tximport (Soneson, Love, & Robinson, 2015), and differential gene expression analysis was performed using DESeq2 (Love, Huber, & Anders, 2014) after removing genes with summed counts <10. For Kallisto pseudoaligment of samples without available library information, an average fragment length of 250 and a standard deviation of 120 were used.

For TF motif analysis, RNA-seq reads were checked for quality using FASTQC (Andrews, 2014). Reads were then trimmed using Trimmomatic (Bolger, Lohse, & Usadel, 2014) to remove Illumina adapters and regions of reads with PHRED quality scores below 30, as well as the leading and trailing 15 base pairs of each read. Reads with a minimum length of 30 after trimming were retained. Reads were then aligned to the GRCh38.p12 transcriptome (Ensembl release 94) using Bowtie2 (Langmead & Salzberg, 2012) and summarized at the gene level using tximport (Soneson et al., 2015). Differential expression analysis was performed using DESeq2 (Love et al., 2014).

scRNA-seq Data Analysis

FASTQ files were aligned to a dual-species transcriptome made up of the human GRCh38.p12 transcriptome (Ensembl release 95) and the mouse GRCm38 transcriptome (Ensembl release 95) using CellRanger (v2.2.0) with default commands and an expected cell count of 5,500. Following alignment, all barcodes that were identified in the mouse alignment were removed from the human dataset.

Bulk RNA-seq Data Visualization

Data was normalized and converted to a $\log_2$ scale for visualization using DESeq2's varianceStabilizingTransformation followed by batch correction using the removeBatchEffect function from limma (Ritchie et al., 2015). Heatmaps were generated using the R "Pheatmap" package (Kolde, 2018) while volcano and bar plots were generated using the "ggplot2" package (Wickham, 2016).

scRNA data Visualization and Differential Gene Analysis

UMI count tables, for 13,597 MITRG xMG and 11,054 5X-MITRG xMG, were read into Seurat (v2.3.4) (Butler, Hoffman, Smibert, Papalexi, & Satija, 2018) for preprocessing and clustering analysis. First, cells were log normalized, centered, and scaled (Default settings) followed by PCA using all genes in the dataset. PCs 1:10 were used for clustering with a resolution parameter of 0.3. Clusters identified as doublets, dividing, or gene poor (representing damaged cells) were then discarded before further analysis. Cells passing these QC parameters were then merged by genotype (e.g. Male and Female 5X-MITRG) using the MergeSeurat function.

Secondary QC cutoffs were then applied to include only cells with less than 32% ribosomal genes, 7% mitochondrial genes, greater than 800 genes but less than double the median gene count, and greater than 500 UMI but less than double the median UMI count. This resulted in 10,184

MITRG and 8,673 5X-MITRG cells with average UMI counts of 3,201 for MITRG and 3,242 for 5X-MITRG, and average genes counts of 1,583 and 1,593, respectively. Data for these cells were log normalized, centered, and scaled, using the 'negbinom' general linear model, while regressing out library size differences, percent mitochondrial genes, and sex. A second round of PCA was then performed on the cleaned data and interrogation of the PCs revealed a set of 41 highly variable genes contained across all samples, regardless of genotype or sex. These genes were present across multiple PCs and had a large effect on clustering but, as a gene set, had no discernable biological relevance. Therefore, we treated these genes as a technical artifact and removed the set from the variable gene list before repeating subsequent PCA analysis.

PCA was then performed using a set of variable genes selected according to expression and dispersion cutoffs (low expression cutoff = 0.01, high expression cutoff = 3, low dispersion cutoff = 1.1). Subsequent tSNE clustering was performed using PCs 1:14 for xMG isolated from the MITRG mouse and PCs 1:10 for xMG isolated from the 5X-MITRG mouse, both at a resolution of 0.45. tSNE plots were generated using the same PCs used for clustering and variable genes were determined between clusters using the Wilcoxon Rank Sum Test.

Comparison of Human and Mouse DAM Genes

Differential genes analysis was performed between the DAM and Homeostatic clusters for 5X-MITRG xMG with an FDR cutoff of 0.01 and the requirement that the gene be expressed in at least 10% of the cluster. Murine DAM genes were obtained from Keren-Shaul et al. (Keren-Shaul et al., 2017) and filtered to remove pseudogenes, genes without a verifiable official name (e.g. GM*), as well as ambiguous genes without 1:1 mouse to human homologs, as specified by either Ensembl or NCBI Homologene. The subsequent comparison utilizing qPCR, microarray, and bulk RNA-seq microglia gene lists (Kamphuis et al., 2016; Krasemann et al., 2017; Yin et al., 2017)

was performed by merging the unique genes from all four lists and filtering the list for genes with 1:1 homologs.

xMG Response to Laser Ablation

All image stacks were processed and analyzed using the image processing package FIJI, a distribution of NIH Image J software. Stacks were temporally binned (5 min) and the average GFP intensity within a circle (r = 50μm) centered at site of damage was used to assess local microglial response to laser ablation. A second circle (r = 50μm) at least 100μm away from the site of damage was used to assess distal changes in intensity following laser ablation. The intensity at any timepoint (t_x) was normalized to the intensity in that area at t_{5min}. To determine differences in GFP intensity within and between groups we used a repeated measures two-way ANOVA corrected for multiple comparison (Sidak).

Gene set enrichment analysis

Pathway analysis was performed using the Broad Institute's Gene Set Enrichment Analysis (GSEA) desktop application version 3.0 (Subramanian et al., 2005). Differential expression results, generated by comparing saline and LPS-treated samples, were taken from DESeq2 and ranked according to the sign of the fold change * $-\log_{10}$(adjusted p-value). The entire list of ranked genes present in both samples was then input into GSEA's pre-ranked analysis module and the module was set to perform 1000 permutations using the weighted enrichment statistic. The gene list was compared to MSigDB's gene ontology database (c5.all.v6.2.symbols.gmt) consisting of the entire set of Gene Ontology terms (Ashburner et al., 2000; The Gene Ontology, 2017) and results were output, excluding any gene sets less than 15 genes or more than 5000 genes in length.

Gene Ontology Analysis

Gene ontology (GO) analysis was performed using PANTHER (Mi et al., 2017). Upregulated or downregulated genes (|log fold change| >= 2) were compared to genes with a log fold change between 2 and -2 using a statistical overrepresentation test. Significantly ($p<0.05$) overrepresented GO terms were clustered and visualized using the EnrichmentMap plugin (Merico, Isserlin, Stueker, Emili, & Bader, 2010) in Cytoscape 3.6.1 (Shannon et al., 2003).

Transcription Factor Binding Prediction and Co-Occurrence

Potential transcription factor binding sites were identified by searching the region 500bp upstream of genes using FOCIS (D. E. Webster, 2013) for binding motifs from the JASPAR database (2018 release) (Khan et al., 2018). Upregulated (log fold change >= 2) or downregulated (log fold change <= -2) genes were compared to genes with a log fold change between 2 and -2 as background. Transcription factors with putative binding sites upstream of the same gene were considered to be co-occurring. Co-occurrence frequency of a transcription factor pair was described using the Jaccard index.

Literature search

Pubmed searches were performed using the term "microglia" or "Alzheimer" plus the name of each differentially expressed gene and transcription factor of interest. At least one publication result matching both terms was considered a positive result.

Statistical Analysis

All statistical analyses were performed in either R programming language or utilizing GraphPad Prism.

Data and Code Availability

The bulk and single-cell RNA-seq datasets generated during this study are available through GEO SuperSeries accession number GSE133434 or individual series accession numbers GSE133432 or GSE133433, respectively. The bulk RNA-seq datasets generated by Gosselin et al. are available through NCBI dbGaP, accession number phs001373.v1.p1. The bulk RNA-seq datasets generated by Abud et al. are available through GEO, series accession number GSE89189. The bulk RNA-seq datasets generated by McQuade et al. are available through GEO, series accession number GSE117829.

RESULTS

Human iPSC-derived hematopoietic progenitor cells engraft and differentiate into cells expressing mature microglia markers

Given the developmental ontogeny of microglia, which arise from yolk sac-derived primitive hematopoietic progenitor cells (HPCs) (Prinz, Erny, & Hagemeyer, 2017), we hypothesized that transplantation of iPSC-derived HPCs (iHPCs), as generated in McQuade et al. (2018) which express multiple genes associated with primitive HPCs (**Figure 1.1A**), into the early postnatal MITRG brain would result in robust engraftment of human cells that would differentiate into mature microglia. To test this, we transplanted GFP-expressing iHPCs directly into the lateral ventricles and overlying cortex of postnatal day 1 (P1) MITRG mice (Rongvaux et al., 2014) (**Figure 1.1B**). After allowing the mice to age for two months, immunohistochemical (IHC) analysis revealed robust engraftment of human cells throughout the forebrain that strongly expressed the homeostatic microglial marker P2RY12 (**Figure 1.1C**), IBA1 (**Figure 1.2A**), the myeloid transcription-factor PU.1 (**Figure 1.2B**), and the brain resident microglia-specific marker

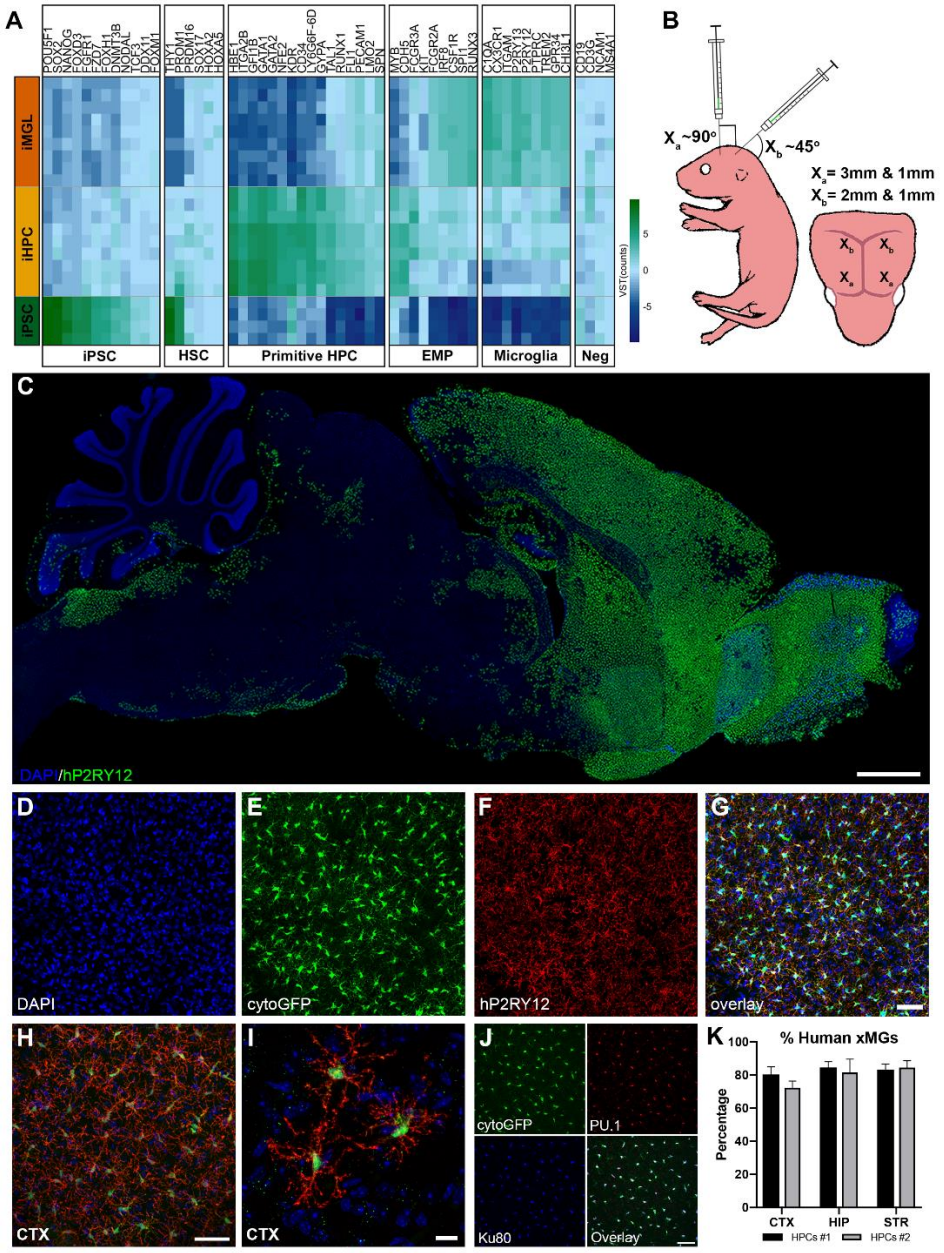

Figure 1.1. iPSC-derived human HPCs differentiate into microglia and display robust engraftment within the forebrain of MITRG mice. (A) A heatmap comparing iPSC, iHPC, and iMG (McQuade et al., 2018) across a sampling of genes related to iPSC, hematopoietic stem cell (HSC), primitive HPC, erythromyeloid progenitor (EMP), and microglia lineages, along with lineage negative (Neg) genes, shows that iHPCs most closely resemble primitive HPCs but also express some EMP markers. (B) Schematic of transplantation paradigm. (C) Human P2RY12 staining displays the overall migration and distribution of xMG 2 months after P1 transplantation (P2RY12, pseudocolored green; DAPI, blue). (D-G) Transplanted cells display near complete co-localization of cytosolic eGFP (green) with human P2RY12 (red). (H-I) Engrafted cells uniformly tile in the cortex and take on a highly ramified morphology. (J) Colocalization of (Green, cytoGFP), PU.1 (Red, all myeloid nuclei) and Ku80 (pseudocolored blue, human nuclei only) was used to quantify xMG engraftment. (K) Percentage of xMG engraftment in the cortex (CTX), the hippocampus (HIP), and the striatum (STR) from two separate experiments (HPCs #1 and HPCs #2). In some cases, brightness and contrast settings of confocal images were adjusted to reveal fine structures and morphology. Scale = 1mm (C), 50μm (G, H, & J), 10μm (I)

TMEM119, along with the human nuclei marker, Ku80 (**Figure 1.2C-D**). Further analysis revealed a high degree of concordance between the expression of GFP and P2RY12 (**Figure 1.1D-G**) as well as the complex, ramified morphology adopted by the transplanted iHPCs (**Figure 1.1H-I**) strongly suggesting that the engrafted iHPCs had differentiated into microglia.

Quantification of microglia within the targeted regions, including the cortex, hippocampus, and striatum, demonstrated that ~80% of the PU.1+ microglia co-expressed the human-specific nuclear marker Ku80 (**Figure 1.1J-K**). Furthermore, no significant differences in engraftment were observed between different batches of iHPC transplants ($F_{1,18}$=0.6923, p=0.4163), across different brain regions ($F_{2,18}$=1.462, p=0.2580), or in the interaction between iHPC batch and region ($F_{2,18}$=0.4417, p=0.6497) (**Figure 1.1K**) demonstrating the reproducibility of this approach.

Expression of human CSF1 is necessary and sufficient for the long-term engraftment of human microglia in the murine brain

We previously demonstrated that human microglia could survive for at least 2 months following transplantation into adult MITRG immune-deficient mice (Rag2 KO, IL2rγ KO) (Abud et al., 2017). However, we remained curious as to whether all three humanized genes present in the MITRG; hCSF1, hCSF2, or Thrombopoietin (hTPO) (Rongvaux et al., 2014), were necessary for xMG survival. Given the importance of CSF1R signaling for microglia survival, and previous reports that the murine CSF1 ligand cannot fully activate human CSF1R signaling (Elmore et al., 2014; Rathinam et al., 2011; Sieff, 1987), we hypothesized that expression of humanized CSF1 alone was necessary for robust engraftment of human microglia in the murine brain. To test this, we performed transplantations of GFP^+ iHPCs into MITRG mice (**Figure 1.3A**) and MITRG mice which had the humanized hCSF2 and hTPO genes bred out (**Figure 1.3B**), revealing virtually identical engraftment of human cells in both strains and confirming that expression of hCSF2 and

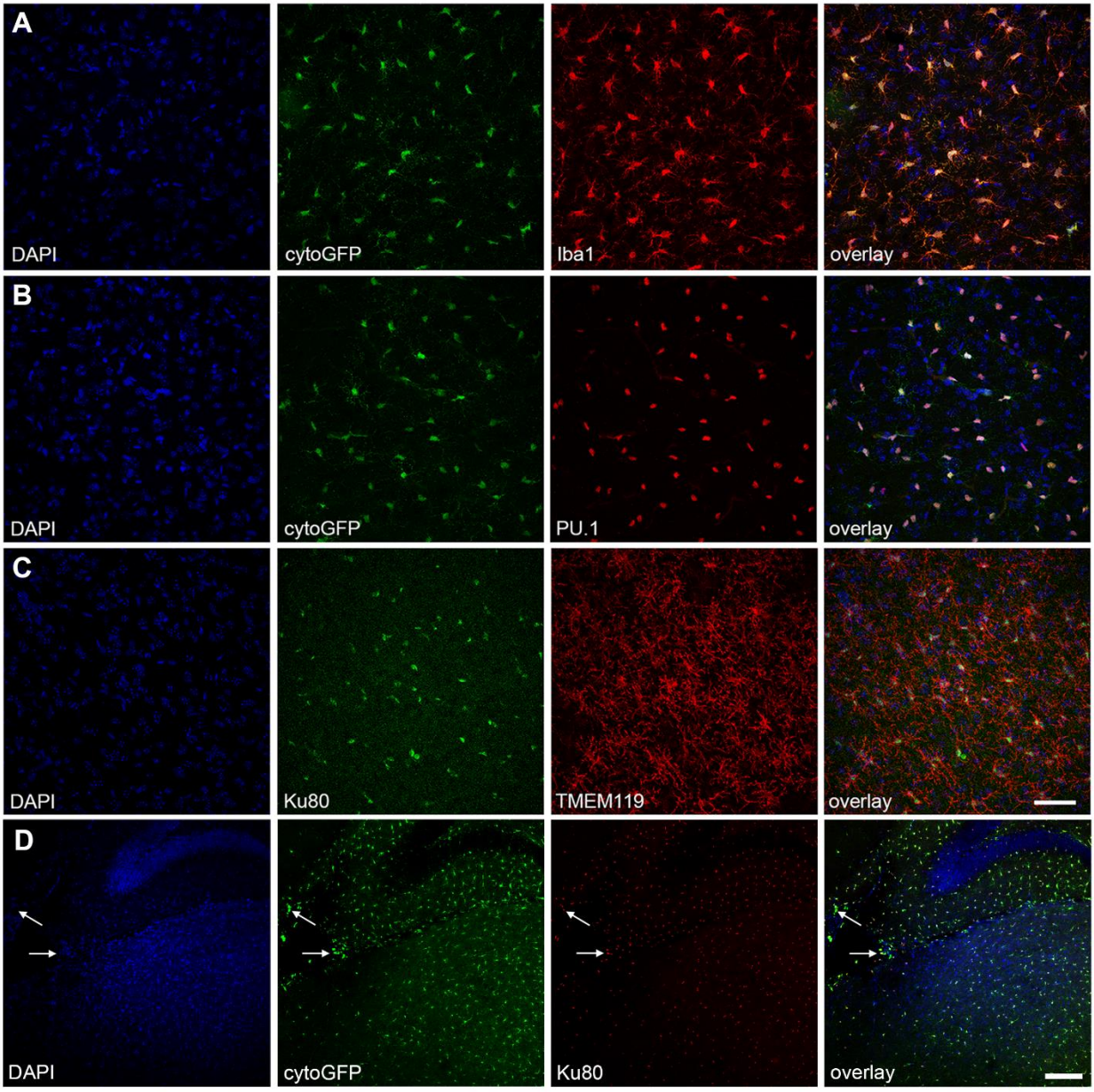

Figure 1.2. Xenotransplanted human cells express microglia markers. (A) Individual channels reveal co-localization of the cytosolic eGFP (green) with the myeloid cell marker Iba1 (red) (all nuclei, blue; DAPI). (B) Transplanted human cells are also positive for the myeloid-lineage transcription factor PU.1 (red). (C) Additionally, human cells express the homeostatic microglia-specific marker TMEM119 (red). The human nuclei maker Ku80 (AlexaFluor 633, pseudocolored green) is also used to identify human cells as TMEM119 staining requires an antigen retrieval step that quenches endogenous GFP fluorescence. (D) Transplanted human cells in the parenchyma, resembling microglia, and choroid plexus, with a more ameboid morphology (white arrows), both demonstrate colocalization of GFP and Ku80. Scale = 20μm (A-C), 140um (D)

hTPO is not necessary for xMG survival. In stark contrast, no xMG were detected in mice that expressed hCSF2 and hTPO but lacked hCSF1 expression (**Figure 1.3C**). Interestingly, the necessity for hCSF1 was also dose-dependent, as heterozygous hCSF1 mice exhibited partial survival of xMG (**Figure 1.3D**). Lastly, transplantations into the parental mouse strain from which the MITRG model was developed (JAX# 017708), which includes Rag2/IL2rγ deletion and hCSF1 but lacks hCSF2 and hTPO, demonstrated that human iHPCs differentiate into microglia which engraft at levels that are consistent with transplantation into MITRG mice (**Figure 1.3E**). Taken together, these data demonstrate that human CSF1 is both necessary and sufficient to enable the long-term engraftment and survival of human microglia in the mouse brain.

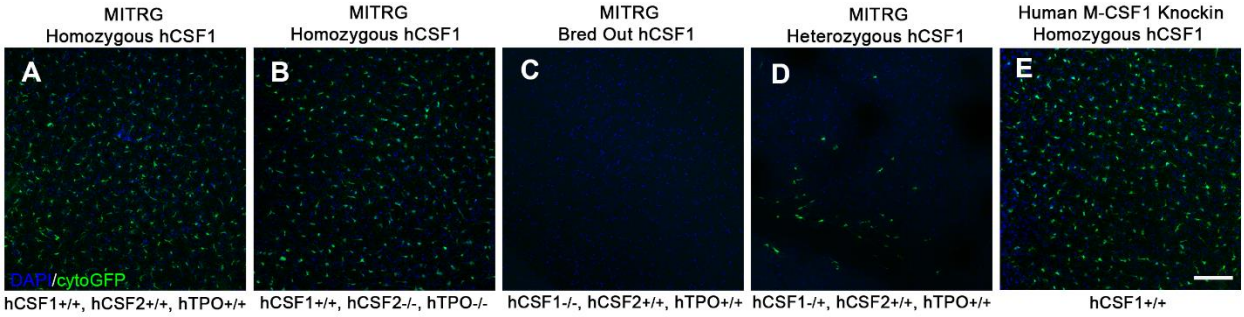

Figure 1.3. Chimeric distribution of human xMG is influenced by age of transplantation and hCSF1 expression level. (A) Human iHPCs transplanted into the MITRG mouse homozygous for all three humanized knockin genes; CSF1, CSF2, and TPO, survive and display robust engraftment (GFP: green; all nuclei, DAPI, blue). (B) Replacement of hCSF2 and hTPO expression with the murine gene, while maintaining hCSF1 expression yields equivalently robust engraftment. (C) In contrast, when hCSF1 is replaced with murine Csf1, no human cells survive. (D) The necessity of hCSF1 appears to be dose-dependent as heterozygous expression of hCSF1 dramatically reduces human microglial engraftment. (E) Human iHPCs transplanted into the parental human M-CSF1 knockin mouse strain ($Rag2^{-}$/IL2Rγ^{-}; JAX Stock No: 017708) which lacks hCSF2 and hTPO expression, display equivalent engraftment to the MITRG model. Scale = 20μm (A-B), 100μm (C-G).

Transplanted iHPCs acquire altered morphologies and phenotypic signatures in a niche-dependent manner

xMG were observed throughout the forebrain and had adopted characteristic, region-specific distributions, morphologies, and marker expression levels. For example, within the cortex and olfactory bulb, xMG created a mosaic network of ramified cells that tiled neatly with neighboring microglia, establishing distinct microdomains (**Figure 1.4A-C**). Within the

hippocampus and overlying corpus collosum, the expected contrasting morphologies were present, with ramified $GFP^+/P2RY12^+$ cells appearing within CA1, and more elongated microglia expressing lower levels of P2RY12 within the overlying white matter of the corpus callosum (**Figure 1.4D**). In addition, relatively few xMG were observed within the granule cell layer (**Figure 1.4E**), a hippocampal subregion that exhibits the lowest number of microglia (De Lucia et al., 2016; Shapiro, Perez, Foresti, Arisi, & Ribak, 2009). Within the striatum (**Figure 1.4F**), xMG engrafted predominantly within the gray matter, avoiding the white matter bundles, again consistent with the typical distribution of microglia within this region (Savchenko, McKanna, Nikonenko, & Skibo, 2000). Interestingly, limited engraftment of $GFP^+/P2RY12^+$ xMG could also be observed far from the transplantation sites, including parts of the cerebellum (**Figure 1.4G**) and the spinal cord, where xMG adopted a more linear, less ramified morphology (**Figure 1.4H**).

In addition to these varying populations of $P2RY12^+$ xMG, we observed subsets of human cells that expressed GFP, yet exhibited a more ameboid morphology (**Figure 1.2D, arrows**). When further examined, these cells were found to lack P2RY12 expression, instead exhibiting morphology, localization, and markers typical of other CNS-myeloid cells (**Figure 1.4I-T**). This finding suggests that transplanted iHPCs maintain the potential to differentiate into the other yolk

Figure 1.4. Transplanted iHPCs adapt to diverse niches within the brain and differentiate into the four CNS macrophage subtypes in a context-dependent manner. (A-H) High power images demonstrate the variety of morphological features xMG display during homeostatic conditions, including neat tiling and complex ramifications in (A) the olfactory bulb (OB) and (B-C) the neocortex (CTX). (D) Within the corpus callosum (CC) overlying the hippocampus (Hip), xMG exhibit a more elongated morphology with a diminished expression of P2YR12. (E-F) Consistent with normal anatomical distributions, xMG also tend to avoid the granule cell layer of the dentate gyrus (GrDG) and the axon-bundles within the striatum (STR). (G-H) Remarkably, xMG also migrate to parts of the cerebellum (CRB) and spinal cord (SC). (I-L) A subset of GFP^+ cells exhibit an amoeboid morphology, linear organization, and lack the homeostatic microglia marker, P2RY12. These cells also encircle $GLUT1^+$ blood vessels, localize to the perivascular space (J, K), and express CD163 (L) suggesting a perivascular macrophage (pvMϕ) phenotype. (M) Another population of $GFP^+/PU.1^+$ cells display robust engraftment in meningeal whole mounts. (N-O) These ameboid shaped meningeal macrophages (mMϕ) and can also be found in sections where parts of the meninges (MN) were preserved and are distinct from the fully ramified $GFP^+/hP2RY12^+$ microglia within the parenchyma (PAR). (P) Similar to the pvMϕ, these mMϕ are also $GFP^+/hP2RY12^-/CD163^+$ (arrows). (Q-T) A few $GFP^+/hP2RY12^-/CD163^+$ choroid plexus macrophage-like (cpMϕ) cells can be found within the choroid plexus (arrows). In some images, brightness and contrast settings were adjusted. Scale = 50μm (A, D-J, N-Q, S, T), 25μm (C, K), 20μm (L), 100μm (B, M, R).

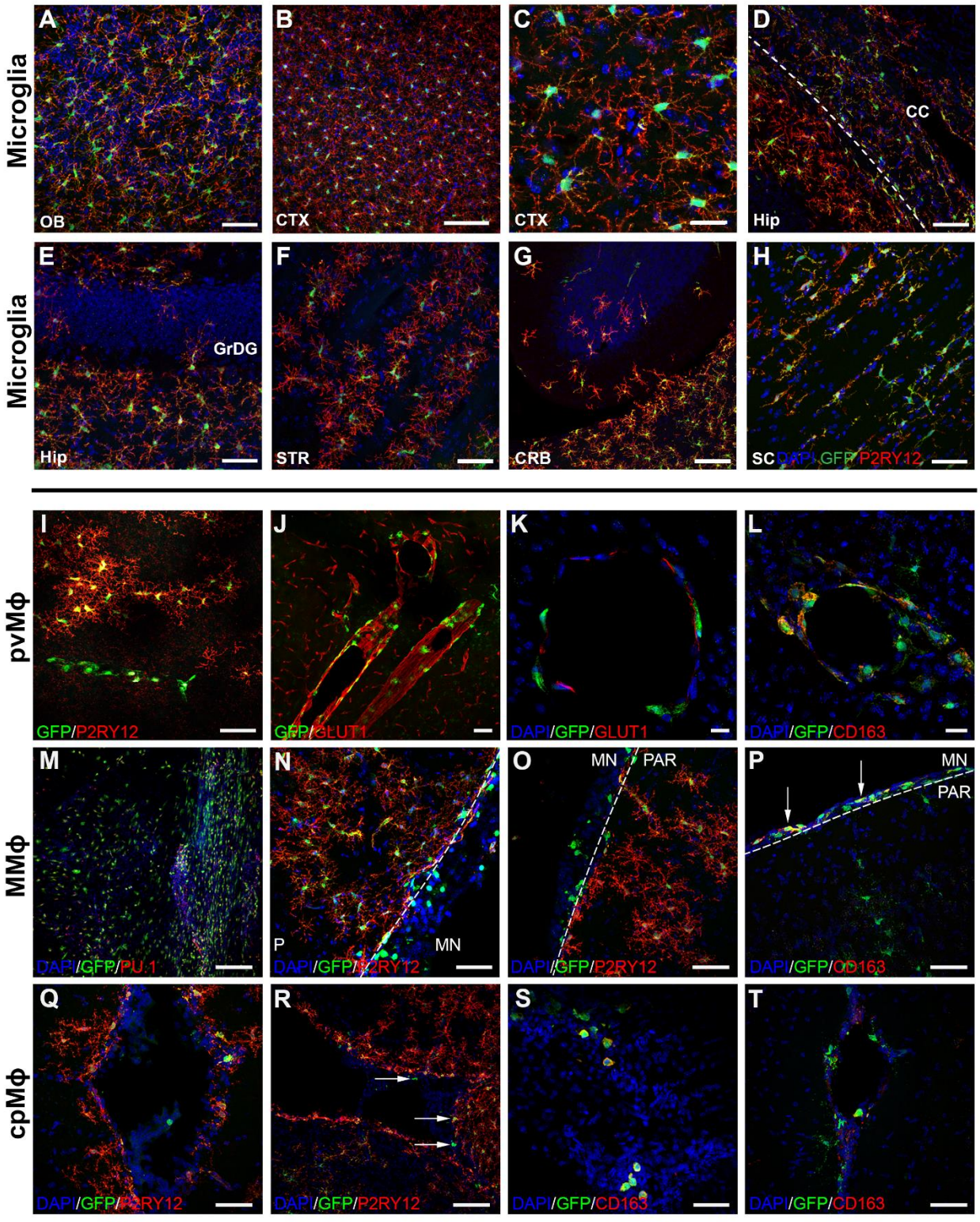
Microglia
A
OB
B
CTX
C
CTX
D
CC
Hip
Microglia
E
GrDG
Hip
F
STR
G
CRB
H
SC DAPI GFP P2RY12
pvMΦ
I
GFP/P2RY12
J
GFP/GLUT1
K
DAPI/GFP/GLUT1
L
DAPI/GFP/CD163
MMΦ
M
DAPI/GFP/PU.1
N
P
MN
DAPI/GFP/P2RY12
O
MN
PAR
DAPI/GFP/P2RY12
P
MN
PAR
DAPI/GFP/CD163
cpMΦ
Q
DAPI/GFP/P2RY12
R
DAPI/GFP/P2RY12
S
DAPI/GFP/CD163
T
DAPI/GFP/CD163

sac-derived CNS-myeloid cell types: perivascular (pvMϕ), meningeal (mMϕ), and choroid plexus (cpMϕ) macrophages. For example, $GFP^+/P2RY12^-$ pvMϕ-like cells were found along the vasculature, in close opposition to GLUT1-expressing murine blood vessel endothelial cells (**Figure 1.4I-K**). These pvMϕ-like cells also exhibited colocalized expression of CD163 (**Figure 1.4L**), an established marker of non-microglial CNS myeloid cells (Goldmann et al., 2016). Whole meningeal mounts (**Figure 1.4M**) confirmed engraftment of more amoeboid $GFP^+/P2RY12^-$ mMϕ-like cells which were also observed in sections where the meninges were preserved during cryosectioning (**Figure 1.4N-O**). As with the pvMϕ-like cells, these meningeal-localized cells also expressed CD163 (**Figure 1.4P**). Additionally, a small population of $GFP^+/P2RY12^-/CD163^+$ cells was found within the choroid plexus (**Figure 1.4Q-T**). The relatively small number of cpMϕ-like cells is consistent with the understanding that cpMϕs are maintained in the adult brain through a partial turnover from definitive bone marrow hematopoietic stem cells, whereas microglia, pvMϕ, and mMϕ continually self-renew (Prinz et al., 2017). Overall, these results suggest that transplantation of iHPCs into the early postnatal brain permits the context-dependent maturation of microglia and other CNS myeloid cells.

xMG acquire a transcriptomic signature that closely resembles *in vivo* human microglia

While IHC analysis revealed that xMG expressed many microglial markers and adopted the morphology of homeostatic microglia, an in-depth transcriptomic analysis of multiple cell lines was needed to test whether xMG fully acquire a microglial fate. Therefore, we developed methods to recover pure populations of xMG, derived from fluorescent or non-fluorescent iPSC lines, from transplanted brains in order to perform RNA-sequencing (**Figure 1.5**). To assess xMG in comparison to endogenous human microglia, transcriptomes were compared between xMG, brain-derived human microglia (ExVivo), cultured human microglia (InVitro), and iMG

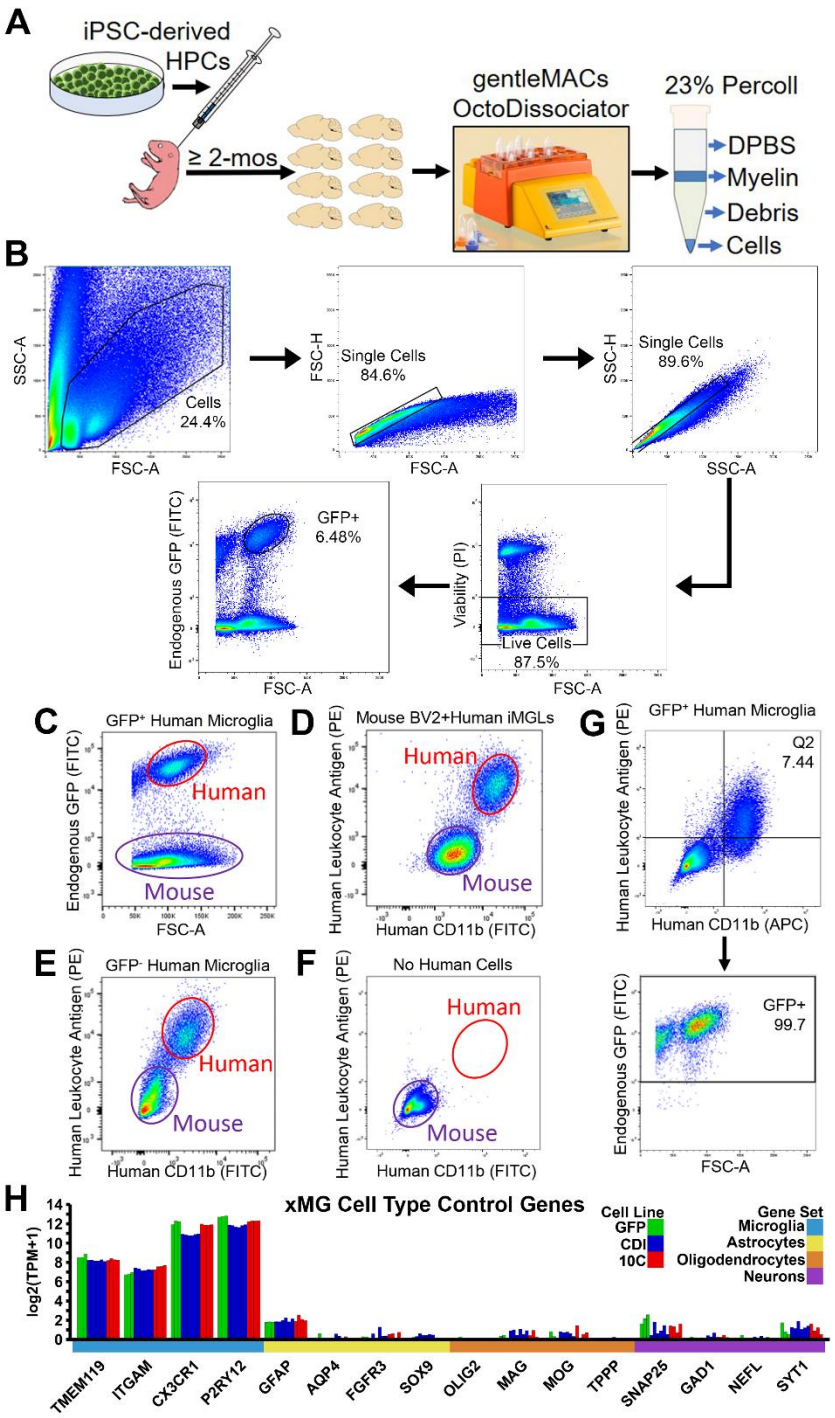

Figure 1.5. Methods of tissue dissociation and validation of the human microglia flow cytometry paradigm. (A) Graphical overview of the transplantation and cell isolation workflow with up to 8 mouse brains being dissociated in parallel via enzymatic digestion on the Miltenyi gentleMACS OctoDissociator. Dissociated tissue is then separated from myelin and debris by centrifuging in 23% Percoll and the cell pellet is processed for flow cytometry. (B) Example gating strategy used during isolation of GFP$^+$ microglia from the mouse brain. Cells were first separated from debris via a liberal P1 gate. Doublets were then selected against in both the forward and side-scatter directions, followed by selection of the PI negative population (live cells), and conservative gating on the larger, brighter GFP$^+$ cells. A similar strategy was employed for isolation of non-GFP expressing human cells with final gating performed using human-specific HLA$^+$ and CD11b$^+$ antibodies. (C) GFP$^+$ human microglia are readily distinguished from mouse cells without additional fluorophores. (D) Initial validation of the HLA/CD11b staining paradigm consisted of identifying GFP negative human iMG mixed in a 9:1 (mouse:human) ratio with mouse BV2 microglia-like cells. (E) Subsequent, *in vivo* staining validation involved isolating transplanted non-GFP expressing human microglia from a dissociated mouse brain. (F) Negative staining control showing that there are no HLA/CD11b double-positive cells in a non-transplanted mouse brain. (G) Final validation of the HLA/CD11b isolation paradigm was performed on brains transplanted with GFP$^+$ human microglia. Applying a conservative gate based on FMO controls to the HLA/CD11b double-positive cells selects for a population that is 99.7% GFP+. (H) RNA-seq data on xMG derived from 3 unique cell lines shows little to no contamination of transcripts that are typically associated with astrocytes (yellow), oligodendrocytes (orange), or neurons (purple), while microglia genes (light blue) are highly expressed, demonstrating successful isolation of a pure microglia population.

differentiated from iPSCs. To further increase the power of these comparisons, a previously published dataset (Gosselin et al., 2017) that included additional ExVivo and InVitro samples was also included (**Figure 1.6**).

To explore the overall similarities and differences between these 49 human microglial samples, the studies were batch corrected (**Figure 1.7A-B**) and principal component analysis (PCA) was performed. This analysis revealed a clear separation of microglia groups based on environment, with a high degree of clustering between the xMG and ExVivo microglia (**Figure 1.6A**). However, as we were primarily interested in determining if transplantation had induced an *in vivo* transcriptomic profile, we used the dataset published by Gosselin et. al. to define a list of 3,432 brain-dependent microglial genes that were differentially expressed between the ExVivo and InVitro samples. PCA analysis with this gene list further enhanced clustering of xMG with ExVivo microglia, whereas iMG and InVitro microglia formed distinct, segregated clusters, demonstrating that *in vivo* differentiation of iHPCs within the murine brain induces a brain-dependent microglia transcriptome (**Figure 1.6B**).

Figure 1.6. Transplantation of human iHPCs into the murine brain recapitulates an *in vivo* human transcriptome. (A) PCA plot, including 16,413 genes, comparing freshly isolated human microglia (ExVivo, green; n=17 patients), xMG (purple; 3 iHPC cell lines, n=3-6 mice per line, 13 mice total), iMG (yellow; n=6 wells), and cultured human microglia (InVitro, orange; n=13 patients) from our lab (MBJ, circles) or the Gosselin samples (triangles). ExVivo microglia and xMG cluster together while both *in vitro* groups (iMG and InVitro) cluster separately. (B) PCA comparing the 3,432 differentially expressed genes between the Gosselin ExVivo and InVitro microglia (FDR=0.05, LFC cutoff=±2). Again, xMG cluster closely with ExVivo microglia, demonstrating that transplantation recovered a brain-dependent microglia signature. (C) Heatmap comparing sample groups from our lab (MBJ, Blue) and Gosselin et al. (Red) based on the top 190 brain-dependent microglia signature genes. Euclidean clustering shows samples cluster by environment (*in vivo* or *in vitro*) and xMG samples are intermixed with ExVivo microglia samples. (D) xMG express transcription factors at levels that are comparable to ExVivo microglia, many of which were either lowly or not expressed *in vitro* (red text). (E) xMG express microglia signature genes and activation markers, including *P2RY12*, *TGFB1*, and *CX3CR1*, at comparable levels to ExVivo microglia, suggesting that xMG have taken on a homeostatic transcriptomic profile. xMG also express the brain-dependent microglial gene *TMEM119*, which was not previously expressed in iMG. (F) xMG express AD risk genes at levels that coincide with non-AD ExVivo microglia. This finding demonstrates that xMG could be accurate surrogates for AD studies in mouse models. Heatmaps in D-F represent VST normalized expression values, averaged for all samples in a group.

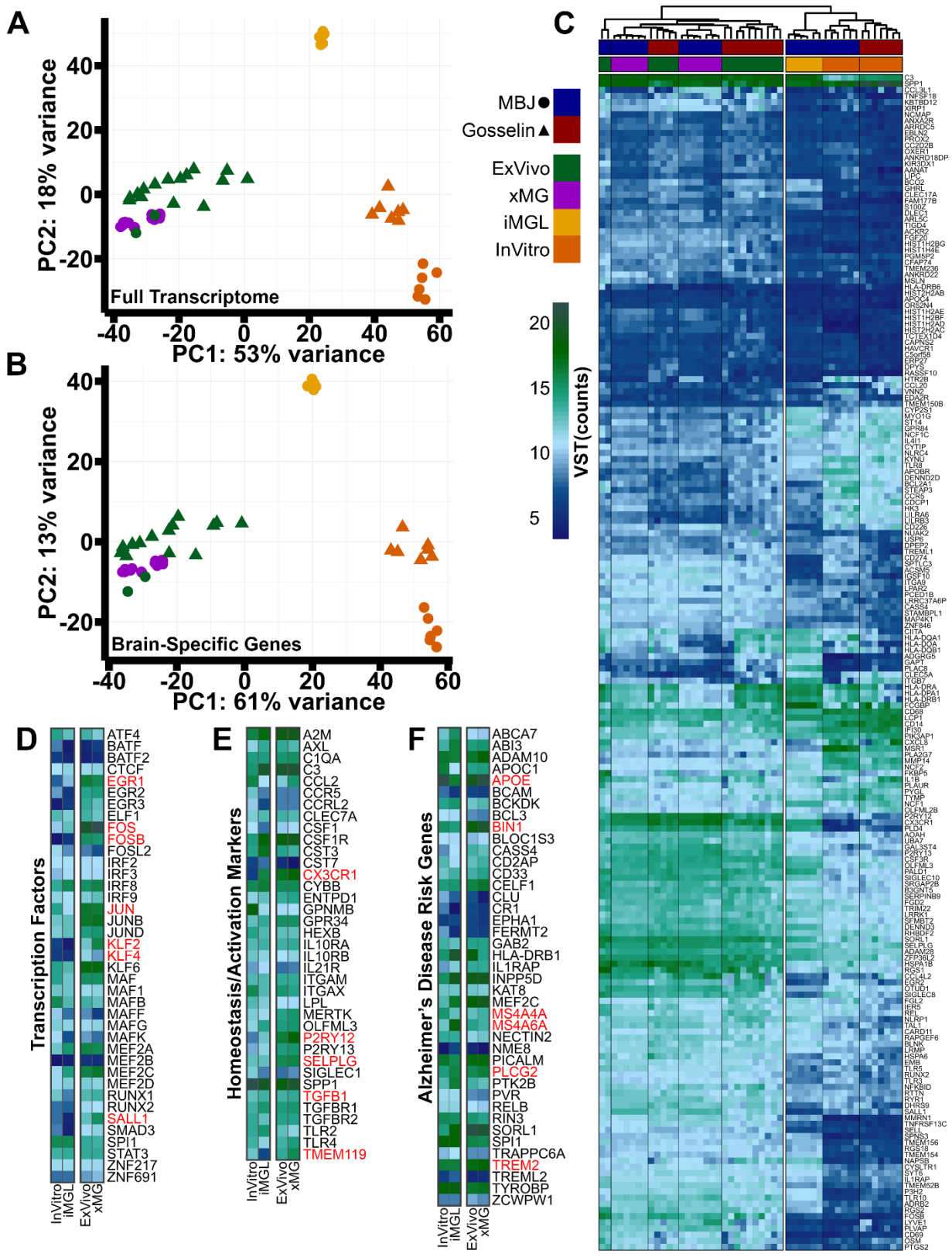
A
PC2: 18% variance
PC1: 53% variance
Full Transcriptome
B
PC2: 13% variance
PC1: 61% variance
Brain-Specific Genes
C
MBJ
Gosselin
ExVivo
xMG
iMGL
InVitro
VST(counts)
D
Transcription Factors
ATF4
BATF
BATF2
CTCF
EGR1
EGR2
EGR3
ELF1
FOS
FOSB
FOSL2
IRF2
IRF3
IRF8
IRF9
JUN
JUNB
JUND
KLF2
KLF4
KLF6
MAF
MAF1
MAFB
MAFF
MAFG
MAFK
MEF2A
MEF2B
MEF2C
MEF2D
RUNX1
RUNX2
SALL1
SMAD3
SPI1
STAT3
ZNF217
ZNF691
E
Homeostasis/Activation Markers
A2M
AXL
C1QA
C3
CCL2
CCR5
CCRL2
CLEC7A
CSF1
CSF1R
CST3
CST7
CX3CR1
CYBB
ENTPD1
GPNMB
GPR34
HEXB
IL10RA
IL10RB
IL21R
ITGAM
ITGAX
LPL
MERTK
OLFML3
P2RY12
P2RY13
SELPLG
SIGLEC1
SPP1
TGFB1
TGFBR1
TGFBR2
TLR2
TLR4
TMEM119
F
Alzheimer's Disease Risk Genes
ABCA7
ABI3
ADAM10
APOC1
APOE
BCAM
BCKDK
BCL3
BIN1
BLOC1S3
CASS4
CD2AP
CD33
CELF1
CLU
CR1
EPHA1
FERMT2
GAB2
HLA-DRB1
IL1RAP
INPP5D
KAT8
MEF2C
MS4A4A
MS4A6A
NECTIN2
NME8
PICALM
PLCG2
PTK2B
PVR
RELB
RIN3
SORL1
SPI1
TRAPPC6A
TREM2
TREML2
TYROBP
ZCWPW1
InVitro
iMGL
ExVivo
xMG

To perform an enhanced, gene-level analysis, the brain-dependent gene list was cross-referenced to the 881-gene microglial signature published by Gosselin et al., resulting in 190 brain-dependent microglial signature genes (**Figure 1.6C**). Euclidean clustering of the samples mirrored the PCA clustering, with iMG and InVitro groups on one branch and the xMG and ExVivo samples intermixed within the other branch (**Figure 1.7C**). However, while the xMG profile was highly similar to the ExVivo signature, differential gene expression (DGE) analysis between xMG and ExVivo samples demonstrated that 97 of the 881 signature genes were differentially expressed (**Figure 1.7D**). Interestingly, Euclidean clustering of all *in vivo* samples using these 97 differentially expressed genes revealed that, while xMG clustered separately from most of the ExVivo samples, three of the youngest ExVivo samples (avg. age 16.5 months) were intermixed with the xMG samples (**Figure 1.7E**). This finding potentially suggests that xMG have yet to fully mature at the examined time points. However, there were also many MHC Class II genes (**Figure 1.7D**) that were expressed at higher levels in the older ExVivo samples, possibly indicating an increased activation state. One explanation could be that xMG were isolated from the healthy mouse brain whereas the ExVivo samples were isolated from patient tissue affected by epilepsy or collected from tumor margins, resulting in an activated state. Longer-term aging studies may provide the evidence needed to understand these small, albeit intriguing, differences.

Further gene-level analysis showed that transplantation into the brain environment induced a number of important microglia gene sets. Key microglia-associated transcription factors, including *EGR1, FOS, FOSB, JUN, KLF2, KLF4, and SALL1* (**Figure 1.6D**), that were either not expressed or lowly expressed *in vitro*, were fully recovered following transplantation. We also focused on a number of microglia genes that have been proposed to be important for homeostasis or activation (Keren-Shaul et al., 2017; Krasemann et al., 2017), as it has been suggested that

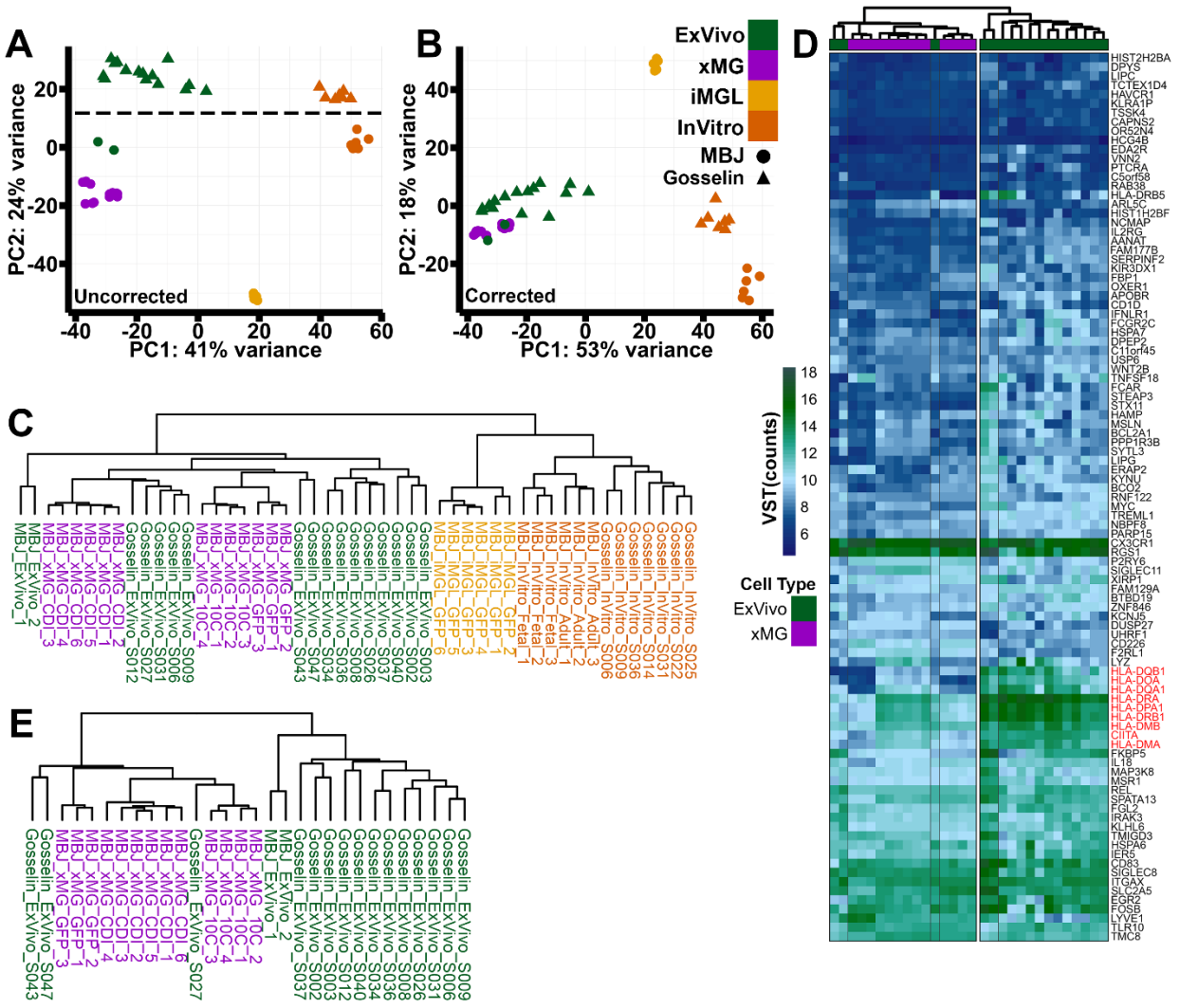

Figure 1.7. xMG cluster closely with brain-derived human microglia. (A) PCA analysis, based on transcriptome genes expressed >10 reads/sample (n=16,413 genes), comparing cultured human microglia (n=13, InVitro, orange), iMG (n=6, yellow), freshly isolated human microglia (n=17, ExVivo, green), and xMG (n=13, purple). While clustering of cell types from our lab (MBJ, circles) and Gosselin et al. (triangles) was similar, a lab-dependent batch effect (dashed line) was clearly observed between samples of equivalent cell types. (B) Applying batch correction to the VST normalized expression values using limma's removeBatchEffect function improves clustering of equivalent cell types, regardless of the lab that performed sequencing. (C) Dendrogram showing the Euclidean clustering (Related to Figure 3C) according to the 190 brain-specific, microglia signature genes resulting from cross referencing the 3,432 brain-specific genes with the 881 gene signature from Gosselin et al. 2017. Note that samples are separated according to environment (*in vivo* vs *in vitro*) and xMG samples are interspersed with ExVivo microglia. (D) Heatmap displaying the 96 genes that are differentially expressed between xMG and ExVivo samples (FDR<0.05; LFC=±2) and also present in the Gosselin 881-gene signature. ExVivo samples collected from the three youngest patients continue to cluster with the xMG. Additionally, a number of MHC class II genes (red text) are upregulated in the ExVivo samples, possibly suggesting an increased activation state. (E) Dendrogram showing the Euclidean clustering of xMG and ExVivo samples for the heatmap presented in D.

microglia derived from transplanted cells can exhibit an 'activated' profile (F. C. Bennett et al., 2018). With regards to homeostatic genes such as *CX3CR1, P2RY12, SELPLG* and *TGFB1*, xMG expression is similar to that of the ExVivo samples, with xMG displaying slightly elevated expression (**Figure 1.6E**). In contrast, xMG do not appear to present with increased expression of genes that have been implicated in microglia activation states including *CLEC7A, ITGAX, IL21R,* or *SIGLEC1*. Additionally, whereas *in vitro* iMG express very low levels of *TMEM119*, transplantation fully recovers expression, consistent with the recent demonstration that *TMEM119* is a brain-dependent microglia gene (M. L. Bennett et al., 2016) (**Figure 1.6E**).

Finally, as we are interested in utilizing this model to study microglia responses to AD pathology, we compiled a list of AD risk genes to ensure that xMG were not aberrantly expressing these transcripts. As with the previous analyses, xMG presented with an expression profile closely mirroring that of the ExVivo samples (**Figure 1.6F**). Notably, genes of current interest in the field such as *APOE, TREM2, BIN1, PLCG2, MS4A4A* and *MS4A6A*, are expressed at ExVivo levels. These findings, in conjunction with the previously presented transcriptomic profiling, not only suggest that xMG have the potential to be utilized in future disease studies but also, considering the human iPSC origin of these cells, offer a level of genetic similarity to human microglia that cannot currently be matched by other approaches.

xMG survey the local environment and rapidly respond to focal brain injury

While validating the morphological, histological, and transcriptomic properties of human microglia within the rodent brain was critical, the utility of this chimeric approach is also dependent on whether xMG can accurately recapitulate microglial function *in vivo*. Therefore, we utilized 2-photon microscopy to visualize the *in vivo* behavior of GFP^+ xMG. Live imaging of xMG revealed an array of neatly tiled, highly ramified human cells that were actively surveying

their immediate environment (**Figure 1.8A)**, as evidenced by constant extension and retraction of processes at rates consistent with endogenous murine microglia (**Figure 1.8B**). Based on previously reported descriptions of endogenous murine microglia behavior (Nimmerjahn et al., 2005), these observations are highly consistent with the activity and morphology of homeostatic microglia.

Since xMG appeared to be actively surveying the brain parenchyma, we next sought to challenge that behavior with a localized, parenchymal injury. Due to the limited availability of *in vivo*, functional microglia data from humans, we concentrated our analysis on focal laser ablation, an approach that has been used to induce a highly reproducible microglial response in mice (Davalos et al., 2005; Nimmerjahn et al., 2005). We again used 2-photon imaging to visualize xMG in the immediate vicinity of the damage site as well as those distally located to the damage site and microglial response was monitored for up to 50 minutes post-injury (**Figure 1.8C-D**). In concordance with previously characterized murine microglial responses, laser damage elicited a rapid and highly localized response in which xMG within 40□m of the damage site immediately responded by sending processes to assess the injury, while distal xMG showed no obvious deviations from homeostatic surveillance activity. Accordingly, quantification of mean GFP intensity within the damage site showed a steady increase for 30 minutes post-injury followed by a sustained intensity for up to 50 minutes of imaging, whereas distal GFP intensity remained consistent across all timepoints (**Figure 1.8D**). Importantly, the extension rate and magnitude of this human microglial injury response is similar to that of murine microglia (**Figure 1.8E**) (Davalos et al., 2005; Nimmerjahn et al., 2005), indicating that xMG respond to local CNS injury in a manner that is consistent with *in vivo* microglia.

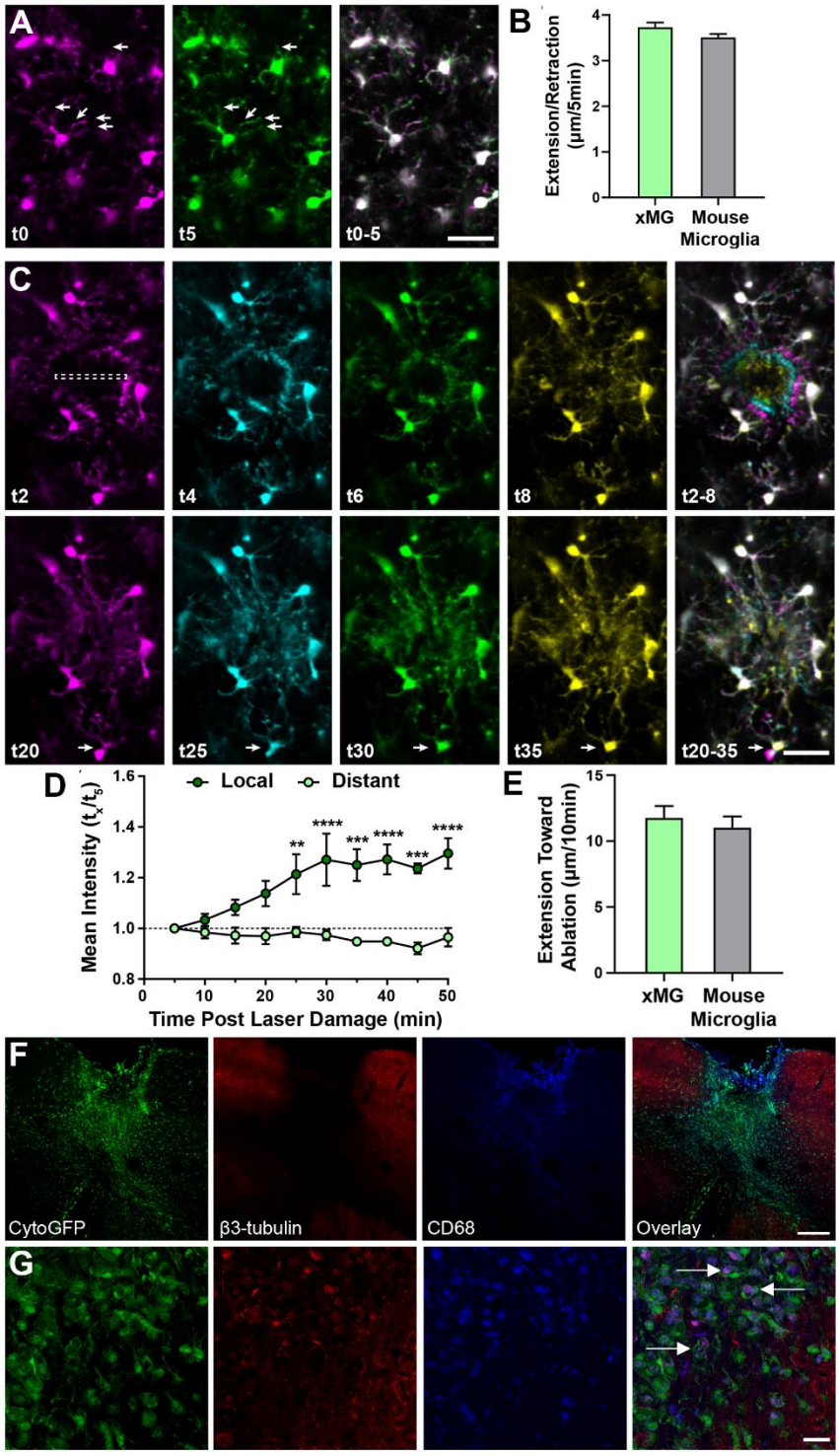

Figure 1.8. xMG survey their surroundings, rapidly respond to laser ablation, and interact with neuronal components after trauma. Human microglia were visualized using multiphoton *in vivo* imaging in (A) homeostasis and (C) following focal, high intensity laser exposure. (A) Time coded colorization of homeostatic xMG demonstrate high process motility, actively surveying their niches. Overlaid color images of t0-5 min. (right) more clearly reveals the morphological dynamics of individual cells. (B) The average length of extension/retraction in 5 minutes found in xMG (3.73±0.10µm, n=300 observations, 3 mice) was not different from those found in mouse microglia (3.51±0.08µm, n=300 observations, 3 mice) (p=0.25, U=42581). (C) Time coded colorization of microglial response to focal damage reveals that processes rapidly move toward and surround the site of injury within 8 minutes post laser ablation. At later timepoints (t25-t35), some microglia outside the direct injury region translocate (white arrow), positioning their cell bodies closer to the injury. (D) The mean intensity at the injury site (local, dark green) is higher than the mean intensity 150um away (distant, light green), showing that xMG processes rapidly localize to the injury site (repeated measures two-way ANOVA, p = 0.006. Scale = 50µm). (E) The average length of extension toward the ablation site in 10 minutes by xMG (11.76±0.90µm, n=22 observations, 3 mice) is similar to those by mouse microglia (11.01±0.87µm, n=37 observations, 3 mice) (p=0.34, U=346). (F-G) Transplanted MITRG mice underwent repeat mild closed head injury (rmCHI) and histological analysis was performed 2-months post-injury. (F) GFP^+ xMG infiltrate the injury site and express increased levels of CD68 (blue). (G) Higher-power images of GFP^+ xMG reveal β3-tubulin (red) and CD68 (blue) colocalized within xMG (white arrows), indicative of microglial phagocytosis of neuronal components. All error bars reflect SEM. Scale = 200µm (F), 20µm (G).

xMG phagocytose neuronal components after brain trauma

In several murine models, repeat mild closed head injury (rmCHI) has been shown to induce sustained microglial activation and interaction with neurons post injury (Gold et al., 2018; Shitaka et al., 2011). Thus, to determine if xMG can interact with murine neuronal components, mice were exposed to rmCHI two months post-transplantation and histological assessment of the injury site was performed 8-weeks later (**Figure 1.8F-G**). Low-power images reveal that GFP^+ xMG infiltrated the injury site (**Figure 1.8F**), while higher-power imaging revealed that lysosomes (CD68; blue) within GFP^+ xMG colocalized with β3-tubulin (red), indicative of phagocytosis of neuronal microtubule components and debris (**Figure 1.8G**; white arrows indicate colocalization of CD68 and β3-tubulin). Thus, xMG can readily interact with and phagocytose degenerating neurons.

xMG respond robustly to a systemic inflammatory challenge

Our next functional assessment focused on characterizing the xMG response to the commonly used peripheral immune challenge lipopolysaccharide (LPS). Mice transplanted with GFP^+ iHPCs were aged 2 months and then administered either saline or LPS via intraperitoneal injection. Quantification of IHC images revealed a significant reduction in the homeostatic marker P2RY12 following LPS treatment and, conversely, a significant upregulation of CD45 (**Figure 1.9A-C**), consistent with an LPS-induced increase in microglial activation state. Interestingly, LPS also induced increased GFP expression, likely because of the activating effect of inflammatory stimuli on CMV-based promoters such as the CAG promoter used to drive GFP expression (**Figure 1.9A-C**) (Varley, Coulthard, Meidell, Gerard, & Munford, 1995).

In addition to the observed morphological and protein-level changes, xMG were isolated from saline and LPS-treated mice in order to examine transcriptomic alterations. DGE analysis

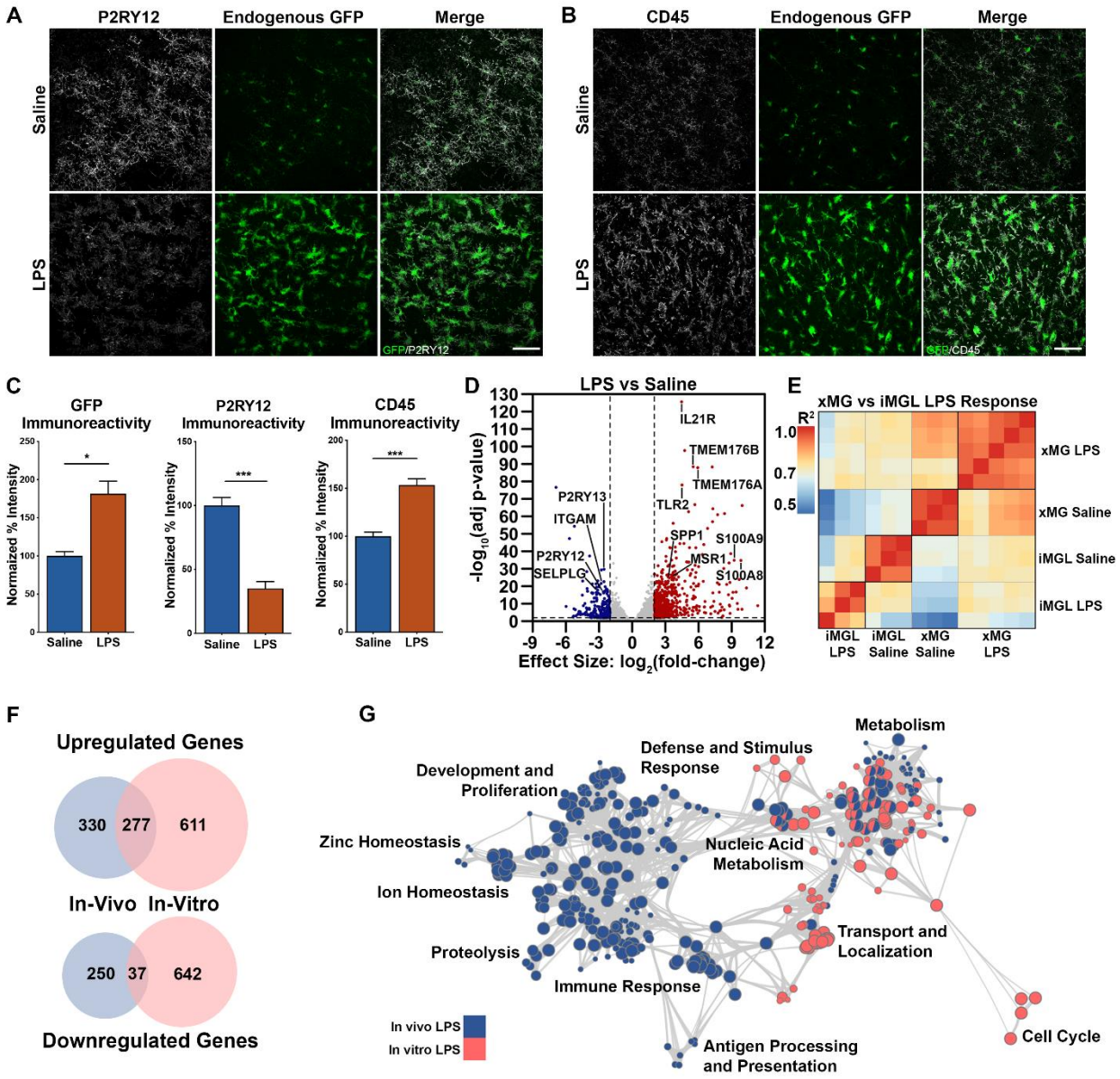

Figure 1.9. Differential responses of xMG and iMG to lipopolysaccharide administration. (A) xMG treated with saline exhibit strong staining for the homeostatic microglial protein P2RY12 (pseudocolored gray) and cytosolic GFP expression (green). In contrast, LPS-treated xMG downregulate P2RY12, whereas GFP intensity increases along with distinct alterations in microglial morphology (Scale=50μm). (B) An upregulation of CD45 immunoreactivity (gray) can been seen after LPS treatment (Scale=50μm). (C) Quantification of GFP reveals a significant increase in intensity with LPS stimulation (p=0.0107) accompanied by a significant decrease in P2RY12 intensity (p=0.0003), and a significant increase in CD45 intensity (p=0.0004). (D) DGE analysis between microglia isolated from saline and LPS-treated animals revealed 607 upregulated genes (red, right) and 287 downregulated genes (blue, left) (FDR=0.01, LFC cutoff=±2). Many upregulated genes (labeled, right) have been implicated in immune activation while a number of downregulated genes (labeled, left) have been described as markers of microglia homeostasis. (E) Pearson correlation matrix comparing the entire transcriptome of each *in vivo* (xMG) saline and LPS treated sample with each *in vitro* (iMG) saline and LPS treated sample. Heatmap colors correspond to R^2 values and samples are clustered via Euclidean distancing. (F) Venn diagram comparing *in vivo* and *in vitro* LPS-induced, differentially expressed genes (FDR=0.01, LFC cutoff=±2), demonstrating few conserved changes. (G) Gene ontology overrepresentation analysis and GO term clustering reveals unique regulation depending on LPS treatment environment, with limited overlap between *in vivo* (blue) and *in vitro* (pink) groups. Bar plots represent mean±SEM.

revealed that LPS treatment resulted in 607 up-regulated and 287 down-regulated genes (**Figure 1.9D**). As anticipated, several of the highly upregulated genes (e.g. *TMEM176A/B*, *IL21R*, *SPP1*, *MSR1*, *TLR2*) are involved in cytokine recognition, phagocytosis, and pathogen responses while many downregulated genes (e.g. *P2RY12*, *P2RY13*, *ITGAM*, *SELPLG*) are typical markers of microglia homeostasis. Further assessment of gene ontology via gene set enrichment analysis (Subramanian et al., 2005) demonstrated a coordinated upregulation of pathways related to immune response, antigen presentation, and translation initiation (**Figure 1.10A-C**). Additionally, examination of the differentially expressed xMG signature genes from **Figure 1.7D** showed that many genes were normalized toward ExVivo levels following LPS treatment, including some of the previously noted MHC Class II genes (**Figure 1.10D, red text**). This finding lends some preliminary support to our aforementioned hypothesis that, rather than being immature, xMG transplanted into the healthy mouse brain may present with a less activated profile than microglia isolated from disease-affected human tissues.

The human microglia response to systemic inflammation is not accurately modeled by LPS *in vitro*

Many studies regarding microglia responses to LPS have been performed *in vitro*, by treating murine or human microglia directly with LPS (Abud et al., 2017; Pulido-Salgado, Vidal-Taboada, Barriga, Sola, & Saura, 2018). We therefore decided to recapitulate this approach by treating iMG made from the same GFP^+ cell line as the LPS-exposed xMG, with LPS *in vitro*. RNA-seq and DGE analysis revealed 888 up-regulated genes and 679 down-regulated genes following *in vitro* LPS treatment. Compared to the *in vivo* results of 607 up-regulated and 287 down-regulated genes, it was immediately clear that the response to LPS in a dish was more dramatic than the response *in vivo*. Correlation analysis between saline and LPS samples

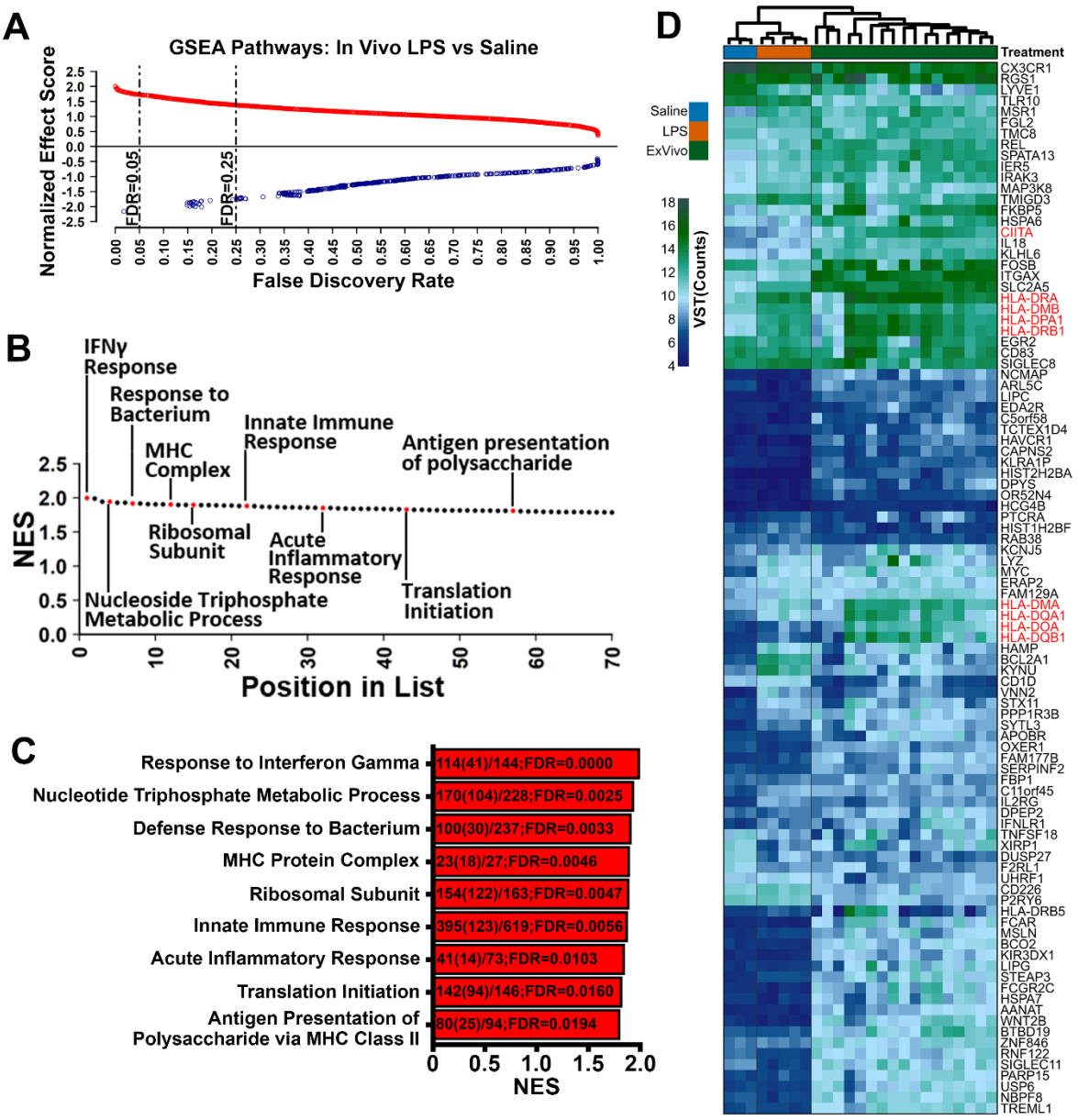

Figure 1.10. LPS treatment upregulates numerous inflammatory pathways and induces a transcriptomic profile resembling disease-affected microglia. (A) All gene ontology pathways identified by gene set enrichment analysis (GSEA) as upregulated (red, open circles) or downregulated (blue, open circles) following *in vivo* peripheral LPS treatment. False discovery rate (FDR) cutoffs of 0.25 (for hypothesis generation) and 0.05 (for validation) were applied. 23 downregulated pathways were significant at an FDR or 0.25 and only 1 was significant at the 0.05 cutoff. In contrast, 869 upregulated pathways were significant at an FDR≤0.25 and 112 were significant at an FDR≤0.05. (B) The top 70 GSEA pathways ordered by normalized expression score (NES) score and position in the list (ordered by NES). The pathways listed in C are identified by red dots and labels showing where each falls in the list. (C) A representative selection of pathways identified by GSEA. Identified pathways were highly related to metabolic processes, immune responses to bacteria, antigen presentation, and ribosomal/translational processes. The numbers shown within the bar graph indicate: # of genes mapped (# genes contributing to the enrichment score)/Total genes in the pathway; FDR. (D) Heatmap of the 96 microglia signature genes that were shown to be differentially expressed in xMG. While LPS treatment did not fully recover these genes, a partial recovery of many genes related to immune activation, including many of the MHC Class II genes that were previously shown to be deficient in xMG (red text), was observed following inflammatory insult. This finding may suggest that ExVivo human samples isolated from patients affected by epilepsy or collected from tumor margins may exhibit a partially activated state.

from both environments demonstrated limited correlation between *in vitro* and *in vivo* groups, with the least correlated groups being *in vivo* LPS and *in vitro* LPS (**Figure 1.9E**). Unsurprisingly, the lack of correlation further manifested as a limited overlap between the DGE lists, with the LPS groups only sharing 22.7% of the up-regulated genes and an abysmal 4% of down-regulated genes (**Figure 1.9F**). To determine if these gene-level differences also manifested at the pathway level, we performed gene ontology (GO) analysis, which similarly revealed very little overlap between the two environments (**Figure 1.9G**).

Transitions in the expression profile of xMG are orchestrated by well-established microglial transcriptional regulators

An overarching goal of our approach was to develop a predictive experimental model that could be used to study human microglia *in vivo.* Therefore, we next sought to perform an unbiased analysis of the two environmental transitions that we had exposed human microglia to: one from *in vitro* to *in vivo* and another from *in vivo* to peripheral stimulation with LPS. We began by performing DGE analysis, to assess how these transitions altered the transcriptional state of xMG, and then utilized k-means clustering (Lloyd, 1982) to identify 8 clusters of genes with expression profiles that were unique to each of the states (**Figure 1.11A**). Exemplifying the powerful predictive potential of this approach, a subsequent literature-based search of all differentially expressed genes revealed that a large majority of these genes are highly relevant to microglial biology (**Figure 1.11A**). Likewise, many of these genes have been implicated in AD (S. Hickman, Izzy, Sen, Morsett, & El Khoury, 2018). Next, we performed GO analysis to determine which gene classes changed in response to each transition (**Figure 1.11B**). Comparison of GO terms revealed that when xMG undergo transplantation, genes related to synapse assembly,

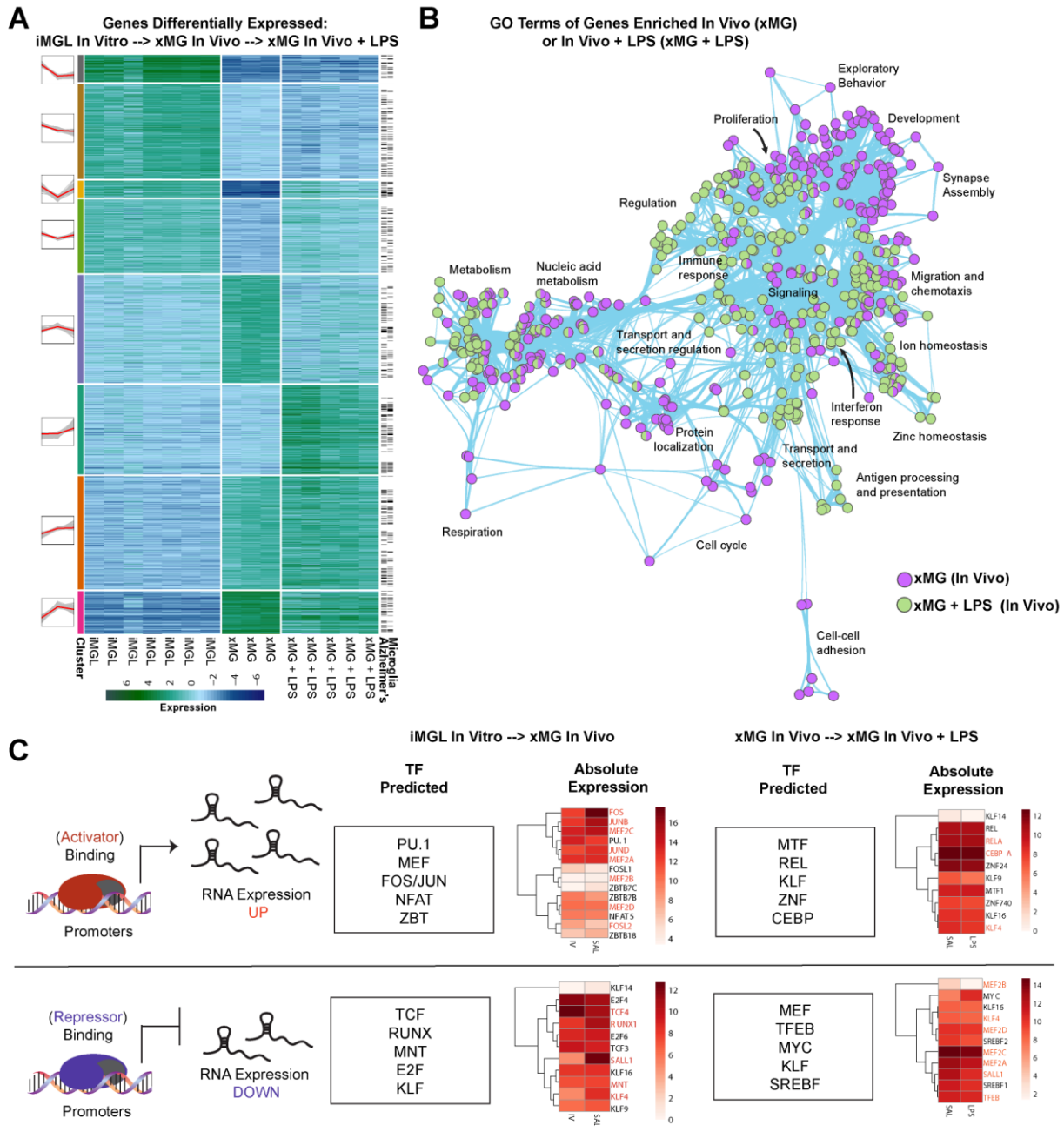

Figure 1.11: xMG gene expression profiles are indicative of known microglial activation signatures. (A) Heatmap of differentially expressed genes from the same GFP iPSC line differentiated into microglia *in vitro* versus GFP-xMG *in vivo*, versus *in vivo* GFP-xMG activated with LPS. Black lines on the right indicate genes that have previously been implicated in Alzheimer's Disease and/or microglial biology. (B) Network graph of enriched GO terms generated from (A), when comparing up-regulated genes from *in vitro*, to *in vivo*, to *in vivo* with LPS stimulation. Nodes represent individual GO terms (gene sets), and edges represent the relatedness between them. (C) Summary of predicted transcription factors and their association with genes up- or down-regulated between states. Heatmaps represent their expression levels at each state.

exploratory behavior, and cell-cell adhesion are strongly induced, all of which would be predicted to increase following xMG integration into the brain. In contrast, GO terms associated with genes that were upregulated following peripheral LPS stimulus were instead consistent with immune activation, interferon response, antigen presentation, and a hallmark of *in vivo* microglia activation: zinc homeostasis (Kauppinen et al., 2008).

To further test if the observed expression signatures were influenced by known microglial gene regulatory factors, we performed an unbiased search to identify transcription factor (TF) motifs enriched within the promoter regions of all genes that exhibited differential expression with each transition state (**Figure 1.11C**). Using this approach, we were able to identify several TF motifs that were highly enriched during the *in vitro* to *in vivo* transition and known to be critical regulators of microglial homeostatic function (e.g. *RUNX2*, *MEF*, *JUN*, *FOS*, *KLF*). Similar analysis on the xMG+LPS samples identified unique TF motifs that have been implicated in the transformation of microglia to an activated state (e.g. *IRF8, STAT3, RelA, CEBPA, MTF-1*).

xMG adjacent to beta-amyloid plaques exhibit a Disease Associated Microglia (DAM)-like phenotype

Since we confirmed that xMG were capable of appropriately responding to both exogenous and endogenous inflammatory insults, we next sought to determine if xMG could be utilized in a disease modeling application. As it was recently reported that murine microglia transition into distinct and highly specialized subpopulations upon chronic exposure to pathological beta-amyloid (Aβ) in AD mouse models (Keren-Shaul et al., 2017; Krasemann et al., 2017), we sought to verify whether a similar phenotype may occur in xMG. We, therefore, transplanted GFP^+ iHPCs into the newly developed 5X-MITRG mouse model and allowed the

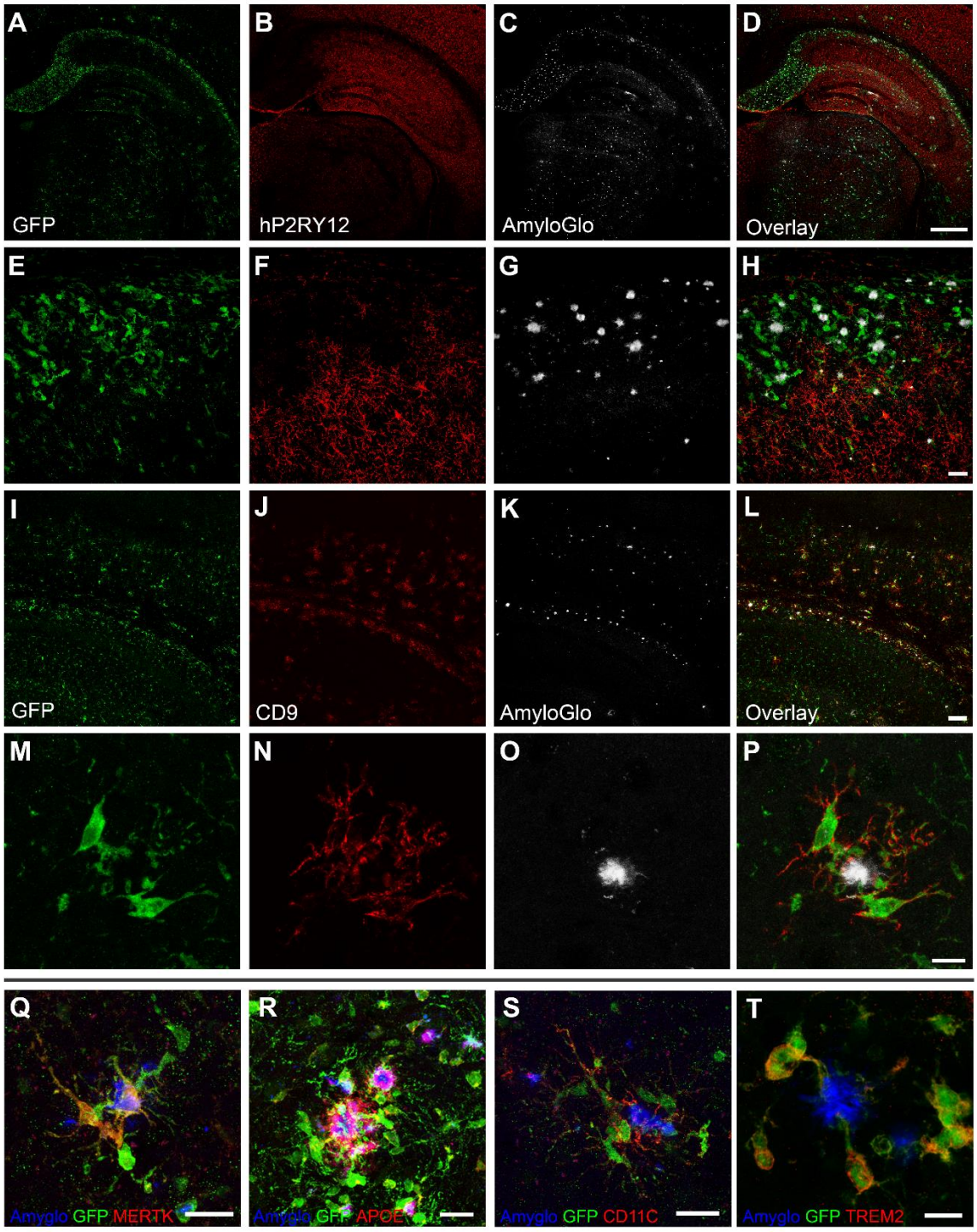

Figure 1.12. xMG down-regulate homeostatic markers and upregulate activation markers around Aβ plaques. Representative images of xMG in the hippocampus and subiculum of the 5X-MITRG at 9-months. (A-H) The homeostatic marker P2RY12 is downregulated in plaque-associated xMG while more distal xMG continue to express P2RY12. (cytosolic GFP, green; P2RY12, pseudocolored red; fibrillar amyloid (AmyloGlo), gray). (I-P) Plaque-associated xMG also display and increase in the DAM gene CD9, while distal cells do not (cytosolic GFP, green; CD9, red; fibrillar amyloid (AmyloGlo), gray). (Q-T) Additionally, plaque-associated xMG upregulate other DAM markers, including MERTK (Q), human APOE (R), CD11C (S), and TREM2 (T). scale=500um (A-D), 100um (E-L), 20um (M-S), 10um (T).

mice to age for 9 months. Subsequent histological analysis revealed a clear and marked difference in the expression of numerous DAM markers in xMG near Aβ plaques (**Figure 1.12**). Similar to mouse DAMs and neurodegeneration-associated microglia (MGnD), xMG in contact with plaques downregulated the homeostatic marker P2RY12 (**Figure 1.12A-H**) and adopted an activated, ameboid morphology. Additionally, plaque-associated xMG upregulated the DAM markers CD9 (**Figure 1.12I-P**), MERTK (**Figure 1.12Q**), APOE (**Figure 1.12R**), CD11C (**Figure 1.12S**), and TREM2 (**Figure 1.12T**).

Single-cell RNA-seq reveals transcriptomic alterations in response to AD pathology that are unique to human xMG

While our histological analyses appeared promising, we sought to further characterize the xMG response to amyloid pathology at the transcriptomic level by isolating xMG from the brains of aged MITRG (n=2) and 5X-MITRG (n=4) mice. Single-cell RNA sequencing (scRNA-seq) resulted in 10,184 MITRG and 8,673 5X-MITRG cells and average gene counts of 1,583 and 1,593 per cell, respectively. tSNE clustering of xMG from both MITRG and 5X-MITRG mice (**Figure 1.13A-B**), from male and female mice (**Figure 1.14A-B**), showed similar groups of MHC Class II cells (Orange; *HLA-DRB1*, *HLA-DPB1*, *HLA-DQA1*, and *CD74*), cells responding to Type I Interferon *(*Blue; *IFI6*, *IRF7*, *ISG15*, *STAT1*, and *IFIT3*), a group resembling murine DAMs (Salmon; *CD9*, *TREM2*, *LPL*, and *ITGAX*), as well as a cluster that was defined by a lack of the other cluster markers, which we deemed homeostatic (Green). Additionally, the MITRG xMG displayed a cluster defined by high levels of inflammatory cytokines (Purple; *CCL2*, *CXCL10*, *CCL8*, and *CXCL11*) while the 5X-MITRG xMG did not have a clearly defined chemokine cluster but, instead, displayed a cluster of cells defined by genes related to secretory function. Interestingly, canonical microglia markers (*P2RY12*, *P2RY13*, *CX3CR1*, and *TMEM119*) showed

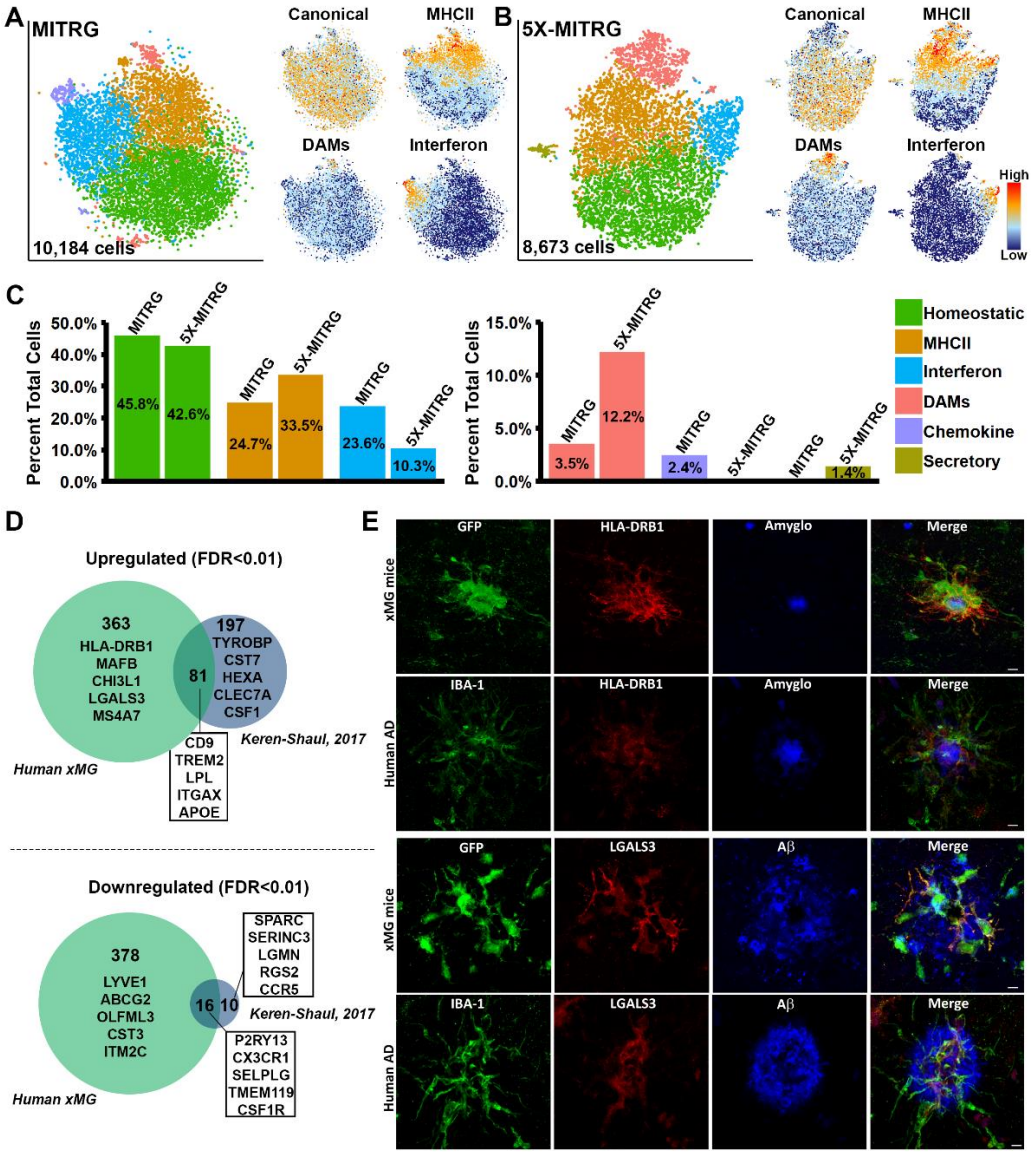

Figure 1.13. Single-cell sequencing of xMG from MITRG and MITRG-5X mice reveals altered population distributions and human-specific genetic responses. (A) tSNE plot of 10,184 xMG isolated from 10.5-month-old MITRG mice (n=2) reveals multiple clusters defined by genes related to MHC class II (Orange; *HLA-DRB1*, *HLA-DPB1*, *HLA-DQA1*, and *CD74*), Type I Interferon (Blue; *IFI6*, *IRF7*, *ISG15*, *STAT1*, and *IFIT3*), DAMs (Salmon; *CD9*, *TREM2*, *LPL*, and *ITGAX*), Inflammatory cytokines (Purple; *CCL2*, *CXCL10*, *CCL8*, and *CXCL11*), and a "homeostatic" cluster (Green) that was mainly defined by a lack of activation markers. Additionally, canonical microglia markers (*P2RY12*, *P2RY13*, *CX3CR1*, and *TMEM119*) showed a uniform distribution across all clusters besides DAMs. (B) tSNE plot of 8,673 xMG isolated from 10.5 and 12-month-old 5X-MITRG mice (n=4) reveals similar clusters to the MITRG xMG. Exceptions include the addition of a secretory cluster (Olive; *ANAX3*, *AGR2*, *PLAC8*, and *PLA2G7*) the loss of a clearly defined chemokine cluster. (C) Bar plot comparing the percentage of total cells making up each cluster in WT MITRG and 5X-MITRG tSNE plots. (D) DAM genes, reported by Keren-Shaul et al. (2017), from 5XfAD murine microglia were filtered to contain only genes defined by Ensembl or NCBI Homologene to have 1:1 human orthologs. Remaining genes were then compared to the differentially expressed genes between DAM and homeostatic xMG (FDR≤0.01) demonstrating that limited overlap exists between the human xMG and mouse DAM genes. (E) Protein-level validation of human-specific DAM genes *HLA-DRB1* (top) and *LGALS3* (bottom) in both 5X-MITRG and human AD brain sections.

a relatively even distribution across most clusters, but decreased expression within the DAM clusters (**Figure 1.13A-B**; **Figure 1.14C-D**; **Supplemental Table 1**). Additionally, despite general similarities between the clusters present in the MITRG and 5X-MITRG xMG, differences existed in the proportion of microglia within each cluster (**Figure 1.13C**), with the DAM and MHCII clusters being larger in the 5X-MITRG and the Interferon cluster being reduced.

We next sought to further examine the expression levels of AD risk genes within the 5X-MITRG xMG. Analysis of the expression levels of 50 AD risk genes revealed that 39 of these genes were expressed in at least one cluster and many were differentially expressed in specific clusters (FDR≤0.01; **Figure 1.14E**). Furthermore, analysis of the amino acid sequences of these genes demonstrated that a number of AD risk genes display low amino acid homology when compared to their human counterparts and/or ambiguous gene homologs, and with *CD33* lacking any reliable homolog in the mouse (**Figure 1.14E**).

This observation led us to investigate whether the xMG approach was capable of revealing novel human-specific aspects of the microglia response to Aβ. To do so, we performed DGE analysis between the DAM and homeostatic clusters in the 5X-MITRG and compared these genes to the DAM genes published by Keren-Shaul et al. (2017), as this was the most directly comparable

Figure 1.14. Analysis of scRNA-seq by individual sex or genes reveals additional aspects of xMG transcriptomics. (A) Merged scRNA-seq libraries from male (n=1) and female (n=1) MITRG mice demonstrates that male and female cells are evenly distributed across clusters. (B) Merged scRNA-seq libraries from male (n=2) and female (n=2) 5X-MITRG mice demonstrates that male and female cells are evenly distributed across clusters. (C) Individual heatmaps of genes comprising the aggregated heatmap signatures from Figure 1.13A. (D) Individual heatmaps of genes comprising the aggregated heatmap signatures from Figure 1.13B. (E) AD risk genes that are expressed at a minimum of 5% of cells in one cluster in the 5X-MITRG xMG. The large boxes denote the percent homology between the amino acid sequences while the text within the large box denotes the human to mouse gene homology ratio (M=many genes). Gray boxes denote homology of less than 50%. Small boxes display which clusters expressed a given risk gene and the text denotes what percentage of cells in the cluster express the gene. Additionally, up and down arrows indicate that the gene was significantly up or downregulated, respectively, in a given cluster when compared to all other cells. (F) An aggregated list of unique genes, comprised of microglia AD response genes from four studies (Kamphuis et al., 2016; Keren-Shaul et al., 2017; Krasemann et al., 2017; Yin et al., 2017), was filtered to contain only genes defined by Ensembl or NCBI Homologene to have 1:1 human orthologs. Remaining genes were then compared to the differentially expressed genes between DAM and homeostatic xMG (FDR≤0.01) demonstrating that limited overlap exists between the transcriptomic response of human xMG and mouse microglia to amyloid pathology.

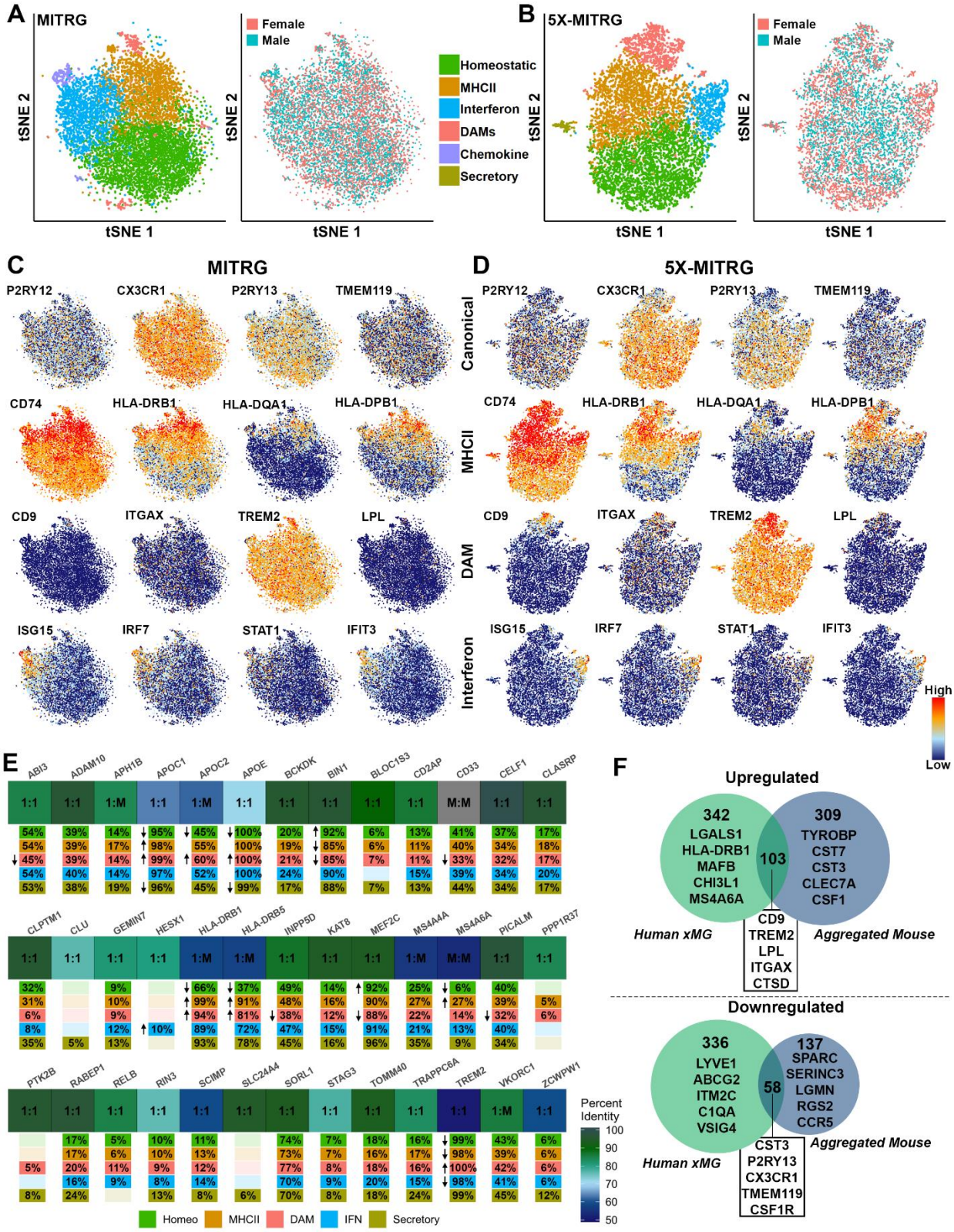
A
MITRG
tSNE 2
tSNE 1
Female
Male
Homeostatic
MHCII
Interferon
DAMs
Chemokine
Secretory
B
5X-MITRG
C
MITRG
D
5X-MITRG
Canonical
MHCII
DAM
Interferon
P2RY12
CX3CR1
P2RY13
TMEM119
CD74
HLA-DRB1
HLA-DQA1
HLA-DPB1
CD9
ITGAX
TREM2
LPL
ISG15
IRF7
STAT1
IFIT3
High
Low
E
ABI3
ADAM10
APH1B
APOC1
APOC2
APOE
BCKDK
BIN1
BLOC1S3
CD2AP
CD33
CELF1
CLASRP
CLPTM1
CLU
GEMIN7
HESX1
HLA-DRB1
HLA-DRB5
INPP5D
KAT8
MEF2C
MS4A4A
MS4A6A
PICALM
PPP1R37
PTK2B
RABEP1
RELB
RIN3
SCIMP
SLC24A4
SORL1
STAG3
TOMM40
TRAPPC6A
TREM2
VKORC1
ZCWPW1
Percent Identity
100
90
80
70
60
50
Homeo
MHCII
DAM
IFN
Secretory
F
Upregulated
342
LGALS1
HLA-DRB1
MAFB
CHI3L1
MS4A6A
103
309
TYROBP
CST7
CST3
CLEC7A
CSF1
Human xMG
Aggregated Mouse
CD9
TREM2
LPL
ITGAX
CTSD
Downregulated
336
LYVE1
ABCG2
ITM2C
C1QA
VSIG4
58
137
SPARC
SERINC3
LGMN
RGS2
CCR5
Human xMG
Aggregated Mouse
CST3
P2RY13
CX3CR1
TMEM119
CSF1R

study published to date. This comparison revealed a substantial number of both up (363 genes) and down (378 genes) regulated genes that were unique to human xMG (**Figure 1.13D**). However, it is important to note that while the study published by Keren-Shaul et al. (2017) is the only currently published study examining the 5XfAD murine microglia response to Aβ pathology at the single-cell level, other studies have attempted to elucidate a similar phenotype via bulk sequencing, microarray, and qPCR in APP/PS1 and 5XfAD mice (Kamphuis et al., 2016; Krasemann et al., 2017; Yin et al., 2017). Therefore, we also performed a comparison of our xMG
DAM genes to an aggregated gene list composed of all the unique genes specified in these studies plus the Keren-Shaul study (**Figure 1.14F**). While this comparison yielded slightly altered genes lists, there was still a high degree of discordance between the datasets, with 342 upregulated and 336 downregulated genes uniquely attributed to human xMG.

In order to confirm that these differences were indeed relevant to the human microglial response to Aβ, we selected two genes, *HLA-DRB1* and *LGALS3* (galectin 3), which have both been implicated in AD (Allen et al., 2015; Boza-Serrano et al., 2019), for histological validation at the protein level in both xenotransplanted mice and AD-patient tissue. As shown in **Figure 1.13E**, both proteins are highly expressed in xMG adjacent to murine Aβ plaques and this expression pattern bears a striking resemblance to the plaque-associated microglial labeling in AD-patient tissue. While an in-depth validation of all the unique xMG genes discovered in this analysis goes beyond the scope of the current article, this model clearly provides ample opportunity to investigate novel aspects of the *in vivo* microglial response to amyloid pathology. We, therefore, propose that xMG are not just capable of recapitulating general *in vivo* microglia behavior, but that utilizing xMG in conjunction with disease models provides a method of uncovering new genetic insights into human neurological disease.

DISCUSSION

Over the last decade, the field has increasingly recognized the importance of microglia in both homeostatic brain function and neurological disease. As our understanding has grown, so too has the need to develop more predictive models of human microglia to study these highly adaptable cells. Traditionally, this has meant collecting and culturing microglia from postmortem or surgically resected tissue or trusting that rodent microglia faithfully recapitulate human microglial phenotypes. While these approaches continue to be fundamental to our understanding of microglial biology, recent advancements have led to a more widely applicable toolkit. With the development of the first protocols to generate microglia from patient-derived stem cells *in vitro*, researchers are now able to model and manipulate the complex, polygenic landscapes that potentially underlie human microglia function and dysfunction. However, the field has also recently recognized that, despite these exciting new capabilities, the plasticity that makes microglia so fascinating represents a double-edged sword that complicates our attempts at *in vitro* modeling.

To address this challenge, we turned to transplantation of human iPSC-derived HPCs into the humanized, immune-deficient mouse brain. This paradigm induces robust microglial engraftment and differentiation of the complete complement of CNS macrophage subtypes. Additionally, microglia arising from this approach recapitulate the complex expression profile that is characteristic of their endogenous human counterparts, dynamically react to local and peripheral insults, and robustly respond to Aβ pathology on both the morphological and transcriptomic levels. Taken together, these results support the conclusion that xMG serve as suitable surrogates for endogenous human microglia, enabling new and informative *in vivo* studies of this important cell type.

Despite the many potential advantages of this chimeric model, it is important to note that xMG expectedly come with caveats of their own, the most prominent being the requirement of an immune-deficient recipient organism. With recent studies demonstrating the interactive relationship between microglia and peripheral immune cells, especially in the context of neurodegeneration (Marsh et al., 2016), this deficiency is important to acknowledge. While this problem is by no means unique to this model, as *in vitro* models inevitably suffer from the same pitfall, determining the most effective method of rectifying this shortcoming will require many additional studies.

Our hope is that the assessments herein provide sufficient demonstrations of the utility of this model that will encourage further studies examining the complex *in vivo* interactions between human microglia and neurological disease. The experiments utilizing the 5X-MITRG model and subsequent single-cell analysis have already revealed a substantial genetic response to Aβ plaques that appears to be unique to human microglia. Moving forward, it is our hope that leveraging CRISPR technology and the growing availability of patient iPSC lines will allow this approach to be broadly used to examine the impact of mutations, genetic diversity, and polygenic risk on human microglial function, thereby improving our understanding of these complex and fascinating cells.

CHAPTER 2

THE ALZHEIMER'S DISEASE-ASSOCIATED *TREM2* R47H GENETIC POLYMORPHISM DRIVES TRANSCRIPTOMIC AND FUNCTIONAL ALTERATIONS IN XENOTRANSPLANTED MICROGLIA

INTRODUCTION

In 2013, two independent studies identified the R47H mutation in exon 2 of the *TREM2* gene as a significant risk factor for AD, conferring approximately the same amount of risk as a single copy of an APOE ε4 allele (Guerreiro, Wojtas, et al., 2013; Jonsson et al., 2013). Since this initial discovery, the role of *TREM2* has been investigated in a multitude of AD studies utilizing mouse models (Jay et al., 2015; Keren-Shaul et al., 2017; Krasemann et al., 2017; Song et al., 2018; Xiang et al., 2018). These studies have revealed significant deficiencies in microglia ability to sense lipids and migrate to amyloid plaques and have demonstrated that TREM2 is a critical switch in activating microglia, causing TREM2-deficient microglia to become "locked" in a homeostatic state (Keren-Shaul et al., 2017; Krasemann et al., 2017; Mazaheri et al., 2017; Yuan et al., 2016b).

However, it has also been reported that the murine TREM2 receptor does not function identically to the human TREM2 receptor (Xiang et al., 2018), as only 69% of the protein sequence is homologous between the species, suggesting that the role of this gene in microglia function is best studied in human form. Indeed, studies have been performed which have generated mouse models containing humanized *TREM2* (Song et al., 2018; Xiang et al., 2018), although this approach requires the development of a new transgenic mouse model in order to examine any additional biological variation and does not allow for the direct study of the human microglia response to AD pathology. As these considerations present substantial drawbacks to the humanized

mouse approach, leveraging the versatility of human iPSC-derived microglia offers a more adaptable and efficient method for studying the effects of this mutation.

Therefore, this project was aimed at examining the role of human *TREM2* on the response of human microglia to amyloid pathology. In collaboration with Dr. Christel Claes, Amanda McQuade, and Jean-Paul Chadarevian in the Blurton-Jones lab, isogenic iPSC lines possessing either the *TREM2* WT or R47H variants were established and these cells were differentiated into iHPCs and transplanted into either 5X-MITRG or 5X-hCSF1 mice. Histological and single-cell transcriptomic analyses revealed that *TREM2* R47H xMG display certain characteristics that mimic *TREM2* knockout (KO) and murine studies, such as a reduction in Aβ-plaque interactions and a reduction in the DAM population. However, *TREM2* R47H xMG also displayed unique cell population distributions when compared to *TREM2* WT or KO xMG, with an interferon response cluster being substantially affected by the mutation while the DAM cluster was reduced to a lesser degree. Overall, these data suggest that while murine and KO studies have clarified aspects of *TREM2*'s role in amyloid responsive microglia, there are still unexplored lines of questioning as to the role of the role of the R47H mutation in human microglia.

MATERIALS AND METHODS

Animals

All animal procedures were conducted in accordance with the guidelines set forth by the National Institutes of Health and the University of California, Irvine Institutional Animal Care and Use Committee. The M-CSFh mouse line (hCSF1) was purchased form Jackson Laboratories (stock # 017708) and includes deletion of Rag2 and Il2rg and humanized M-CSFh (Rathinam et al., 2011), which are necessary for human microglial engraftment. The MITRG mouse was purchased from Jackson Laboratories (stock #017711); this BALB/c/129 model includes two

knockouts alleles, Rag2^{-} (Rag2$^{tm1.1Flv}$), γc^{-} (Il2rg$^{tm1.1Flv}$), and three humanized knock-in alleles, M-CSFh (Csf1$^{tm1(CSF1)Flv}$), IL-3/GM-CSFh (Csf2/Il3$^{tm1.1(CSF2,IL3)Flv}$), TPOh (Thpo$^{tm1.1(TPO)Flv}$). The 5X-hCSF1 (5X-hCSF1) and 5X-MITRG models were created by backcrossing the M-CSFh mouse or the MITRG mouse, respectively, with the well-established 5xFAD transgenic model which overexpress co-integrated transgenes for Familial Alzheimer's Disease (FAD) mutant APP (Swedish, Florida, and London) and mutant FAD PS1 (M146L and L286V) (Oakley et al., 2006).

Maintenance and acquisition of iPSC lines

Maintenance of all iPSC lines involved culturing in feeder-free conditions in complete mTeSR E8 medium (Stemcell Technologies), in a humidified incubator (5% CO2, 37°C), with medium changed daily. Passaging was performed every 7-8 days using ReLeSR (Stemcell Technologies) and cells were plated onto 6-well plates (Corning), coated with growth factor-reduced Matrigel (1mg/mL; BD Biosciences), in mTeSR E8 medium, supplemented with 0.5μM Thiazovivin (Stemcell Technologies) for the first 24 hours post-passage. The pluripotency, karyotype, and sterility of all iPSC lines was confirmed via trilineage differentiation (Stem Cell Tech.), array comparative genomic hybridization (aCGH performed by Cell Line Genetics), and MycoAlert (Lonza) testing.

The WT iPSC line (EBisc #BIONi010-C) was modified by CRISPR gene editing to generate the TREM2 R47H isogenic iPSC line (EBiSC #BIONi010-C-7). These isogenic lines were acquired from the European Bank for induced Pluripotent Stem Cells (EBiSC).

The GFP-expressing iPSC line was purchased from Coriell (AICS-0036 GFP line) and was generated by CRISPR modification of the parental WTC11 line to insert mEGFP into the AAVS1 safe harbor locus (chromosomal location 19q13.4-qter) under the control of a CAG promoter. We used CRISPR-Cas9 modification to generate isogenic *TREM2* R47H homozygous line on the

AICS-0036 GFP cell line backgrounds: 2 x 10^5 induced pluripotent stem cells were isolated following Accutase enzymatic digestion for 3 min at 37°C. Cells were resuspended in 60μL nucleofection buffer from Human Stem Cell Nucleofector™ Kit 2 (Lonza). The suspension was combined with 50μg of RNP complex formed by incubating Alt-R® S.p. HiFi Cas9 Nuclease V3 (IDTDNA) with fused crRNA:tracrRNA (IDTDNA) duplex for 15 min at 23°C. The suspension was transferred to the Amaxa Nucleofector cuvette and transfected using program B-016. Cells were plated in TeSR™-E8™ (STEMCELL Technologies) media with 0.25μM Thiazovivin (STEMCELL Technologies) overnight to recover. Cells were digested the following day with Accutase and single-cell plated to 96-well plates in TeSR™-E8™ media with 0.25μM Thiazovivin and CloneR™ (STEMCELL Technologies) supplement for clonal isolation and expansion. Genomic DNA was extracted using Extracta DNA prep for PCR (Quantabio) from a sample of each clone upon passage and amplified for sequencing using Taq PCR Master Mix (ThermoFisher Scientific) at the cut site. PCR product from promising clones was transformed using TOPO™ TA Cloning™ Kit for Subcloning, with One Shot™ TOP10 (ThermoFisher Scientific) for allele-specific sequencing.

Differentiation of Hematopoietic Progenitor Cells from iPSCs

iHPCs were differentiated according to our published protocol (McQuade et al., 2018). To begin iHPC differentiation, iPSCs were passaged in mTeSR-E8 to achieve a density of 40-60 colonies per 6-well. On day 0, cells were transferred to Medium A from the STEMdiff™ Hematopoietic Kit (Stem Cell Technologies). On day 3, flattened endothelial cell colonies were transferred to Medium B and cells remained in medium B for 7 additional days while iHPCs began to lift off the colonies. On day 11, non-adherent CD43+ iHPCs were collected by removing medium and cells with a pipette. At this point, HPCs can be frozen in Bambanker (Wako) and

stored in liquid nitrogen at a concentration of 4 million cells/mL. Cells used for early-postnatal iHPC transplantation were thawed and resuspended at 50K cells/uL in 1X DPBS (low Ca^{2+}, low Mg^{2+}).

Early Postnatal Intracerebroventricular Transplantation of iHPCs

P1 to P2 5X-hCSF1 or 5X-MITRG mice were placed in a clean cage over a heating pad with a nestlet from the home cage to maintain the mother's scent. Female pups were then placed on ice for 2-3 minutes to induce hypothermic anesthesia. Free-hand transplantation was performed using a 30-gauge needle affixed to a 10μL Hamilton syringe, mice received 1μL of iHPCs suspended in sterile 1X DPBS at 50K cells/μL at each injection site (8 sites) totaling 400K cells/pup. Bilateral injections were performed at $2/5^{th}$ of the distance from the lambda suture to each eye, injecting into the lateral ventricles at 3mm and into the overlying anterior cortex at 1mm, and into the posterior cortex in line with the forebrain injection sites, and perpendicular to lambda at a 45° angle. Transplanted pups were then returned to their home cages and weaned at P21. For further details and validation of this chimeric approach please see: (Hasselmann et al., 2019a).

Immunohistochemistry and Confocal Microscopy

Animals were administered Euthasol and monitored for loss of consciousness. Once animals no longer responded to toe pinch, mice were intracardially perfused with ice cold 1X DPBS. If xMG were being isolated from ½ brains, the remaining half brain was drop fixed in 4% (w/v) PFA for 48 hours, otherwise, the mice were intracardially perfused with 4% PFA and post-fixed for 24 hours. Samples were then cryoprotected in 30% (w/v) sucrose until the tissue sank in the solution. Brains were then cut either coronally or sagittally at a section thickness of 40um on a sliding microtome cooled to -79°C. Tissue sections were collected as free-floating sections in PBS with and 0.05% sodium azide. For staining, tissue was blocked for 1 hour in 1X PBS, 0.2%

Triton X-100, and 10% goat or donkey serum. Immediately following blocking, sections were placed in primary antibodies diluted in 1X PBS and 1% goat or donkey serum and incubated overnight on a shaker at 4°C. Sections were then incubated in conjugated secondary antibodies for 1 hour, before washing and mounting on microscope slides. Immunofluorescent sections were then visualized and captured using an Olympus FX1200 confocal microscope. In some cases, brightness and contrast settings of confocal images were slightly adjusted to reveal fine structures and morphology. Importantly, no such changes were made to any images used for quantification.

Plaque Proximity and Total Plaque Area

To examine the impact of the *TREM2* R47H mutation on plaque migration, iHPCs derived from isogenic wild-type and R47H mutant iPSCs (EBiSC # BIONi010-C and #BIONi010-C-7) were transplanted into P1 5X-MITRG mice. 9-months later, immunohistochemistry was performed, and confocal Z-stacks collected within the Piriform Cortex at 40x magnification using identical confocal settings (n=3 mice per *TREM2* genotype). Human microglia numbers and locations were detected and quantified through Ku80 immunofluorescence using the "Spots" function in IMARIS software. IMARIS based quantification of human microglial proximity to plaques was done by first identifying Aβ plaques using the "Surfaces" function, then using the "Spots close to Surfaces" Matlab extension (threshold set to 10μm). Total plaque area was measured from sum of surfaces for each image. Proximity to plaque and total plaque area were tested for statistical significance ($p<0.05$) though Welch's t test using Prism 7.

Tissue dissociation for scRNA-seq

All steps were performed on ice or at 4°C with ice cold reagents and all centrifuge steps were performed for 10 minutes at 400xg with full brake and acceleration unless otherwise stated. Anesthetized mice were intracardially perfused with 1X DPBS, half brains were dissected, the

cerebellum was removed, and tissue was stored in RPMI 1640 until subsequent perfusions were completed. Brains were manually homogenized using a 7mL Dounce homogenizer by adding 4mL of RPMI 1640 and performing 10 strokes with the "loose" pestle followed by 10 strokes with the "tight" pestle. Samples were then run through a pre-soaked 70uM filter and the filter was washed with 10mL of RPMI 1640. The sample was pelleted by centrifugation and myelin was removed by resuspension in 30% Percoll overlaid with 2mL of 1X DPBS centrifuged at 400xg for 20 minutes with acceleration and brake set to 0. The myelin band and supernatant were discarded and cell pellets were resuspended in 80µL MACS buffer (0.5% BSA in 1X DPBS) + 20µL Mouse Cell Removal beads (Miltenyi) and incubated at 4°C for 15 minutes. Magnetically labelled mouse cells were separated using LS columns and the MidiMACs separator (Miltenyi) while the unlabeled human cells were collected in the flow through. Human cells were then pelleted by centrifugation and dead cells were magnetically removed using the Dead Cell Removal kit, Annexin V (Stem Cell Technologies) by resuspending the pellets in 100uL of buffer (2% BSA + 1mM $CaCl_2$ in 1X PBS) in 5mL polystyrene round-bottom tubes and the following manufacturer protocol. Live cells were centrifuged, resuspended in 50-100mL of MACS buffer, and concentrations were determined by counting on a hemocytometer. Final cell concentrations were then adjusted to 900-1,000 cells/uL.

scRNA-seq library preparation and sequencing

scRNA-seq library preparation was performed according to the 10X Genomics Chromium Single Cell 3' Reagents kit v3 user guide except that sample volumes containing 25,000 cells were loaded onto the 10X Genomics flow cell in order to capture ~10,000 total cells. The 10X Genomics workflow was then followed according to the manufacturer protocol and libraries were pooled at equimolar concentrations for sequencing on an Illumina NovaSeq 6000, targeting ~50,000 reads

per cell. FASTQ files were aligned to both the human GRCh38 transcriptome (Ensembl release 95) (Yates et al., 2020) using the CellRanger v3.0.2 "count" command, with the expected cells set to 10,000 and no secondary analysis performed.

scRNA-seq Data Visualization and Differential Gene Analysis

UMI count tables were read into Seurat v3 (Butler et al., 2018) or preprocessing and clustering analysis. Initial QC was performed by log normalizing and scaling (default settings) each dataset followed by PCA performed using all genes in the dataset. Seurat's 'ElbowPlot' function was used to select principal components (PCs) to be used for clustering along with a resolution parameter of 0.35 and clusters identified as being doublets, gene poor, or dividing were removed from the dataset prior to downstream analysis. Secondary QC cutoffs were then applied to retain only cells with less than 27.5% ribosomal genes, 12.5% mitochondrial genes, greater than 500 genes but less than double the median gene count, and greater than 500 UMI but less than double the median UMI count. Additionally, subsequent analysis identified a small cell population (179 cells) primarily present in only a single sample, which were removed as the cluster did not appear to be biologically relevant.

Cells passing QC for each sample were then merged using Seurat's 'merge' function and datasets were processed using Seurat's integrated analysis workflow (Fabbrini et al., 2019). In short, samples from individual mice were integrated using the 'FindIntegationAnchors' and 'IntegrateData' commands using dimensions 1:25. Datasets were then scaled and sources of technical variation were regressed out (library size differences, percent ribosomal genes, and percent mitochondrial genes) and PCA was performed using Seurat's 'RunPCA' command. A shared nearest neighbor (SNN) plot was generated using Seurat's 'FindNeighbors' function using PCs 1:15 as input, clustering was performed using the 'FindClusters' function and a resolution

parameter of 0.3, and dimension reduction was performed using the 'RunUMAP' function with the same PCs used for generating the SNN plot. Differentially expressed genes were determined between clusters using the 'FindAllMarkers' function, which employs a Wilcoxon Rank Sum Test, with and FDR cutoff of 0.01, an LFC cutoff of 0.25, and the requirement that the gene be expressed in at least 10% of the cluster and clusters were labeled according to manual curation of the differential gene lists.

RESULTS

xMG possessing homozygous *TREM2* KO respond to amyloid pathology as previously reported in mice

Isogenic *TREM2* WT and homozygous KO xMG were transplanted into 5X-MITRG mice and the mice were aged for 6 months (McQuade et al., 2020). scRNA-seq analysis performed on the isolated xMG revealed both xMG genotypes were distributed across 5 clusters which displayed similar gene signatures to previous data from the 5X-MITRG (**Figure 2.1A; Figure 1.13B**). Upon closer examination of the clusters, differences were evident in the population distributions between *TREM2* WT and KO cells, primarily driven by a reduction in the MHCII and DAM populations along with a subsequent increase in the Homeostatic population (**Figure 2.1B**). This finding correlates well with previous results describing the loss of *TREM2* function disrupting the transition of microglia out of the homeostatic state (Keren-Shaul et al., 2017; Krasemann et al., 2017; Mazaheri et al., 2017; Yuan et al., 2016b). However, while the *TREM2* R47H mutation has been reported to be a loss of function mutation due to the substitution being within the ligand binding domain of the receptor (Guerreiro, Wojtas, et al., 2013; Kleinberger et al., 2014), complete knockout of the *TREM2* gene is not a condition that has been widely described in human patients.

As such, the possibility that the effects of the R47H mutation may only partially overlap with those of *TREM2* KO needed to be further examined.

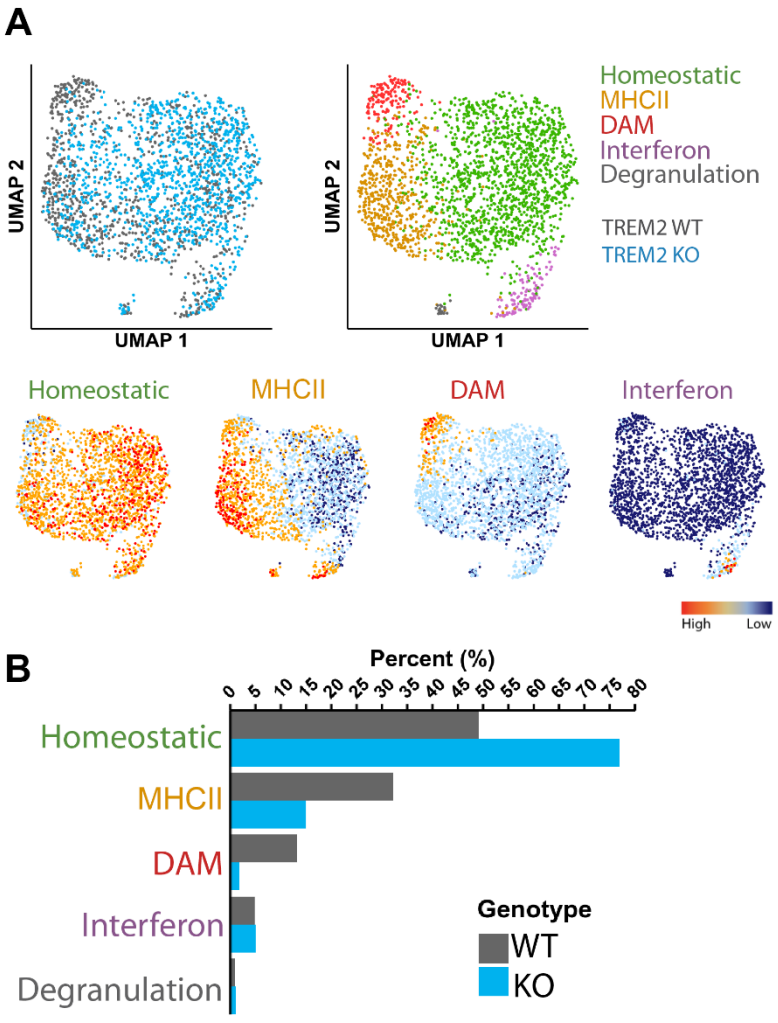

Figure 2.1. Deletion of *TREM2* suppresses the development of Disease-Associated Microglia in vivo. A) UMAP plots from WT and *TREM2* knockout microglia transplanted into a 5x-MITRG mouse. The upper UMAP plots show the clustering of *TREM2* WT and KO cells alongside clustering of human microglia subpopulations in 5X-MITRG mice. The lower four UMAP plots demonstrate the relative expression of known homeostatic, HLA, interferon and DAM markers. Homeostatic: CX3CR1, P2RY12, P2RY13, TMEM119, SALL1. HLA: HLA-DRA, HLA-DRB1, HLA-DRB5, HLA-DPA1, HLA-DPB1, HLA-DMA, HLA-DQA1, HLA-DQA2, HLA-DQB1, CD74. Interferon: IFIT1, IFIT2, ISG15, IFI6, IFITM3, MX1, MX2, STAT1. DAM: CD9, TREM2, SPP1, ITGAX, CD83, APOC1, LGALS3. B) Bar plot showing cluster percentages for each cell type for each *TREM2* genotype.

Confirmation of the generation of isogenic *TREM2* R47H iPSC lines using CRISPR/Cas9

Therefore, we utilized CRISPR gene editing to introduce the *TREM2* R47H mutation into the Coriell GFP human iPSC line (Coriell #AICS-0036). DNA sequencing of the resulting isogenic line revealed four nucleotide substitutions present in the codons for amino acids 43, 45, 46, and 47 (**Figure 2.2**). The nucleotide substitutions present in codons 43, 45, and 46 all resulted in silent mutations, while the G to A substitution in codon 47, resulted in the WT CGC codon, coding for

Arginine, to be converted to a CAC codon, coding for a Histidine. Additionally, this mutation was present on both alleles, and while *TREM2* mutations in AD patients are predominantly heterozygous, it has been reported that patients possessing homozygous R47H mutations present with an earlier age of onset or more frontal lobe pathology (Cuyvers et al., 2014; Slattery et al., 2014), possibly due to a compounding phenotype of increased AD severity and neurodegenerative symptoms of Nasu-Hakola disease (Paloneva, Autti, Hakola, & Haltia, 1993).

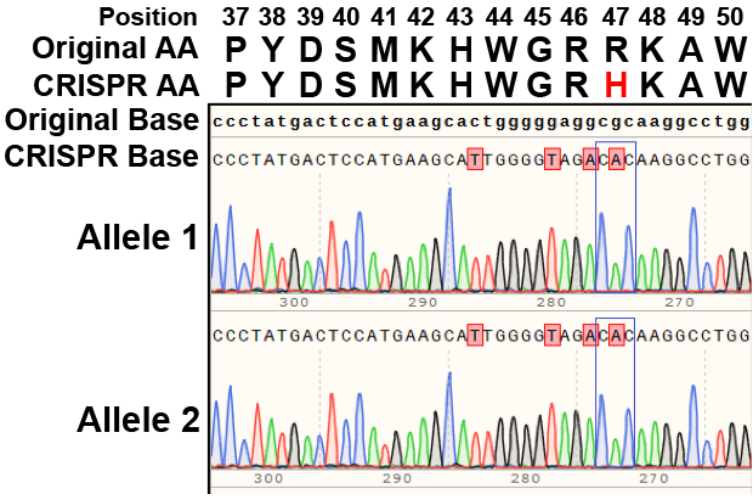

Figure 2.2. CRISPR/Cas9 editing to create a homozygous TREM2 R47H mutant human iPSC line. The chromatogram demonstrates CRISPR/Cas9 induced targeting of CGC (Arginine (R)) in the wild-type allele of TREM2 exon 2, to CAC (Histidine (H)) (together with the insertion of some additional silent mutations) in both alleles, resulting in a TREM2 homozygous R47H mutation in the commercially available GFP iPSC line from Coriell.

Homozygous *TREM2* R47H xMG display altered responses to amyloid plaques

We next sought to examine the effect of the R47H mutation in xMG in regard to their response to amyloid plaques. To determine whether *TREM2* R47H mutation plays a similar role in disrupting the migration of xMG to Aβ plaques as has been previously reported for microglia in human AD subjects (Yuan et al., 2016a) and the 5XfAD mouse model of AD (Song et al., 2018), we transplanted 5X-MITRG mice with iHPCs derived from *TREM2* WT or R47H iPSC lines (EBisc #BIONi010-C and EBiSC #BIONi010-C-7). 9-months later, brains were examined by confocal microscopy and the association between plaques and xMG was examined by IMARIS 3D-quantification of confocal Z-stacks. This analysis revealed significantly less R47H xMG

clustering around Aβ plaques when compared to WT xMG (**Figure 2.3A-C**) despite there being no significant difference in overall plaque burden across mice (**Figure 2.3D**).

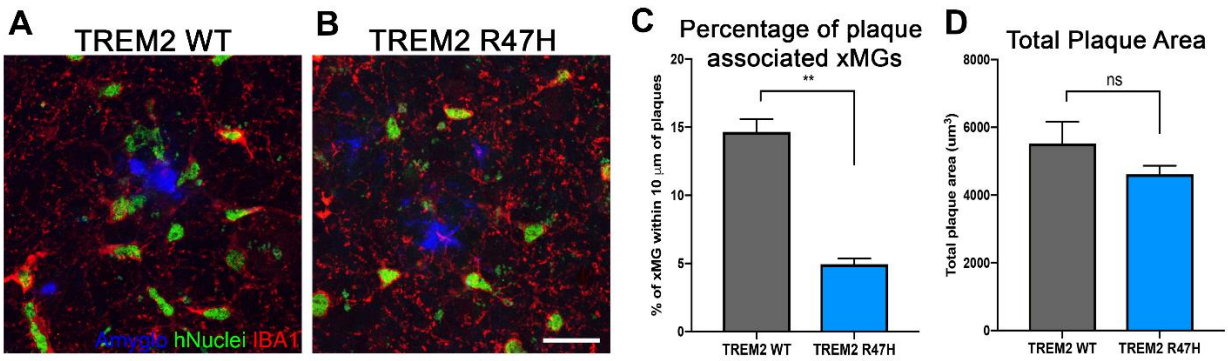

Figure 2.3. xMG response to Aβ plaques is altered by the *TREM2* R47H mutation. 5X-MITRG mice were transplanted with xMGs possessing either WT TREM2 (A) or a homozygous R47H mutation (B) and aged to 9 months. Quantification of xMG migration towards Aβ plaques (blue, Amyglo) revealed a significant decrease in plaque-associated R47H-expressing xMGs (C) (green, hNuclei/Ku80; red, IBA1), but no significant difference in total plaque burden (D). ** $p<0.001$, scale= 20um (A-B).

Amyloid pathology induces unique population distributions in *TREM2* R47H xMG

As xMG possessing the R47H mutation clearly demonstrated an impairment in response to amyloid, we next sought to examine the effects of this mutation on the population distribution of xMGs in the 5X-hCSF1 mouse. *TREM2* WT and *TREM2* R47H xMGs were isolated from the brains of 5X-hCSF1 mice after 7 months of aging and subjected to scRNA-seq (**Figure 2.4**). While similar clusters were observed as those identified in our previous *TREM2* KO study (**Figure 2.1**), the population distribution between *TREM2* WT (**Figure 2.4A**) and R47H (**Figure 2.4B**) xMG only partially recapitulated the *TREM2* KO results. In both cases, the *TREM2* WT cells appeared to more readily transition towards amyloid responsive populations than the R47H cells, evidenced by a reduced percentage of WT cells in the Homeostatic cluster and an increased percentage of WT cells in the MHCII and DAM populations (**Figure 2.3C; Figure 2.1B**). However, unlike the *TREM2* KO results, the activation deficiency observed in the *TREM2* R47H xMG was less due to a reduction in the percentage of DAM and was, instead, more prominently driven by a reduction in the IFN cluster (**Figure 2.4C**).

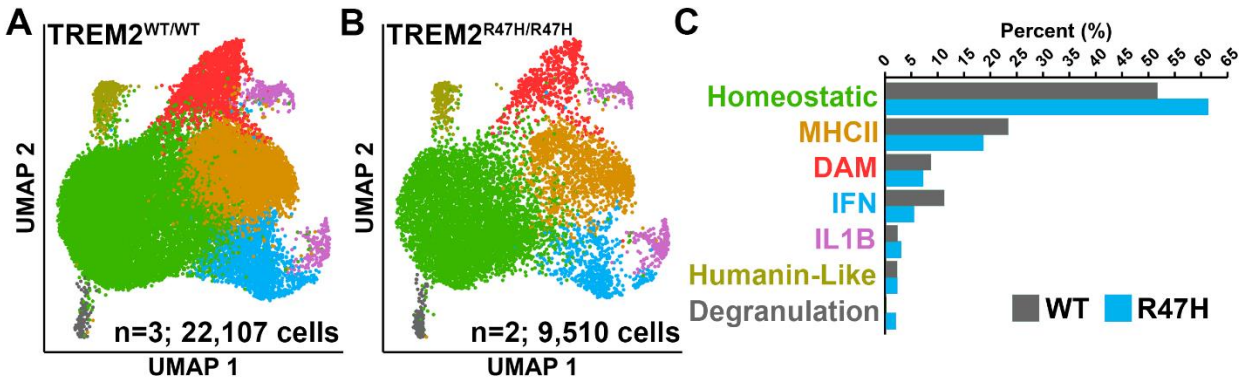

Figure 2.4. The *TREM2* R47H mutation alters the population-level response to amyloid in xMG. A) UMAP plot displaying clustering of TREM2$^{WT/WT}$ xMGs isolated from 7-month-old 5X-hCSF1 mice (n=3 mice; 22,107 cells B) UMAP plot displaying clustering of TREM2$^{R47H/R47H}$ xMGs isolated from 7-month-old 5X-hCSF1 mice (n=2 mice; 9,510 cells C) Bar plot displaying the average percentage of cells making up the 7 unique xMG clusters.

TREM2 R47H affects distinct gene programs related to the DAM and IFN clusters

To further examine the specific genes that were altered in relation to these population shifts, a pseudo-bulk comparison of WT xMG to R47H xMG across all clusters was performed. This analysis generated a list of 38 genes (12 upregulated and 26 downregulated) that are significantly altered in xMG containing the R47H mutation (**Table 2.1**). The upregulated genes primarily consisted of cytokines (*CCL2*, *CCL3*, *CCL3L1*, *CCL4*, *CCL4L2*, *CXCL10*) while the downregulated genes were related to antigen presentation (*CD74*, *FCER1G*, *HLA-A*, *HLA-B*, *HLA-C*, *HLA-DRA*, *HLA-DRB1*, *HLA-DPA1*, *HLA-DMA*, *HLA-DQA2*, *HLA-DQB1*), lipoprotein signaling and cholesterol metabolism (*APOC1*, *APOE*, *LIPA*, *OLR1*, *CTSD*), and interferon response (*IFI27*, *LY6E*, *HLA-A*, *HLA-B*, *HLA-C*). Interestingly, while 30/38 (78.9%) of the R47H-dependent genes overlap with the significant DAM signature, only 3 of the overlapping genes (10%) are regulated in the same direction as WT TREM2 (e.g., upregulated WT DAM and R47H DAM) (**Table 2.1, asterisks**). Similarly, 23/38 (60.5%) of the R47H-dependent genes overlap with

Table 2.1. Genes significantly dysregulated by the *TREM2* R47H mutation and the overlap with the DAM and IFN cluster signatures. Pseudobulk analysis of all *TREM2* R47H cells vs all *TREM2* WT cells generated a list of 38 genes that were significantly dysregulated by the mutation. 30/38 genes are part of the DAM gene signature (WT DAM vs all remaining WT xMG; FDR ≤ 0.01) and 23/38 genes overlapping with the IFN gene signature (WT IFN vs all remaining WT xMG; FDR ≤ 0.01). Asterisks represent the limited number of genes that were regulated in the same direction between WT and R47H (e.g., upregulated in WT DAM and R47H DAM).

Up-regulated in R47H xMG						
Gene	**Log2(FC)**	**WT %**	**R47H %**	**Adjusted p**	**IFN Signature**	**DAM Signature**
CXCL10	0.50136	46.5	67.3	2.01E-23	Yes*	No
CCL4L2	0.33666	40.8	47.7	2.20E-68	Yes	No
CCL4	0.30451	36.3	50.4	1.40E-05	Yes	Yes
CCL3L1	0.27247	40.0	58.8	3.25E-05	Yes	Yes*
HAMP	0.25723	43.0	51.3	1.04E-35	No	Yes
CCL2	0.19786	43.8	53.4	3.94E-17	No	Yes
CCL3	0.18919	44.5	66.1	2.39E-31	No	Yes*
IER2	0.13989	63.1	76.3	5.02E-11	Yes*	No
PLAT	0.13298	44.7	61.0	6.86E-05	No	Yes
SERPINB9	0.13283	60.6	77.3	3.71E-33	No	Yes
EGFL7	0.12837	62.5	75.8	1.28E-12	Yes	Yes
FCGR1B	0.10505	77.3	86.3	2.71E-09	No	No
Down-regulated in R47H xMG						
Gene	**Log2(FC)**	**WT %**	**R47H %**	**Adjusted p**	**IFN Signature**	**DAM Signature**
CTSD	-0.1	86.5	88.3	1.20E-29	Yes*	Yes
LIPA	-0.10002	74.0	79.3	5.12E-17	Yes*	Yes
WIPF3	-0.10095	37.7	64.8	9.65E-79	No	Yes
HLA-A	-0.10177	93.4	96.1	1.11E-45	Yes	No
NAP1L1	-0.11147	65.1	74.0	1.53E-11	No	Yes
HLA-B	-0.11266	97.9	98.4	7.51E-62	Yes	Yes
HLA-DQB1	-0.11394	56.7	80.5	1.24E-30	No	Yes
OLR1	-0.11866	82.5	83.5	2.91E-34	Yes*	Yes
HLA-C	-0.11955	98.1	98.7	2.31E-75	Yes	No
LY6E	-0.12855	60.9	93.9	2.33E-277	Yes	No
APOE	-0.13145	100.0	100.0	1.17E-96	Yes	Yes
TMSB10	-0.13676	97.5	96.3	5.37E-75	Yes	Yes
SCIN	-0.14807	54.3	82.8	2.49E-91	No	Yes
LILRB4	-0.15022	51.8	72.9	1.52E-19	Yes	Yes
FCER1G	-0.15061	91.7	89.6	9.54E-63	No	No
ALOX5AP	-0.15837	90.6	91.2	1.85E-51	Yes*	Yes*
S100A11	-0.15958	93.1	90.5	1.97E-81	Yes	Yes
HLA-DQA2	-0.17419	57.3	76.3	0.002725399	No	Yes
SPP1	-0.1954	99.6	99.2	1.87E-97	No	Yes
IFI27	-0.21782	59.2	86.4	1.76E-112	Yes	No
HLA-DMA	-0.24245	69.0	80.1	2.69E-20	No	Yes
APOC1	-0.27412	95.6	92.6	1.19E-163	No	Yes
CD74	-0.28667	96.4	97.5	5.06E-189	Yes	Yes
HLA-DRB1	-0.35857	80.7	90.8	6.75E-111	Yes	Yes
HLA-DPA1	-0.36035	79.5	87.2	3.58E-114	Yes	Yes
HLA-DRA	-0.36635	86.9	95.6	2.46E-167	Yes	Yes

*R47H mutation regulates this gene in the same direction as WT *TREM2*

the significant genes of the IFN signature, while 6 of the 23 genes (26.1%) are regulated in the same direction as WT *TREM2*. It is also important to note that we do not see a significant reduction in the expression of *TREM2* in this model, as has been reported in when using *TREM2* R47H knock-in mice (Xiang et al., 2018) but not when utilizing human cells (Claes et al., 2019).

DISCUSSION

These experiments suggest that examining the R47H mutation in human microglia is an important approach for uncovering effects that are not clearly modeled in mouse models or *TREM2* KO studies. In particular, the reduction not only in the MHCII and DAM clusters, but also largely in the IFN cluster, is a response that has yet to be fully explored in the literature. Interestingly, the IFN cluster is typically increased in WT xMG when compared to 5X xMG (**Figure 1.13C**), suggesting that, while the *TREM2* R47H cells are less capable of becoming activated, the phenotype observed is not entirely reminiscent of the healthy condition. This idea is reinforced by the fact that R47H xMG upregulate a variety of inflammatory cytokines, demonstrating that these cells aren't simply locked in a homeostatic state, but, rather, they are inflamed while being unable to transition into the appropriate activation states that would allow them to respond to pathological brain conditions.

Taken as a whole, these results show that we have yet to completely understand the complex roles of *TREM2* in human microglia. While the effects of the R47H mutation on genes related to lipid signaling and cholesterol metabolism are currently being investigated in greater detail by members of the Blurton-Jones lab, as they are particularly relevant to amyloid processing in AD, there are still significant outstanding questions. One such question is related to the origin of these transcriptomic alterations, since it is unclear whether the observed alterations were due directly to the *TREM2* R47H mutation or if these deficiencies are secondary to the reduction in

xMG interaction with Aβ plaques. While this question and others like it will be complicated to tackle, the xMG model will provide ample opportunities for further experimentation on the role of genetic mutations in microglia.

CHAPTER 3

ALTERATIONS TO CHROMATIN STRUCTURE AND TRANSCRIPTOMIC PROGRAMMING UNDERLIE THE MICROGLIA RESPONSE TO AMYLOID PATHOLOGY

INTRODUCTION

It has been demonstrated that during microglia development in mice, alterations in the transcriptomic landscape are associated with robust modifications to chromatin structure over time. These changes are what drive the population shifts from early embryonic microglia (E10.5-E14), to pre-microglia (E14 to postnatal day 9), and eventually to adult microglia, which are established between 2 and 4 weeks of age in the mouse (Matcovitch-Natan et al., 2016). Furthermore, the highly responsive nature of these immune cells means that even once they reach the fully differentiated "adult" stage, it is still possible to modify these landscapes. This was clearly demonstrated in a set of studies that observed the effects of removing murine microglia from the brain and maintaining them in a cell culture environment. Gosselin and colleagues showed that upon removal from the brain, microglia undergo dramatic shifts in both their transcriptomic and epigenomic landscapes (Gosselin et al., 2017). Additionally, Bohlen and colleagues reported that microglia that have "de-differentiated" following removal from the brain still have the capacity to revert to a mature phenotype following re-transplantation into the CNS (Bohlen et al., 2017).

These findings suggest that controlling the induction or removal of specific microglia populations primarily requires an understanding of the transcriptomic and epigenomic alterations that drive that phenotype. Further developing this level of understanding for various microglia phenotypes would mean that a protective population of cells could be induced to rectify a specific pathological state and then be reverted back to a homeostatic state once the problem has subsided.

In the case of Alzheimer's disease, one could hypothesize that increasing the DAM population could result in a more robust response to amyloid pathology and a reduction in disease severity.

Therefore, the goal of these experiments is to examine the transcriptomic and epigenomic landscapes that define the DAM population in comparison to the additional xMG subpopulations that have that have been previously reported (Hasselmann et al., 2019b; McQuade et al., 2020). However, as previous reports have been performed using scRNA-seq, which does not provide the depth necessary to perform these comparisons, a new approach for performing bulk analysis on individual xMG subpopulations is needed. Towards this goal, I have developed a method that allows for the bulk isolation of individual xMG subpopulations from the 5X-MITRG mouse brain by leveraging surface markers defined from scRNA-seq analyses. In collaboration with Drs. Chris Glass and Alexander Nott as well as graduate student Eric Kofman at UCSD, I have begun to examine these populations by both bulk RNA-seq, offering a much more robust examination of the transcriptomic landscape of these activation states, as well as by utilizing the assay for transposase-accessible chromatin followed by sequencing (ATAC-seq), allowing for a parallel analysis of the population-specific chromatin alterations. While these results are currently being replicated with an increased number of cell lines, the data thus far have provided a promising look at the analytical potential of this approach.

MATERIALS AND METHODS

Animals

All animal procedures were conducted in accordance with the guidelines set forth by the National Institutes of Health and the University of California, Irvine Institutional Animal Care and Use Committee. The 5X-MITRG model was created by backcrossing the MITRG mouse with 5xFAD mice which overexpress co-integrated transgenes for Familial Alzheimer's Disease (FAD)

mutant APP (Swedish, Florida, and London) and mutant FAD PS1 (M146L and L286V). Progeny of these pairings were then genotyped and backcrossed with MITRG mice to return the 5 MITRG genes to homozygosity and maintain the APP/PS1 transgenic loci in the hemizygous state, resulting in the 5X-MITRG ($Rag2^{-}$; γc^{-}; $M\text{-}CSF^{h}$; $IL\text{-}3/GM\text{-}CSF^{h}$; TPO^{h}; Tg(APPSwFlLon,PSEN1*M146L*L286V)6799Vas).

Acquisition and maintenance of iPSC lines

The GFP cell line, purchased from Coriell (AICS-0036), was generated by CRISPR modification of the line WTC11 to insert a monoallelic mEGFP into the AAVS1 safe harbor locus (chromosomal location 19q13.4-qter) under the control of a CAG promoter. Maintenance of the iPSC line involved culturing in feeder-free conditions in complete mTeSR E8 medium (Stemcell Technologies), in a humidified incubator (5% CO2, 37°C), with medium changed daily. Passaging was performed every 7-8 days using ReLeaSR (Stemcell Technologies) and cells were plated onto 6-well plates (Corning), coated with growth factor-reduced Matrigel (1 mg/mL; BD Biosciences), in mTeSR E8 medium, supplemented with 0.5uM Thiazovivin (Stemcell Technologies) for the first 24 hours post-passage. The cell line was tested for mycoplasma on a monthly basis, and confirmed to be negative, and cell line karyotyping was performed every ten passages.

Differentiation of Hematopoietic Progenitor Cells and *in vitro* Microglia from iPSCs

iHPCs were differentiated according to the protocol published by McQuade et al. (McQuade et al., 2018). To begin iHPC differentiation, iPSCs were passaged in mTeSR-E8 to achieve a density of 80 colonies of 100 cells each per 35mm well. On day 0, cells were transferred to Medium A from the STEMdiff™ Hematopoietic Kit (Stem Cell Technologies). On day 3, flattened endothelial cell colonies were exposed to Medium B and cells remained in medium B for 7 additional days while iHPCs began to lift off the colonies. On day 10, non-adherent CD43+

iHPCs were collected by removing medium and cells with a serological pipette. At this point, d10-d11 iHPCs can be frozen in Bambanker (Wako). Cells used for early-postnatal iHPC transplantation were thawed in iPS-Microglia medium (DMEM/F12, 2X insulin-transferrin-selenite, 2X B27, 0.5X N2, 1X glutamax, 1X non-essential amino acids, 400μM monothioglycerol, and 5 μg/mL human insulin freshly supplemented with 100 ng/mL IL-34, 50 ng/mL TGFβ1, and 25 ng/mL M-CSF (Peprotech)) and allowed to recover for 24 hours, then resuspended at 62,500 cells/uL in 1X DPBS (low Ca^{2+}, low Mg^{2+}).

Early Postnatal Intracerebroventricular Transplantation of iHPCs

P1 5X-MITRG mice were placed in a clean cage over a heating pad with a nestlet from the home cage to maintain the mother's scent. Pups were then placed on ice for 2-3 minutes to induce hypothermic anesthesia. Free-hand transplantation was performed using a 30-gauge needle affixed to a 10μL Hamilton syringe, mice received 1μL of iHPCs suspended in sterile 1X DPBS at 62.5K cells/μL at each injection site (8 sites) totaling 500K cells/pup. Bilateral injections were performed at 2/5th of the distance from the lambda suture to each eye, injecting into the lateral ventricles at 3mm and into the overlying anterior cortex at 1 mm, and into the posterior cortex in line with the forebrain injection sites, and perpendicular to lambda at a 45° angle. Transplanted pups were then returned to their home cages and weaned at P21.

Tissue dissociation and xMG isolation

Following perfusion with ice cold PBS containing 5 ug/ml actinomycin D (act D), half brains were dissected, and the cerebellum was removed. Tissue was stored briefly in RPMI 1640 containing 5 ug/mL act D, 10uM triptolide, and 27.1 ug/mL anisomycin until subsequent perfusions were completed. Tissue dissociation was then performed utilizing the Tumor Dissociation kit, human (Miltenyi) and the gentleMACS OctoDissociator with Heaters (Miltenyi)

according to manufacturer guidelines with modifications. Briefly, tissue was cut into ~1mm^3 pieces and placed into the C-tubes with the kit's enzymes, 5 ug/mL act D, 10uM triptolide, and 27.1 ug/mL anisomycin and samples were dissociated using the preprogrammed protocol. Following enzymatic digestion, samples were strained through a 70um filter and pelleted by centrifugation. Myelin and debris were removed by resuspending the pellet in 8mL 23% Percoll, overlaid with 2mL of 1X DPBS, spinning at 400xg for 25 minutes at 4°C, with acceleration and brake set to 0, and discarding the myelin band and supernatant. Cell pellets were then resuspended in 80uL FACS buffer (0.5% BSA in 1X DPBS) + 20uL Mouse cell removal beads (Miltenyi) and incubated at 4°C for 15 minutes. Samples were then separated using LS columns and the MidiMACs separator (Miltenyi) and the human cells were collected in the flow through. Cells were pelleted via centrifugation (10 minutes, 400xg) and processed for flow cytometry.

Fluorescence activated cell sorting of xMG

For sorting of xMG, cell pellets were resuspended in 100uL of FACS buffer containing 5ug of mouse and human Fc block (BD) and incubated for 5 minutes on ice. 100uL of FACS buffer including the following antibodies was then added to the sample for a final staining volume of 200uL: Mouse anti-HLA-DR-PE clone LN3 (Biolegend, 1:200) and mouse anti-CD9 clone HI9a (Biolegend, 1:200). Samples were then spun down and resuspended in 400uL of FACS buffer containing DAPI (Biolegend, 1:400) as a viability marker. Samples were then sorted on a FACSARIA Fusion II (BD Biosciences) directly into 700uL of Trizol (Thermo Fisher), for RNA sequencing, or 200uL of FACS buffer, for ATAC-seq.

Bulk RNA Isolation from xMG

FACS sorted xMG were stored in Trizol at -80°C until RNA isolation. Samples were then thawed on ice and RNA was isolated by adding 140uL of TET (10mM Tris 8.0/0.01mM

EDTA/0.05% Tween20) followed by 140uL Chloroform:Isolamyl alcohol 24:1 (Sigma). Samples were centrifuged at 15,000xg for 10 min. at 4°C and the aqueous phase was collected and added to 1.5uL of GlycolBlue (Thermo Fisher). 55uL (~1/10 supernatant volume) of 3M sodium acetate and 550uL (~1 supernatant volume) of isopropanol (Sigma) were added and the samples were mixed by inverting then stored at -20°C overnight. Samples were then spun at 15,000xg for 30 min. at 4°C, supernatants were removed from pellets, and 500uL of 75% ethanol was added to the pellet. Samples were then spun at 15,000xg for 30 min. at 4°C, and supernatants were removed from pellets. RNA pellets were dried at RT to remove any residual ethanol, resuspended in 14uL of RNase-free H_2O.

RNA analysis, Library Construction and Bulk RNA-seq

RNA integrity (RIN) values were determined using an Agilent Bioanalyzer 2100 series and RNA concentrations were assayed by Qubit and the average RIN value for RNA samples used in sequencing was 9.8. 2.5ng of RNA was used for library construction using ClonTech SMART-seq V4 Ultra Low Input kit (Takara Bio) which utilized poly-A selection to enrich for mRNAs. The quality of the DNA libraries was assayed using the Agilent 2100 bioanalyzer high sensitivity DNA assay and the DNA high sensitivity Qubit. The libraries were quantified by Kapa qPCR, normalized to 2nM and then multiplexed for sequencing on the Illumina NovaSeq 6000 platform with single read 100 base chemistry.

Bulk RNA-seq Data Analysis

FASTQ files were preprocessed using BBDuk (Bushnell, 2018) to filter out ribosomal RNA and PhiX reads, trim Illumina adapters, and to quality trim any base pairs below a PHRED score of 10. FASTQC (Andrews, 2014) was then performed to verify the quality of the sequencing files and all files were determined to be of sufficient quality for downstream processing. Reads

were then pseudoaligned to the human GRCh38 transcriptome (Ensembl release 97) (Schneider et al., 2017; Zerbino et al., 2018) using Kallisto (Bray et al., 2016), transcripts were summarized to the gene level via tximport (Soneson et al., 2015), and differential gene expression analysis was performed using DESeq2 (Love et al., 2014) after removing genes with summed counts <10.

Bulk RNA-seq Data Visualization

Data was normalized and converted to a $\log_2$ scale for visualization using DESeq2's varianceStabilizingTransformation followed by batch correction using the removeBatchEffect function from limma (Ritchie et al., 2015). Heatmaps were generated using the R "Pheatmap" package (Kolde, 2018) while volcano and bar plots were generated using the "ggplot2" package (Wickham, 2016).

Cleavage, Tagmentation, and Amplification of Accessible Chromatin

Isolated cells were pelleted and lysed in 50uL of a buffer consisting of 10mM Tris-HCl, 10mM NaCl, 3mM $MgCl_2$, and 0.1% IGEPAL, CA-630. 2.5uL of the Tagment DNA enzyme I (Illumina cat#20034197) was added to the solution and incubated at 37°C for 30 minutes. Tagmented DNA was then purified using the Zymo Research ChIP DNA Clean and Concentrator kit (cat#D5205) and eluted in 11uL of elution buffer. DNA fragments were then PCR amplified using the NEBNext High-Fidelity reagents (cat#M0541) and amplification was monitored by qPCR in a side reaction to stop the amplification run to avoid substantial GC and size biases. Amplified DNA was then purified again using the Zymo ChIP Clean kit and samples were run on a 10% TBE gel at 140V for 1 hour. The gel was stained with SYBRGold and the gel region between 175-225bp was cut out and shredded by centrifugation for 2 minutes at max speed. 150uL of a buffer consisting of 0.5M ammonium acetate, 0.1% SDS, 1mM EDTA, and 10mM magnesium acetate and the samples were shaken at room temperature for 45 minutes. Samples were transferred

to a filter column and DNA was once again purified using the Zymo ChIP DNA Clean kit and eluted into 15uL of elution buffer. Samples were analyzed by qubit to determine sample concentrations.

RESULTS

Isolation of xMG subpopulations using surface markers identified by scRNA-seq

The scRNA-seq data published in Hasselmann et al. (2019) identified four primary xMG subclusters (**Figure 3.1A; Figure 1.13B**). Differential gene expression analysis was performed between each cluster versus all the remaining cells to identify the most highly differentially expressed genes in each cluster. From this list, *CD9*, *IFITM3*, and the *HLA-DR* gene family were selected as cell surface marker genes that could be targeted with fluorescent antibodies to facilitate isolation of each subcluster via fluorescence activated cell sorting (FACS) (**Figure 3.1B; Table 3.1**). However, upon preliminary analysis, it was determined that the IFITM3 antibody labeled a limited number of cells with a maximum observed population of 3.12% of xMG (**Figure 3.1C**). As isolation of the IFN population would not yield enough cells to perform downstream analysis, subsequent isolations were focused solely on CD9 and HLA-DR labeling, without the inclusion of the IFITM3 antibody. As such, identification of the clusters was defined as follows: DAM: $CD9^{+}$/HLA-DR^{+}; MHCII: $CD9^{-}$/HLA-DR^{+}; Homeostatic: $CD9^{-}$/HLA-DR^{-}.

xMG were then sorted out of 5X-MITRG mice that had been transplanted with GFP iHPCs and aged for 9 months. Sorting for both bulk RNA-seq and ATAC-seq utilized fluorescence minus one (FMO) controls to set the gate cutoffs and identified robust cell populations for each cluster of interest at ratios reminiscent of the scRNA-seq data (**Figure 3.1D**). As a preliminary confirmation that the differentially activated populations were being sorted from the brain, endogenous GFP levels were observed to be increasing along with the activation state of the cell

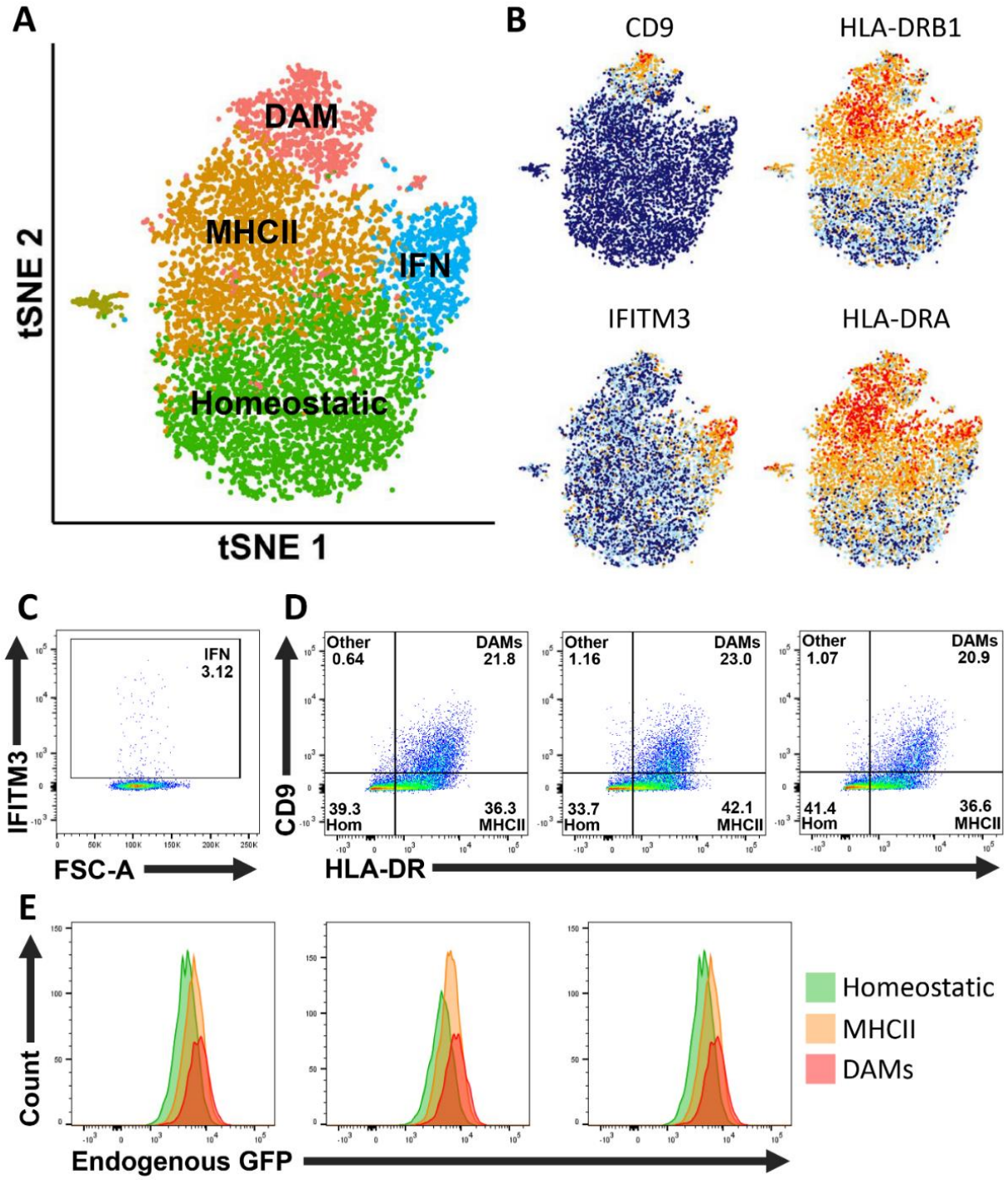

Figure 3.1 Cluster identification and FACS sorting of xMG subpopulations. A) scRNA-seq analysis from Hasselmann et al. (2019) identified four main xMG subpopulations in the brains of 5X-MITRG mice. B) Cluster distributions of selected cell surface genes to be used as targets for fluorescent antibodies and subcluster isolation. C) FACS analysis with an antibody against IFITM3 labeled a maximum of 3.12% of cells in the 5X-MITRG brain. D) Using antibodies against HLA-DR and CD9, robust DAM ($CD9^+/HLA\text{-}DR^+$), MHCII ($CD9^-/HLA\text{-}DR^+$), and Homeostatic ($CD9^-/HLA\text{-}DR^-$) were identified by FACS. E) Endogenous GFP expression under the control of the CAG promoter is increased as the activation state of the sorted population increases (DAM>MHCII>Homeostatic).

population (DAM>MHCII>Homeostatic) (**Figure 3.1E**). This phenomenon was also reported in response to xMG treatment with LPS (**Figure 1.9C**) and in response to amyloid plaques (**Figure 1.12E-H**) (Hasselmann et al., 2019b).

Table 3.1 Differential gene expression results for selected subpopulation cell surface marker genes. Differential gene expression analysis was performed for each subcluster versus all remaining cells to determine cluster-specific gene markers. Based on these results, five genes for cell membrane proteins were selected that would offer the ability to differentiate each subcluster by flow cytometry.

	Gene	Log2(FC)	Cluster %	Remaining %	Adj. p-value
Homeostatic	IFITM3	-0.5076	47.5	57.0	5.38E-35
	CD9	-0.9870	5.0	23.4	5.49E-124
	HLA-DRA	-1.0233	83.0	97.1	0
	HLA-DRB5	-1.0649	43.9	83.9	0
	HLA-DRB1	-1.1122	70.2	94.9	0
MHCII	HLA-DRB1	0.7584	98.0	77.5	0
	HLA-DRB5	0.7569	89.6	55.4	0
	HLA-DRA	0.6710	98.5	87.4	0
	IFITM3	-0.3374	50.1	54.4	8.74979E-06
	CD9	-0.5177	13.4	16.6	1.25E-02
DAM	CD9	1.9038	64.2	8.8	0
	HLA-DRA	0.3263	96.8	90.3	2.94E-39
	HLA-DRB1	0.2845	92.7	83.2	1.79E-28
	HLA-DRB5	0.2699	79.8	65.1	7.53E-24
	IFITM3	-0.1815	49.3	53.5	1
IFN	IFITM3	1.3797	89.7	48.8	4.20E-274
	HLA-DRA	0.1140	92.8	90.9	0.264207807
	HLA-DRB1	0.0891	87.2	84.1	1
	CD9	-0.5548	10.1	16.2	0.001966322

Differential gene expression analysis of bulk RNA-seq confirms the identity of the isolated xMG subpopulations

Initial analyses of the isolated xMG subpopulations by bulk RNA-seq confirmed that the populations sorted by flow cytometry were indeed enriched in the targeted genes (**Figure 3.2A-C**). After performing differential gene expression analysis in DESeq2, results were compared in a pairwise fashion across the three isolated clusters. Comparing the MHCII population, classified by a high level of HLA-DR but being negative for CD9, to the Homeostatic population, primarily

showed an enrichment of multiple MHCII and associated genes (**Figure 3.2A**). Similarly, comparison of the DAM population, classified as CD9 and HLA-DR positive, to the Homeostatic population showed a highly significant increase in *CD9* and MHCII gene transcripts (**Figure 3.2B**). Finally, comparison of the DAM and MHCII populations showed that the DAM population was high in *CD9* expression, but the levels of MHCII gene transcripts were similar between the populations (**Figure 3.2C**). Additionally, many of the top differentially expressed genes observed in the bulk RNA-seq comparisons were aligned with the scRNA-seq cluster genes, such as *GPNMB, LPL, LGLAS3,* and *CHI3L1* being upregulated in the DAM cluster and *CIITA* and *CD74* being upregulated in the MHCII cluster when compared to the Homeostatic cluster (**Supplemental Table 1**; **Supplemental Table 2**).

Next, a heatmap of the 50 most highly expressed genes was generated to determine how these genes were distributed across the clusters (**Figure 3.2D**). Each subpopulation showed distinct regions of overlap and incongruence across these genes with the Homeostatic population being uniquely enriched in expression of the survival gene *CSF1R* as well as *SLCO2B1* and *SELPLG*, all of which have been identified as a members of the microglia "sensome" (S. E. Hickman et al., 2013). The MHCII population was uniquely defined by high expression levels of complement genes *C1QA, C1QB,* and *C1QC* as well as an apparent lack of *ITM2B,* which codes for a protein, BRI2, that binds to amyloid precursor protein and inhibits its cleavage by α-, β-, and γ-secretases, thereby reducing deposition of Aβ in the brain (Matsuda, Giliberto, Matsuda, McGowan, & D'Adamio, 2008; Matsuda, Matsuda, Snapp, & D'Adamio, 2011). The DAM population was uniquely defined by high expression levels of previously described DAM genes, such as *SPP1*, *FTH1*, and *B2M* (Hasselmann et al., 2019b; Keren-Shaul et al., 2017; Mathys et al., 2017) and an

lack of complement signaling as demonstrated by decreased levels of *C1QA*, *C1QB*, *C1QC*, and *C3*. There

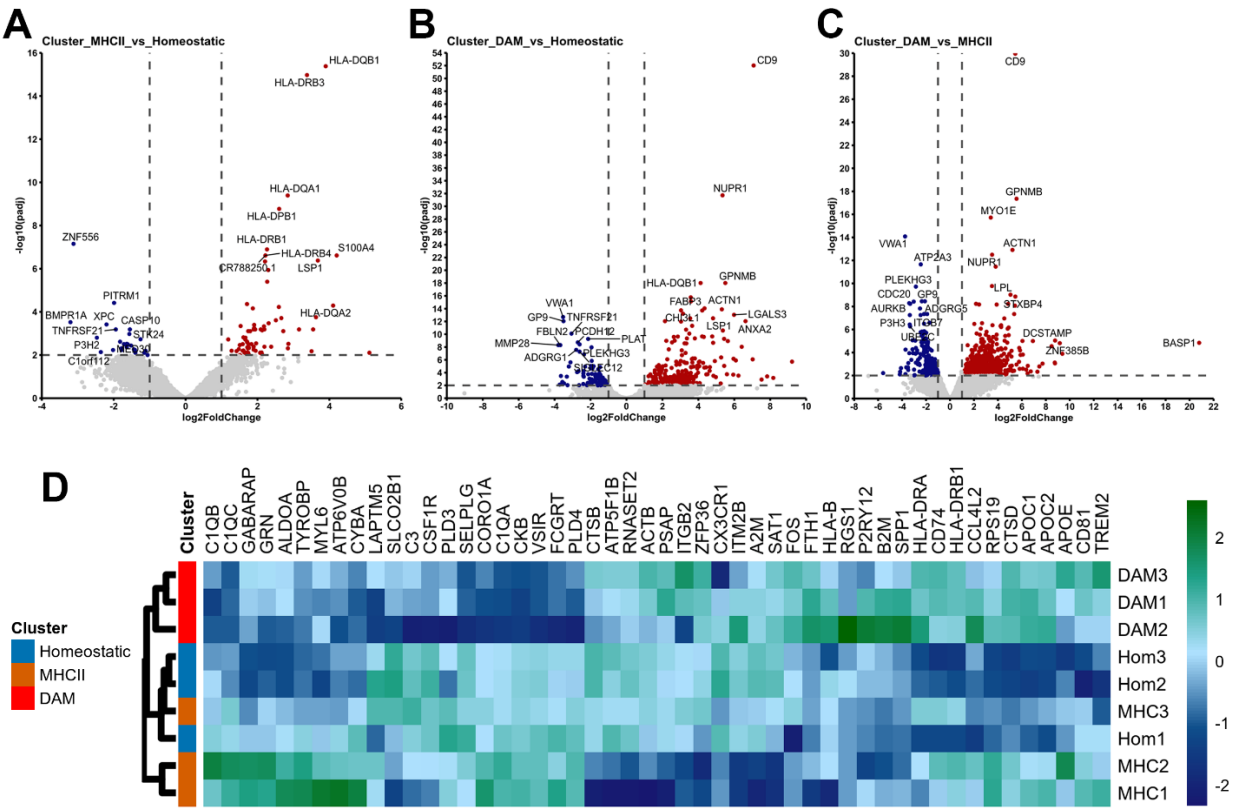

Figure 3.2 Bulk RNA-seq differential gene expression analysis between clusters reveals genetic characteristics of each population. Using DESeq2, differential gene expression analysis was performed on bulk RNA-seq data. Volcano plots showing the differentially expressed genes between the MHCII and Homeostatic clusters (A), the DAM and Homeostatic clusters (B), and the DAM and MHCII clusters (C) demonstrate that the most significant genes for each cluster correspond with the scRNA-seq results and the proteins targeted for subcluster isolation. D) Heatmap showing the $\log_2$(TPM+1) expression levels of the top 50 most highly expressed genes in the bulk RNA-seq dataset. Columns and rows are clustered according to Euclidean distancing.

is also a lack of *GRN* expression in the DAM population, which is interesting considering this gene codes for the protein progranulin and loss of function mutations in this gene have been shown to be causative factors in the development of familial forms of frontotemporal dementia (FTD) and lysosomal storage disorders (Almeida et al., 2016; Baker et al., 2006; Cruts et al., 2006). Additionally, one particularly interesting area of overlap between the populations is *P2RY12*, which is typically considered to be a marker of homeostatic microglia and is downregulated at the protein level following LPS treatment and DAM (**Figure 1.9C**; **Figure 1.12B**), being more highly

expressed in the DAM cluster compared to the Homeostatic cluster (**Figure 3.2D**). While this seems counterintuitive, this finding has recently also been observed in a single nucleotide sequencing study of AD patients (Zhou et al., 2020).

Enriched chromatin binding motifs identify transcription factors potentially regulating the DAM phenotype

In addition to the bulk RNA-seq analysis, the binding motifs identified by ATAC-seq were also compared across the xMG populations to identify possible transcription factor (TF) binding sites specific to each cluster. First, the MHCII cluster was compared to the Homeostatic cluster and, surprisingly, there were no significantly enriched binding motifs in the in either cluster. This suggested that despite significant alterations in gene expression between these populations (**Figure 3.1A**), the changes were not dependent on altered chromatin structure. However, as the expression of MHCII genes is regulated by a set of transcription co-activators belonging to the Regulatory Factor X (RFX) family along with the master regulator *Class II Major Histocompatibility Complex Transactivator* (*CIITA*) (Reith, LeibundGut-Landmann, & Waldburger, 2005), the RNA expression levels of these genes were examined next. Of the genes present in the dataset, including *CIITA*, *RFX1*, *RFX5*, *RFX-associated ankyrin-containing protein* (*RFXANK*), only *CIITA* was found to be significantly upregulated (LFC≥2; FDR cutoff = 0.01) in the MHCII population (**Supplemental Table 2**).

Next, DNA binding motifs were compared between the DAM and Homeostatic clusters as well as the DAM and MHCII clusters. Multiple motifs were enriched in both comparisons (**Figure 3.3A-B**) with binding sites for EGR2, TFEB, and CEBPA being common among both comparisons. The RNA expression levels of the TFs associated with the enriched open chromatin

regions was then examined and revealed a cluster of TFs that appear to be enriched in the DAM population (**Figure 3.3C**). Interestingly, the TFEB motif that was identified by ATAC-seq

A

Enriched Motifs: DAM vs Homeostatic

Rank	Motif	P-value	log P-pvalue	% of Targets	% of Background	STD(Bg STD)	Best Match/Details
1		1e-85	-1.971e+02	32.28%	10.46%	51.6bp (67.3bp)	Egr2(Zf)/Thymocytes-Egr2-ChIP-Seq(GSE34254)
2		1e-38	-8.777e+01	44.27%	26.14%	48.6bp (70.0bp)	TFEB/MA0692.1
3		1e-36	-8.515e+01	26.87%	12.54%	54.8bp (64.8bp)	CEBPA/MA0102.3
4		1e-20	-4.711e+01	12.71%	5.31%	44.4bp (63.8bp)	Atf3(bZIP)/GBM-ATF3-ChIP-Seq(GSE33912)
5		1e-12	-2.790e+01	1.71%	0.18%	54.4bp (70.6bp)	NFKB2/MA078.1

B

Enriched Motifs: DAM vs MHCII

* - possible false positive

Rank	Motif	P-value	log P-pvalue	% of Targets	% of Background	STD(Bg STD)	Best Match/Details
1		1e-22	-5.157e+01	29.24%	9.17%	53.8bp (72.9bp)	Egr2(Zf)/Thymocytes-Egr2-ChIP-Seq(GSE34254)
2		1e-22	-5.066e+01	27.57%	8.33%	46.9bp (73.8bp)	TFEB/MA0692.1
3		1e-15	-3.627e+01	25.91%	9.50%	45.1bp (70.7bp)	FOSL1/MA0477.1
4		1e-13	-3.037e+01	12.96%	3.08%	53.0bp (68.9bp)	CEBPA/MA0102.3
5 *		1e-11	-2.725e+01	23.59%	9.69%	48.1bp (72.7bp)	MAFG::NFE2L1/MA0089.1
6 *		1e-10	-2.533e+01	10.63%	2.49%	45.9bp (74.3bp)	Klf2/MA0742.1
7 *		1e-10	-2.492e+01	3.99%	0.24%	54.6bp (79.6bp)	Gata1/MA035.3
8 *		1e-9	-2.254e+01	1.99%	0.02%	57.1bp (99.1bp)	ZNF282/MA1154.1
9 *		1e-9	-2.194e+01	2.33%	0.05%	34.1bp (69.1bp)	SD0002.1_at_AC_acceptor
10 *		1e-9	-2.143e+01	2.33%	0.05%	68.2bp (91.2bp)	ZNF341(Zf)/EBV-ZNF341-ChIP-Seq(GSE113194)
11 *		1e-9	-2.129e+01	17.61%	6.99%	59.1bp (76.3bp)	NFIC/MA0161.2
12 *		1e-9	-2.122e+01	1.99%	0.03%	48.2bp (57.4bp)	SCRT1(Zf)/HEK293-SCRT1.eGFP-ChIP-Seq

C

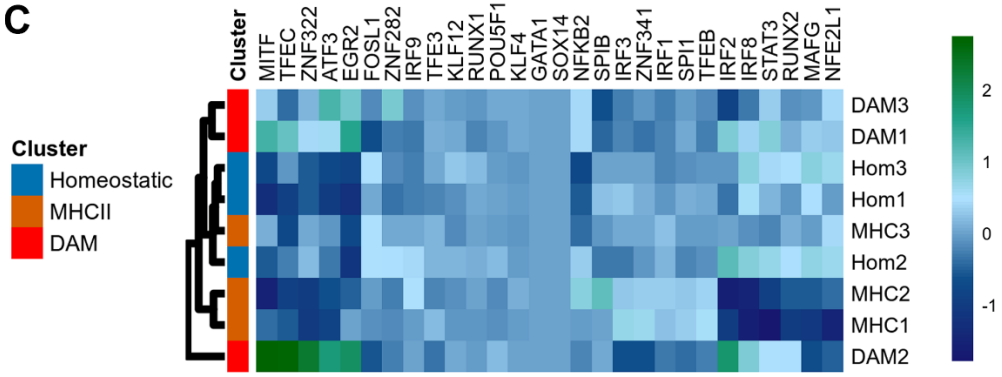

Figure 3.3 ATAC-seq motif analysis reveals population-specific chromatin alterations. Comparisons of the accessible chromatin binding motifs between the A) DAM vs Homeostatic and B) DAM vs MHCII show possible transcription factor binding sites that are significantly enriched in the DAM population. C) Heatmap displaying the RNA expression levels (log_2(TPM+1)) of potential transcription factors identified in A and B. Rows and columns are clustered according to Euclidean distancing.

represents a binding site that is shared among the MiTF/TFE family of TFs consisting of MITF, TFEB, TFEC, and TFE3 (Aksan & Goding, 1998; Hemesath et al., 1994). Of these four TFs, it appears that gene expression of MITF and TFEC are significantly upregulated in the DAM population, rather than the originally identified TFEB (**Figure 3.3C**; **Supplemental Table 2**). However, the "baseMean" expression reported by DESeq2 for *TFEB* was ~33-69 times higher than *MITF* and *TFEC*, respectively, (**Supplemental Table 2**) suggesting that TFEB may still be a critical component of this pathway.

DISCUSSION

Given the recent elucidation of the altered distributions of microglia subpopulations in response to amyloid pathology and AD-related mutations in the *TREM2* gene (**Figure 2.4**) (Hasselmann et al., 2019b; Keren-Shaul et al., 2017; Krasemann et al., 2017), it has become evident that a better understanding of the regulation of these states is crucial to understanding the progression of Alzheimer's disease pathology. However, as single-cell analyses are limited to only assessing 10-40% of the most highly expressed genes in a cell, depending on the platform (Nguyen, Pervolarakis, Nee, & Kessenbrock, 2018), current data does not provide the level of detail necessary to thoroughly assess the full range of genetic regulation that underlies these responses. To address this issue, the goal of these experiments was to leverage my previous scRNA-seq results to develop a method of accurately isolating xMG subpopulations in quantities suitable for more in-depth bulk transcriptomic and epigenomic analyses.

Following initial examination of the differentially expressed genes in each population, it was demonstrated that the targeted populations had been accurately isolated. By further analyzing the most highly expressed genes in each population, it was revealed that the individual populations are defined by various unique gene programs. Identification of increased expression of survival and sensome genes in the Homeostatic cluster, complement genes in the MHCII population, and traditionally identified DAM genes in the DAM population were some of the more predictable findings. However, there were also unexpected findings such as the homeostatic microglia marker *P2RY12* being upregulated in the DAM population, despite previous results showing that this protein is significantly downregulated in microglia near amyloid plaques in both the xMG model and in AD patients (Hasselmann et al., 2019b; Walker et al., 2020). Interestingly, the finding that *P2RY12* mRNA is upregulated in this population is actually in line with a recent study that performed single-nucleus sequencing on AD patients (Zhou et al., 2020). Together, these results seem to suggest that while transcriptomic analyses can provide insight into many aspects of the microglia response to amyloid pathology, there are disconnects between the expression of RNA and the ultimate expression of proteins that have yet to be fully investigated.

Another puzzling aspect of the DAM population RNA expression profile is the apparent downregulation of progranulin. As loss of function mutations in this gene have been shown to cause FTD and lysosomal storage disorders (Almeida et al., 2016; Baker et al., 2006; Cruts et al., 2006), it seems logical that downregulation of this gene would result in a population of microglia that are likely to exacerbate development of neurodegenerative pathologies, like amyloid plaques. However, as mutations in genes such as *TREM2* increase the risk of developing AD while decreasing the prevalence of the DAM population (**Figure 2.1; Figure 2.3; Figure 2.4**), the prevailing assumption in the field is that the DAM population is actually serving to restrain the

development of AD pathology. Interestingly, as counterintuitive as it may seem, the reduction in *GRN* expression may actually be a relevant aspect of the transition to the DAM phenotype. In a recent study that examined the transcriptomic profiles of *GRN* KO mice, it was shown that microglia from mice lacking *GRN* adopted a profile resembling that of DAM and MGnD (Gotzl et al., 2019). However, complete KO of *GRN* was also shown to result in dysfunctional glucose metabolism in microglia, suggesting that controlled downregulation of *GRN*, as opposed to a complete knockout, may be necessary to contribute to the DAM transition without simultaneously disrupting metabolic functions.

While the gene expression data presented herein is not robust enough to fully address the nuances of this regulation, alterations in accessible chromatin structure in the DAM population may have offered some additional insight into a possible epigenetic pathway for lysosomal function regulation. Identification of enriched binding sites for TFEB, a member of the MiTF/TFE family of transcription factors which regulates lysosomal biogenesis, lipid processing, and autophagy (Bala & Szabo, 2018), suggests that this TF may be driving an upregulation in lysosomal genes in DAM. However, this finding is complicated by the fact that all four family members bind the same E- and M-box domains in the promoter regions of the genes they regulate and these TFs are known to form both homo- and heterodimers to regulate their target genes (Pogenberg et al., 2012). Examination of the RNA expression levels of each member of the MiTF/TFE family revealed that MITF and TFEC, rather than TFEB, were the only significant differentially regulated members of this family. However, the baseline expression of TFEB was 33-68 times higher than MITF and TFEC and it is known that TFEB is concentrated in the cytoplasm in homeostatic states and is translocated to the nucleus following dephosphorylation during activation. This may suggest that despite the lack of significant upregulation, TFEB is an

active player in the regulatory process, whose activity is not dependent on gene expression changes, and small changes in the family members that TFEB forms dimers with could lead to subtle alterations in lysosomal gene expression, such as those that would differentiate between *GRN* KO and healthy downregulation. Further studies examining the TFEB phosphorylation state, cellular localization, and dimerization partners in the nucleus would help to further disentangle this phenomenon.

In conclusion, these data have revealed multiple aspects of the genetic and epigenetic landscape of the main xMG subpopulations. While these experiments are in the process of being repeated in multiple cell lines to confirm the validity of these findings, the roadmap provided by these preliminary data will ensure that the next set of experiments are targeted to the most relevant aspects of these differing populations. In particular, future experiments aimed at assessing the transcriptomic and proteomic states of these cells, the subcellular location and activity of various transcription factors, and the epigenetic modifications that are driving chromatin alterations will be critical in furthering the field's understanding of the xMG response to amyloid pathology. It is my hope that this approach will ultimately aid in the identification of new druggable targets that will finally allow us to stop the progression of AD.

CONCLUSIONS AND FUTURE DIRECTIONS

As microglia have continued to be implicated in a wide array of neurological conditions, the need to accurately model these unique cells has become more important than ever. Studies of mouse microglia have been paramount to developing the field's early understanding of these cells, but as our understanding of the intricacies of microglia has grown, so has our ability to discern the species-specific genetic and functional variability that make human microglia unique. Fortunately, recent developments in the fusion of microglia and iPSC research has dramatically increased the modeling capabilities that are available to researchers in the field. This dissertation represents my attempt at rectifying many of the shortcomings of the existing microglia research protocols by demonstrating the efficacy of a model that combines the control and efficiency of *in vitro* work with the biological validity of *in vivo* experimentation.

Despite the improvements that the xMG model offers over certain aspects of its experimental counterparts, it is important to acknowledge that this model also has substantial room to grow. One key area for growth will be the integration of bone marrow transplantation in parallel with iHPC transplant with cells from the same donor to generate a mouse with a fully humanized immune system. As was previously demonstrated by Samuel Marsh during his time in the Blurton-Jones lab, the contributions of the peripheral immune system in the progression of amyloid pathology cannot be ignored (Marsh et al., 2016). Additionally, the fact that slight alterations in individual cytokines like MCSF can dramatically alter microglia ability to degrade amyloid (Majumdar et al., 2007) suggests that the removal of entire cell types is likely resulting in dramatic shifts in microglia function. Until these interactions are restored, it must be assumed that xMG modeling of pathological responses is incomplete.

Another concern is the current lack of murine disease models that are compatible with xMG transplantation. While the use of MITRG, humanized-CSF1 (Jax #017708), or humanized IL34 mice offer an appropriate environment to study homeostatic function, aging, cancer, viral infections, or acute injuries such as traumatic brain injury or stroke, these models do not provide an environment useful for the study of many neurodegenerative disorders. Indeed, only one transplant-compatible transgenic disease model has thus far been published, the 5X-MITRG, and development of that mouse was a substantial undertaking that required restoration of 5 genes to homozygosity and the incorporation of two additional disease-related human genes (Hasselmann et al., 2019b). Therefore, a significant investment into the development of transplant-compatible murine disease models is required before the full power of this technique can be harnessed.

Even with increased availability of transplant-compatible mouse models, there are also still concerns regarding the effects of the murine host cells on xMG functionality. One significant issue is that the host brain tissue possesses a different genome than that of the xMGs. As it has been demonstrated that a number of murine proteins possess limited homology with their human counterparts, the effects that these discrepancies have on cell-cell interactions and the activation or inhibition of microglia signaling cascades are currently unknown. Additionally, the presence of host murine microglia serves as another confounding variable. Although the forebrain regions where engraftment of xMGs was targeted routinely displayed ~80% engraftment of human microglia (Hasselmann et al., 2019b), this was not consistent throughout the brain, as the midbrain and hindbrain exhibited far more limited engraftment. This caveat becomes especially relevant in the context of studying genetic mutations, as host murine microglia that do not possess the mutation may confound observations by exerting beneficial effects on pathology or xMGs and altering the overall inflammatory landscape of the brain. Therefore, generation of reliable

experimental results may well be dependent on models that utilize chemical ablation of murine microglia prior to transplant (Elmore et al., 2014) or the use of a recently developed mouse model that lacks endogenous microglia (Rojo et al., 2019).

Despite these flaws, the xMG model has thus far been successful in generating findings that have yet to be fully described in any other models of microglia function. For example, while current studies into AD-related mutations in *TREM2* have been commonly claimed to lock microglia in a homeostatic state (Mazaheri et al., 2017), xMG studies into this mutation demonstrate that this characterization may be a bit of a misnomer. While it is true that the homeostatic xMG population in *TREM2* KO and R47H microglia was increased compared to WT xMG, xMGs containing the R47H mutation showed a globally significant upregulation in multiple inflammatory cytokines. This suggests that while it is true that cells deficient in functional *TREM2* may be unable to activate appropriately in response to pathological stimuli, even in the "homeostatic" state, these cells may be inflamed in a way that is detrimental to overall brain health. Further examination of the effects of these cells on ageing in the brains of WT mice could provide useful insight into the long-term effects of this increased baseline level of inflammation.

Additionally, the finding that the IFN population was reduced more than the DAM population in R47H xMG also raises some interesting questions as to the involvement of this population in the progression of AD pathology. Recent preliminary data from the Blurton-Jones lab has shown that xMG transplanted into PS19 mice, displaying tau pathology, show a robust increase in the IFN population. If this finding holds true upon further examination, it would suggest that the DAM population responds to amyloid while the IFN population is more responsive to tau pathology, with both signaling through the TREM2 receptor. Due to the pathology-specific expansion of these populations, it could be hypothesized that the responses are facilitated by

binding of different ligands to the TREM2 receptor, likely Aβ and other lipoproteins for the DAM response and possibly phosphatidylserine on the surface of apoptotic cells for the IFN response (Y. Wang et al., 2015). The significant deleterious effects of the R47H mutation in response to AD pathology could then be explained by its diminished ability to respond to both of these pathological ligands, reducing both the number of DAM responding to amyloid and the number of IFN cells responding to the neurons dying due to tau aggregation.

While this is currently a bit speculative, future studies aimed at defining a way to reliably isolate the IFN subcluster in numbers suitable for a more in-depth analysis, from either 5X-fAD or PS19 mice, could provide further insight into this hypothesis. Additionally, although attempts to identify a surface marker antibody for isolation of this population by FACS or MACS have been met with little success, progress has been made in the sequencing of fixed cells (Channathodiyil & Houseley, 2021), so it may be possible to identify an internal protein that can be used as a more robust marker of this elusive xMG subtype. However, it is also possible that the surface labeling of IFITM3 did appropriately label the population and that the apparent lack of a cluster of cells expressing this surface marker is simply another example of a disconnect between the transcriptomic and proteomic profiles of xMG or representative of a primarily RNA-level microglia population that is transcriptomically primed to respond once the appropriate pathology arises (Holtman et al., 2015; Li, Zong, Cao, Tan, & Tan, 2018). Either way, pursuing experiments aimed at determining the *in vivo* state and function of this population could prove to be a valuable endeavor.

Another interesting observation from the population study is that the DAM population displays reduced levels of complement proteins while the MHCII population shows elevated expression levels of C1Q and the Homeostatic population appears to be enriched in C3 (**Figure**

3.2). As was discussed previously, levels of C1Q and C3 appear to regulate microglia phagocytosis of Aβ (Brazil et al., 2000; Fu et al., 2012; S. D. Webster et al., 2000) suggesting that these populations may be involved in modulating the DAM interaction with Aβ plaques rather than quiescent bystanders. Interestingly, while C3 and the C1Q genes are downregulated in DAM, *ITGB2* appears to be enriched and, seeing as this protein is a component of multiple complement receptors, this could suggest that although DAM are not labeling Aβ plaques with complement, they are prepared to modify their response to amyloid plaques based on labeling performed by other subclusters.

The goal of my dissertation was to continue to advance the field of iPSC-derived microglia by developing and validating an *in vivo* model that more accurately captures the microglia states underlying the human response to neurological disease. To accomplish this goal, I took a multipronged approach that began with confirming morphological, transcriptomic, and functional validity of the transplanted cells. From there, these experiments leveraged CRISPR gene editing technology to generate two isogenic cell lines to allow for the direct interrogation of the *TREM2* R47H mutation. This study was able to reproduce multiple findings that had been previously reported in mouse models and human patients in addition to novel observations as to the population-level effects of this mutation. Additionally, this approach was much more efficient and versatile than previous studies that would have required the generation of two different humanized mouse lines to study a similar level of genetic variation. Finally, I utilized data generated in this model to conceive a new experimental design aimed at elucidating the underlying transcriptomic and epigenomic landscapes of recently described microglia subpopulations. While this data is in the process of being reproduced in a more robust manner, the preliminary results appear to fit within what is currently known about microglia biology while simultaneously offering

opportunities to study novel aspects of the microglia response to amyloid at a resolution that is not currently accessible to other models.

In conclusion, while the some of the data presented in this dissertation may seem to raise as many, if not more, questions than they answers, I believe that the continued application of this model in the pursuit of this line of questioning has the potential to lead to answers for many questions that we have yet to realize we need to ask. While there is still a substantial amount of work required to uncover these answers and explore the validity of some of the hypotheses presented herein, the xMG model that has been developed, validated, and expanded upon in this dissertation is perfectly suited to tackle these outstanding questions.

REFERENCES

Abud, E. M., Ramirez, R. N., Martinez, E. S., Healy, L. M., Nguyen, C. H. H., Newman, S. A., . . . Blurton-Jones, M. (2017). iPSC-Derived Human Microglia-like Cells to Study Neurological Diseases. *Neuron, 94*(2), 278-293 e279. doi:10.1016/j.neuron.2017.03.042

Akiyama, H., & McGeer, P. L. (1990). Brain microglia constitutively express beta-2 integrins. *J Neuroimmunol, 30*(1), 81-93. doi:10.1016/0165-5728(90)90055-r

Aksan, I., & Goding, C. R. (1998). Targeting the microphthalmia basic helix-loop-helix-leucine zipper transcription factor to a subset of E-box elements in vitro and in vivo. *Mol Cell Biol, 18*(12), 6930-6938. doi:10.1128/mcb.18.12.6930

Allen, M., Kachadoorian, M., Carrasquillo, M. M., Karhade, A., Manly, L., Burgess, J. D., . . . Ertekin-Taner, N. (2015). Late-onset Alzheimer disease risk variants mark brain regulatory loci. *Neurol Genet, 1*(2), e15. doi:10.1212/NXG.0000000000000012

Almeida, M. R., Macario, M. C., Ramos, L., Baldeiras, I., Ribeiro, M. H., & Santana, I. (2016). Portuguese family with the co-occurrence of frontotemporal lobar degeneration and neuronal ceroid lipofuscinosis phenotypes due to progranulin gene mutation. *Neurobiol Aging, 41*, 200 e201-200 e205. doi:10.1016/j.neurobiolaging.2016.02.019

Alzheimer, A., Stelzmann, R. A., Schnitzlein, H. N., & Murtagh, F. R. (1995). An English translation of Alzheimer's 1907 paper, "Uber eine eigenartige Erkankung der Hirnrinde". *Clin Anat, 8*(6), 429-431. doi:10.1002/ca.980080612

Andrews, S. (2014). FastQC: a quality control tool for high throughput sequence data (Version 0.11.8). Retrieved from https://www.bioinformatics.babraham.ac.uk/projects/fastqc/

Ashburner, M., Ball, C. A., Blake, J. A., Botstein, D., Butler, H., Cherry, J. M., . . . Sherlock, G. (2000). Gene ontology: tool for the unification of biology. The Gene Ontology Consortium. *Nat Genet, 25*(1), 25-29. doi:10.1038/75556

Baker, M., Mackenzie, I. R., Pickering-Brown, S. M., Gass, J., Rademakers, R., Lindholm, C., . . . Hutton, M. (2006). Mutations in progranulin cause tau-negative frontotemporal dementia linked to chromosome 17. *Nature, 442*(7105), 916-919. doi:10.1038/nature05016

Bala, S., & Szabo, G. (2018). TFEB, a master regulator of lysosome biogenesis and autophagy, is a new player in alcoholic liver disease. *Dig Med Res, 1*. doi:10.21037/dmr.2018.09.03

Bennett, F. C., Bennett, M. L., Yaqoob, F., Mulinyawe, S. B., Grant, G. A., Hayden Gephart, M., . . . Barres, B. A. (2018). A Combination of Ontogeny and CNS Environment Establishes Microglial Identity. *Neuron, 98*(6), 1170-1183 e1178. doi:10.1016/j.neuron.2018.05.014

Bennett, M. L., Bennett, F. C., Liddelow, S. A., Ajami, B., Zamanian, J. L., Fernhoff, N. B., . . . Barres, B. A. (2016). New tools for studying microglia in the mouse and human CNS. *Proc Natl Acad Sci U S A, 113*(12), E1738-1746. doi:10.1073/pnas.1525528113

Beutner, C., Roy, K., Linnartz, B., Napoli, I., & Neumann, H. (2010). Generation of microglial cells from mouse embryonic stem cells. *Nat Protoc, 5*(9), 1481-1494. doi:10.1038/nprot.2010.90

Bohlen, C. J., Bennett, F. C., Tucker, A. F., Collins, H. Y., Mulinyawe, S. B., & Barres, B. A. (2017). Diverse Requirements for Microglial Survival, Specification, and Function Revealed by Defined-Medium Cultures. *Neuron, 94*(4), 759-773 e758. doi:10.1016/j.neuron.2017.04.043

Bolger, A. M., Lohse, M., & Usadel, B. (2014). Trimmomatic: a flexible trimmer for Illumina sequence data. *Bioinformatics, 30*(15), 2114-2120. doi:10.1093/bioinformatics/btu170

Boza-Serrano, A., Ruiz, R., Sanchez-Varo, R., Garcia-Revilla, J., Yang, Y., Jimenez-Ferrer, I., . . . Deierborg, T. (2019). Galectin-3, a novel endogenous TREM2 ligand, detrimentally regulates inflammatory response in Alzheimer's disease. *Acta Neuropathol*. doi:10.1007/s00401-019-02013-z

Bray, N. L., Pimentel, H., Melsted, P., & Pachter, L. (2016). Near-optimal probabilistic RNA-seq quantification. *Nat Biotechnol, 34*(5), 525-527. doi:10.1038/nbt.3519

Brazil, M. I., Chung, H., & Maxfield, F. R. (2000). Effects of incorporation of immunoglobulin G and complement component C1q on uptake and degradation of Alzheimer's disease amyloid fibrils by microglia. *J Biol Chem, 275*(22), 16941-16947. doi:10.1074/jbc.M000937200

Bushnell, B. (2018). BBMap (Version 38.32). Retrieved from https://sourceforge.net/projects/bbmap/

Butler, A., Hoffman, P., Smibert, P., Papalexi, E., & Satija, R. (2018). Integrating single-cell transcriptomic data across different conditions, technologies, and species. *Nat Biotechnol, 36*(5), 411-420. doi:10.1038/nbt.4096

Camp, J. G., Badsha, F., Florio, M., Kanton, S., Gerber, T., Wilsch-Brauninger, M., . . . Treutlein, B. (2015). Human cerebral organoids recapitulate gene expression programs of fetal neocortex development. *Proc Natl Acad Sci U S A, 112*(51), 15672-15677. doi:10.1073/pnas.1520760112

Capotondo, A., Milazzo, R., Garcia-Manteiga, J. M., Cavalca, E., Montepeloso, A., Garrison, B. S., . . . Biffi, A. (2017). Intracerebroventricular delivery of hematopoietic progenitors results in rapid and robust engraftment of microglia-like cells. *Sci Adv, 3*(12), e1701211. doi:10.1126/sciadv.1701211

Channathodiyil, P., & Houseley, J. (2021). Glyoxal fixation facilitates transcriptome analysis after antigen staining and cell sorting by flow cytometry. *PLoS One, 16*(1), e0240769. doi:10.1371/journal.pone.0240769

Claes, C., Van Den Daele, J., Boon, R., Schouteden, S., Colombo, A., Monasor, L. S., . . . Verfaillie, C. M. (2019). Human stem cell-derived monocytes and microglia-like cells reveal impaired amyloid plaque clearance upon heterozygous or homozygous loss of TREM2. *Alzheimers Dement, 15*(3), 453-464. doi:10.1016/j.jalz.2018.09.006

Colton, C. A., Needham, L. K., Brown, C., Cook, D., Rasheed, K., Burke, J. R., . . . Vitek, M. P. (2004). APOE genotype-specific differences in human and mouse macrophage nitric oxide production. *J Neuroimmunol, 147*(1-2), 62-67. Retrieved from https://www.ncbi.nlm.nih.gov/pubmed/14741429

Cruts, M., Gijselinck, I., van der Zee, J., Engelborghs, S., Wils, H., Pirici, D., . . . Van Broeckhoven, C. (2006). Null mutations in progranulin cause ubiquitin-positive frontotemporal dementia linked to chromosome 17q21. *Nature, 442*(7105), 920-924. doi:10.1038/nature05017

Cuyvers, E., Bettens, K., Philtjens, S., Van Langenhove, T., Gijselinck, I., van der Zee, J., . . . consortium, B. (2014). Investigating the role of rare heterozygous TREM2 variants in Alzheimer's disease and frontotemporal dementia. *Neurobiol Aging, 35*(3), 726 e711-729. doi:10.1016/j.neurobiolaging.2013.09.009

Davalos, D., Grutzendler, J., Yang, G., Kim, J. V., Zuo, Y., Jung, S., . . . Gan, W. B. (2005). ATP mediates rapid microglial response to local brain injury in vivo. *Nat Neurosci, 8*(6), 752-758. doi:10.1038/nn1472

Dawson, T. M., Golde, T. E., & Lagier-Tourenne, C. (2018). Animal models of neurodegenerative diseases. *Nat Neurosci, 21*(10), 1370-1379. doi:10.1038/s41593-018-0236-8

De Lucia, C., Rinchon, A., Olmos-Alonso, A., Riecken, K., Fehse, B., Boche, D., . . . Gomez-Nicola, D. (2016). Microglia regulate hippocampal neurogenesis during chronic neurodegeneration. *Brain Behav Immun, 55*, 179-190. doi:10.1016/j.bbi.2015.11.001

Deltcheva, E., Chylinski, K., Sharma, C. M., Gonzales, K., Chao, Y., Pirzada, Z. A., . . . Charpentier, E. (2011). CRISPR RNA maturation by trans-encoded small RNA and host factor RNase III. *Nature, 471*(7340), 602-607. doi:10.1038/nature09886

Douvaras, P., Sun, B., Wang, M., Kruglikov, I., Lallos, G., Zimmer, M., . . . Fossati, V. (2017). Directed Differentiation of Human Pluripotent Stem Cells to Microglia. *Stem Cell Reports, 8*(6), 1516-1524. doi:10.1016/j.stemcr.2017.04.023

Dudvarski Stankovic, N., Teodorczyk, M., Ploen, R., Zipp, F., & Schmidt, M. H. H. (2016). Microglia-blood vessel interactions: a double-edged sword in brain pathologies. *Acta Neuropathol, 131*(3), 347-363. doi:10.1007/s00401-015-1524-y

Efthymiou, A. G., & Goate, A. M. (2017). Late onset Alzheimer's disease genetics implicates microglial pathways in disease risk. *Mol Neurodegener, 12*(1), 43. doi:10.1186/s13024-017-0184-x

Eikelenboom, P., & Stam, F. C. (1982). Immunoglobulins and complement factors in senile plaques. An immunoperoxidase study. *Acta Neuropathol, 57*(2-3), 239-242. doi:10.1007/BF00685397

Elmore, M. R., Najafi, A. R., Koike, M. A., Dagher, N. N., Spangenberg, E. E., Rice, R. A., . . . Green, K. N. (2014). Colony-stimulating factor 1 receptor signaling is necessary for microglia viability, unmasking a microglia progenitor cell in the adult brain. *Neuron, 82*(2), 380-397. doi:10.1016/j.neuron.2014.02.040

Erblich, B., Zhu, L., Etgen, A. M., Dobrenis, K., & Pollard, J. W. (2011). Absence of colony stimulation factor-1 receptor results in loss of microglia, disrupted brain development and olfactory deficits. *PLoS One, 6*(10), e26317. doi:10.1371/journal.pone.0026317

Fabbrini, F., Van den Haute, C., De Vitis, M., Baekelandt, V., Vanduffel, W., & Vogels, R. (2019). Probing the Mechanisms of Repetition Suppression in Inferior Temporal Cortex with Optogenetics. *Curr Biol, 29*(12), 1988-1998 e1984. doi:10.1016/j.cub.2019.05.014

Friedman, B. A., Srinivasan, K., Ayalon, G., Meilandt, W. J., Lin, H., Huntley, M. A., . . . Hansen, D. V. (2018). Diverse Brain Myeloid Expression Profiles Reveal Distinct Microglial Activation States and Aspects of Alzheimer's Disease Not Evident in Mouse Models. *Cell Rep, 22*(3), 832-847. doi:10.1016/j.celrep.2017.12.066

Fu, H., Liu, B., Frost, J. L., Hong, S., Jin, M., Ostaszewski, B., . . . Lemere, C. A. (2012). Complement component C3 and complement receptor type 3 contribute to the phagocytosis and clearance of fibrillar Abeta by microglia. *Glia, 60*(6), 993-1003. doi:10.1002/glia.22331

Gibbons, H. M., Smith, A. M., Teoh, H. H., Bergin, P. M., Mee, E. W., Faull, R. L., & Dragunow, M. (2011). Valproic acid induces microglial dysfunction, not apoptosis, in human glial cultures. *Neurobiol Dis, 41*(1), 96-103. doi:10.1016/j.nbd.2010.08.024

Ginhoux, F., Greter, M., Leboeuf, M., Nandi, S., See, P., Gokhan, S., . . . Merad, M. (2010). Fate mapping analysis reveals that adult microglia derive from primitive macrophages. *Science, 330*(6005), 841-845. doi:10.1126/science.1194637

Gold, E. M., Vasilevko, V., Hasselmann, J., Tiefenthaler, C., Hoa, D., Ranawaka, K., . . . Cummings, B. J. (2018). Repeated Mild Closed Head Injuries Induce Long-Term White Matter Pathology and Neuronal Loss That Are Correlated With Behavioral Deficits. *ASN Neuro, 10*, 1759091418781921. doi:10.1177/1759091418781921

Goldmann, T., Wieghofer, P., Jordao, M. J., Prutek, F., Hagemeyer, N., Frenzel, K., . . . Prinz, M. (2016). Origin, fate and dynamics of macrophages at central nervous system interfaces. *Nat Immunol, 17*(7), 797-805. doi:10.1038/ni.3423

Gosselin, D., Skola, D., Coufal, N. G., Holtman, I. R., Schlachetzki, J. C. M., Sajti, E., . . . Glass, C. K. (2017). An environment-dependent transcriptional network specifies human microglia identity. *Science, 356*(6344). doi:10.1126/science.aal3222

Gotzl, J. K., Brendel, M., Werner, G., Parhizkar, S., Sebastian Monasor, L., Kleinberger, G., . . . Haass, C. (2019). Opposite microglial activation stages upon loss of PGRN or TREM2 result in reduced cerebral glucose metabolism. *EMBO Mol Med, 11*(6). doi:10.15252/emmm.201809711

Graeber, M. B., Kosel, S., Egensperger, R., Banati, R. B., Muller, U., Bise, K., . . . Mehraein, P. (1997). Rediscovery of the case described by Alois Alzheimer in 1911: historical, histological and molecular genetic analysis. *Neurogenetics, 1*(1), 73-80. doi:10.1007/s100480050011

Guerreiro, R., Bilgic, B., Guven, G., Bras, J., Rohrer, J., Lohmann, E., . . . Emre, M. (2013). Novel compound heterozygous mutation in TREM2 found in a Turkish frontotemporal dementia-like family. *Neurobiol Aging, 34*(12), 2890 e2891-2895. doi:10.1016/j.neurobiolaging.2013.06.005

Guerreiro, R., Wojtas, A., Bras, J., Carrasquillo, M., Rogaeva, E., Majounie, E., . . . Alzheimer Genetic Analysis, G. (2013). TREM2 variants in Alzheimer's disease. *N Engl J Med, 368*(2), 117-127. doi:10.1056/NEJMoa1211851

Haenseler, W., Sansom, S. N., Buchrieser, J., Newey, S. E., Moore, C. S., Nicholls, F. J., . . . Cowley, S. A. (2017). A Highly Efficient Human Pluripotent Stem Cell Microglia Model Displays a Neuronal-Co-culture-Specific Expression Profile and Inflammatory Response. *Stem Cell Reports, 8*(6), 1727-1742. doi:10.1016/j.stemcr.2017.05.017

Hansen, D. V., Hanson, J. E., & Sheng, M. (2018). Microglia in Alzheimer's disease. *J Cell Biol, 217*(2), 459-472. doi:10.1083/jcb.201709069

Hasselmann, J., Coburn, M. A., England, W., Figueroa Velez, D. X., Kiani Shabestari, S., Tu, C. H., . . . Blurton-Jones, M. (2019a). Development of a Chimeric Model to Study and Manipulate Human Microglia In Vivo. *Neuron, 103*(6), 1016-1033 e1010. doi:10.1016/j.neuron.2019.07.002

Hasselmann, J., Coburn, M. A., England, W., Figueroa Velez, D. X., Kiani Shabestari, S., Tu, C. H., . . . Blurton-Jones, M. (2019b). Development of a Chimeric Model to Study and Manipulate Human Microglia In Vivo. *Neuron*. doi:10.1016/j.neuron.2019.07.002

Hemesath, T. J., Steingrimsson, E., McGill, G., Hansen, M. J., Vaught, J., Hodgkinson, C. A., . . . Fisher, D. E. (1994). microphthalmia, a critical factor in melanocyte development, defines a discrete transcription factor family. *Genes Dev, 8*(22), 2770-2780. doi:10.1101/gad.8.22.2770

Hickman, S., Izzy, S., Sen, P., Morsett, L., & El Khoury, J. (2018). Microglia in neurodegeneration. *Nat Neurosci, 21*(10), 1359-1369. doi:10.1038/s41593-018-0242-x

Hickman, S. E., Kingery, N. D., Ohsumi, T. K., Borowsky, M. L., Wang, L. C., Means, T. K., & El Khoury, J. (2013). The microglial sensome revealed by direct RNA sequencing. *Nat Neurosci, 16*(12), 1896-1905. doi:10.1038/nn.3554

Holtman, I. R., Raj, D. D., Miller, J. A., Schaafsma, W., Yin, Z., Brouwer, N., . . . Eggen, B. J. (2015). Induction of a common microglia gene expression signature by aging and neurodegenerative conditions: a co-expression meta-analysis. *Acta Neuropathol Commun, 3*, 31. doi:10.1186/s40478-015-0203-5

Huang, K. L., Marcora, E., Pimenova, A. A., Di Narzo, A. F., Kapoor, M., Jin, S. C., . . . Goate, A. M. (2017). A common haplotype lowers PU.1 expression in myeloid cells and delays onset of Alzheimer's disease. *Nat Neurosci, 20*(8), 1052-1061. doi:10.1038/nn.4587

Imbimbo, B. P., Solfrizzi, V., & Panza, F. (2010). Are NSAIDs useful to treat Alzheimer's disease or mild cognitive impairment? *Front Aging Neurosci, 2*. doi:10.3389/fnagi.2010.00019

INTREPAD: A randomized trial of naproxen to slow progress of presymptomatic Alzheimer disease. (2019). *Neurology, 93*(8), 371. doi:10.1212/WNL.0000000000007919

Janabi, N. (2002). Selective inhibition of cyclooxygenase-2 expression by 15-deoxy-Delta(12,14)(12,14)-prostaglandin J(2) in activated human astrocytes, but not in human brain macrophages. *J Immunol, 168*(9), 4747-4755. doi:10.4049/jimmunol.168.9.4747

Jansen, I. E., Savage, J. E., Watanabe, K., Bryois, J., Williams, D. M., Steinberg, S., . . . Posthuma, D. (2019). Genome-wide meta-analysis identifies new loci and functional pathways influencing Alzheimer's disease risk. *Nat Genet, 51*(3), 404-413. doi:10.1038/s41588-018-0311-9

Jay, T. R., Miller, C. M., Cheng, P. J., Graham, L. C., Bemiller, S., Broihier, M. L., . . . Lamb, B. T. (2015). TREM2 deficiency eliminates TREM2+ inflammatory macrophages and ameliorates pathology in Alzheimer's disease mouse models. *J Exp Med, 212*(3), 287-295. doi:10.1084/jem.20142322

Jiang, H., Burdick, D., Glabe, C. G., Cotman, C. W., & Tenner, A. J. (1994). beta-Amyloid activates complement by binding to a specific region of the collagen-like domain of the C1q A chain. *J Immunol, 152*(10), 5050-5059. Retrieved from https://www.ncbi.nlm.nih.gov/pubmed/8176223

Jinek, M., Chylinski, K., Fonfara, I., Hauer, M., Doudna, J. A., & Charpentier, E. (2012). A programmable dual-RNA-guided DNA endonuclease in adaptive bacterial immunity. *Science, 337*(6096), 816-821. doi:10.1126/science.1225829

Jonsson, T., Stefansson, H., Steinberg, S., Jonsdottir, I., Jonsson, P. V., Snaedal, J., . . . Stefansson, K. (2013). Variant of TREM2 associated with the risk of Alzheimer's disease. *N Engl J Med, 368*(2), 107-116. doi:10.1056/NEJMoa1211103

Kadoshima, T., Sakaguchi, H., Nakano, T., Soen, M., Ando, S., Eiraku, M., & Sasai, Y. (2013). Self-organization of axial polarity, inside-out layer pattern, and species-specific progenitor dynamics in human ES cell-derived neocortex. *Proc Natl Acad Sci U S A, 110*(50), 20284-20289. doi:10.1073/pnas.1315710110

Kamphuis, W., Kooijman, L., Schetters, S., Orre, M., & Hol, E. M. (2016). Transcriptional profiling of CD11c-positive microglia accumulating around amyloid plaques in a mouse model for Alzheimer's disease. *Biochim Biophys Acta, 1862*(10), 1847-1860. doi:10.1016/j.bbadis.2016.07.007

Karch, C. M., Cruchaga, C., & Goate, A. M. (2014). Alzheimer's disease genetics: from the bench to the clinic. *Neuron, 83*(1), 11-26. doi:10.1016/j.neuron.2014.05.041

Karperien, A., Ahammer, H., & Jelinek, H. F. (2013). Quantitating the subtleties of microglial morphology with fractal analysis. *Front Cell Neurosci, 7*, 3. doi:10.3389/fncel.2013.00003

Kauppinen, T. M., Higashi, Y., Suh, S. W., Escartin, C., Nagasawa, K., & Swanson, R. A. (2008). Zinc triggers microglial activation. *J Neurosci, 28*(22), 5827-5835. doi:10.1523/JNEUROSCI.1236-08.2008

Keren-Shaul, H., Spinrad, A., Weiner, A., Matcovitch-Natan, O., Dvir-Szternfeld, R., Ulland, T. K., . . . Amit, I. (2017). A Unique Microglia Type Associated with Restricting Development of Alzheimer's Disease. *Cell, 169*(7), 1276-1290 e1217. doi:10.1016/j.cell.2017.05.018

Khan, A., Fornes, O., Stigliani, A., Gheorghe, M., Castro-Mondragon, J. A., van der Lee, R., . . . Mathelier, A. (2018). JASPAR 2018: update of the open-access database of transcription factor binding profiles and its web framework. *Nucleic Acids Res, 46*(D1), D260-D266. doi:10.1093/nar/gkx1126

Kierdorf, K., Erny, D., Goldmann, T., Sander, V., Schulz, C., Perdiguero, E. G., . . . Prinz, M. (2013). Microglia emerge from erythromyeloid precursors via Pu.1- and Irf8-dependent pathways. *Nat Neurosci, 16*(3), 273-280. doi:10.1038/nn.3318

Kleinberger, G., Yamanishi, Y., Suarez-Calvet, M., Czirr, E., Lohmann, E., Cuyvers, E., . . . Haass, C. (2014). TREM2 mutations implicated in neurodegeneration impair cell surface transport and phagocytosis. *Sci Transl Med, 6*(243), 243ra286. doi:10.1126/scitranslmed.3009093

Koenigsknecht, J., & Landreth, G. (2004). Microglial phagocytosis of fibrillar beta-amyloid through a beta1 integrin-dependent mechanism. *J Neurosci, 24*(44), 9838-9846. doi:10.1523/JNEUROSCI.2557-04.2004

Kolde, R. (2018). pheatmap: pretty heatmaps (Version 1.0.10). Retrieved from https://CRAN.R-project.org/package=pheatmap

Krasemann, S., Madore, C., Cialic, R., Baufeld, C., Calcagno, N., El Fatimy, R., . . . Butovsky, O. (2017). The TREM2-APOE Pathway Drives the Transcriptional Phenotype of Dysfunctional Microglia in Neurodegenerative Diseases. *Immunity, 47*(3), 566-581 e569. doi:10.1016/j.immuni.2017.08.008

Kunkle, B. W., Grenier-Boley, B., Sims, R., Bis, J. C., Damotte, V., Naj, A. C., . . . Pericak-Vance, M. A. (2019). Genetic meta-analysis of diagnosed Alzheimer's disease identifies new risk loci and implicates Abeta, tau, immunity and lipid processing. *Nat Genet, 51*(3), 414-430. doi:10.1038/s41588-019-0358-2

Lambert, J. C., Heath, S., Even, G., Campion, D., Sleegers, K., Hiltunen, M., . . . Amouyel, P. (2009). Genome-wide association study identifies variants at CLU and CR1 associated with Alzheimer's disease. *Nat Genet, 41*(10), 1094-1099. doi:10.1038/ng.439

Lancaster, M. A., Renner, M., Martin, C. A., Wenzel, D., Bicknell, L. S., Hurles, M. E., . . . Knoblich, J. A. (2013). Cerebral organoids model human brain development and microcephaly. *Nature, 501*(7467), 373-379. doi:10.1038/nature12517

Landry, R. P., Jacobs, V. L., Romero-Sandoval, E. A., & DeLeo, J. A. (2012). Propentofylline, a CNS glial modulator does not decrease pain in post-herpetic neuralgia patients: in vitro evidence for differential responses in human and rodent microglia and macrophages. *Exp Neurol, 234*(2), 340-350. doi:10.1016/j.expneurol.2011.11.006

Langmead, B., & Salzberg, S. L. (2012). Fast gapped-read alignment with Bowtie 2. *Nat Methods, 9*(4), 357-359. doi:10.1038/nmeth.1923

Li, J. W., Zong, Y., Cao, X. P., Tan, L., & Tan, L. (2018). Microglial priming in Alzheimer's disease. *Ann Transl Med, 6*(10), 176. doi:10.21037/atm.2018.04.22

Liao, F., Zhang, T. J., Jiang, H., Lefton, K. B., Robinson, G. O., Vassar, R., . . . Holtzman, D. M. (2015). Murine versus human apolipoprotein E4: differential facilitation of and co-localization in cerebral amyloid angiopathy and amyloid plaques in APP transgenic mouse models. *Acta Neuropathol Commun, 3*, 70. doi:10.1186/s40478-015-0250-y

Liddelow, S. A., Guttenplan, K. A., Clarke, L. E., Bennett, F. C., Bohlen, C. J., Schirmer, L., . . . Barres, B. A. (2017). Neurotoxic reactive astrocytes are induced by activated microglia. *Nature, 541*(7638), 481-487. doi:10.1038/nature21029

Lin, Y. T., Seo, J., Gao, F., Feldman, H. M., Wen, H. L., Penney, J., . . . Tsai, L. H. (2018). APOE4 Causes Widespread Molecular and Cellular Alterations Associated with Alzheimer's Disease Phenotypes in Human iPSC-Derived Brain Cell Types. *Neuron, 98*(6), 1141-1154 e1147. doi:10.1016/j.neuron.2018.05.008

Lloyd, S. (1982). Least squares quantization in PCM. *IEEE Transactions on Information Theory, 28*(2), 129-137. doi:10.1109/TIT.1982.1056489

Loeffler, D. A., Camp, D. M., & Bennett, D. A. (2008). Plaque complement activation and cognitive loss in Alzheimer's disease. *J Neuroinflammation, 5*, 9. doi:10.1186/1742-2094-5-9

Love, M. I., Huber, W., & Anders, S. (2014). Moderated estimation of fold change and dispersion for RNA-seq data with DESeq2. *Genome Biol, 15*(12), 550. doi:10.1186/s13059-014-0550-8

Mackenzie, I. R., Hao, C., & Munoz, D. G. (1995). Role of microglia in senile plaque formation. *Neurobiol Aging, 16*(5), 797-804. doi:10.1016/0197-4580(95)00092-s

Majumdar, A., Cruz, D., Asamoah, N., Buxbaum, A., Sohar, I., Lobel, P., & Maxfield, F. R. (2007). Activation of microglia acidifies lysosomes and leads to degradation of Alzheimer amyloid fibrils. *Mol Biol Cell, 18*(4), 1490-1496. doi:10.1091/mbc.e06-10-0975

Mali, P., Yang, L., Esvelt, K. M., Aach, J., Guell, M., DiCarlo, J. E., . . . Church, G. M. (2013). RNA-guided human genome engineering via Cas9. *Science, 339*(6121), 823-826. doi:10.1126/science.1232033

Mandrekar, S., Jiang, Q., Lee, C. Y., Koenigsknecht-Talboo, J., Holtzman, D. M., & Landreth, G. E. (2009). Microglia mediate the clearance of soluble Abeta through fluid phase macropinocytosis. *J Neurosci, 29*(13), 4252-4262. doi:10.1523/JNEUROSCI.5572-08.2009

Mariani, J., Coppola, G., Zhang, P., Abyzov, A., Provini, L., Tomasini, L., . . . Vaccarino, F. M. (2015). FOXG1-Dependent Dysregulation of GABA/Glutamate Neuron Differentiation in Autism Spectrum Disorders. *Cell, 162*(2), 375-390. doi:10.1016/j.cell.2015.06.034

Marinelli, S., Basilico, B., Marrone, M. C., & Ragozzino, D. (2019). Microglia-neuron crosstalk: Signaling mechanism and control of synaptic transmission. *Semin Cell Dev Biol*. doi:10.1016/j.semcdb.2019.05.017

Marsh, S. E., Abud, E. M., Lakatos, A., Karimzadeh, A., Yeung, S. T., Davtyan, H., . . . Blurton-Jones, M. (2016). The adaptive immune system restrains Alzheimer's disease pathogenesis by modulating microglial function. *Proc Natl Acad Sci U S A, 113*(9), E1316-1325. doi:10.1073/pnas.1525466113

Matcovitch-Natan, O., Winter, D. R., Giladi, A., Vargas Aguilar, S., Spinrad, A., Sarrazin, S., . . . Amit, I. (2016). Microglia development follows a stepwise program to regulate brain homeostasis. *Science, 353*(6301), aad8670. doi:10.1126/science.aad8670

Mathews, S., Branch Woods, A., Katano, I., Makarov, E., Thomas, M. B., Gendelman, H. E., . . . Gorantla, S. (2019). Human Interleukin-34 facilitates microglia-like cell differentiation and persistent HIV-1 infection in humanized mice. *Mol Neurodegener, 14*(1), 12. doi:10.1186/s13024-019-0311-y

Mathys, H., Adaikkan, C., Gao, F., Young, J. Z., Manet, E., Hemberg, M., . . . Tsai, L. H. (2017). Temporal Tracking of Microglia Activation in Neurodegeneration at Single-Cell Resolution. *Cell Rep, 21*(2), 366-380. doi:10.1016/j.celrep.2017.09.039

Matsuda, S., Giliberto, L., Matsuda, Y., McGowan, E. M., & D'Adamio, L. (2008). BRI2 inhibits amyloid beta-peptide precursor protein processing by interfering with the docking of secretases to the substrate. *J Neurosci, 28*(35), 8668-8676. doi:10.1523/JNEUROSCI.2094-08.2008

Matsuda, S., Matsuda, Y., Snapp, E. L., & D'Adamio, L. (2011). Maturation of BRI2 generates a specific inhibitor that reduces APP processing at the plasma membrane and in endocytic vesicles. *Neurobiol Aging, 32*(8), 1400-1408. doi:10.1016/j.neurobiolaging.2009.08.005

Mazaheri, F., Snaidero, N., Kleinberger, G., Madore, C., Daria, A., Werner, G., . . . Haass, C. (2017). TREM2 deficiency impairs chemotaxis and microglial responses to neuronal injury. *EMBO Rep, 18*(7), 1186-1198. doi:10.15252/embr.201743922

McQuade, A., Coburn, M., Tu, C. H., Hasselmann, J., Davtyan, H., & Blurton-Jones, M. (2018). Development and validation of a simplified method to generate human microglia from pluripotent stem cells. *Mol Neurodegener, 13*(1), 67. doi:10.1186/s13024-018-0297-x

McQuade, A., Kang, Y. J., Hasselmann, J., Jairaman, A., Sotelo, A., Coburn, M., . . . Blurton-Jones, M. (2020). Gene expression and functional deficits underlie TREM2-knockout microglia responses in human models of Alzheimer's disease. *Nat Commun, 11*(1), 5370. doi:10.1038/s41467-020-19227-5

Merico, D., Isserlin, R., Stueker, O., Emili, A., & Bader, G. D. (2010). Enrichment map: a network-based method for gene-set enrichment visualization and interpretation. *PLoS One, 5*(11), e13984. doi:10.1371/journal.pone.0013984

Merlini, M., Rafalski, V. A., Rios Coronado, P. E., Gill, T. M., Ellisman, M., Muthukumar, G., . . . Akassoglou, K. (2019). Fibrinogen Induces Microglia-Mediated Spine Elimination and Cognitive Impairment in an Alzheimer's Disease Model. *Neuron, 101*(6), 1099-1108 e1096. doi:10.1016/j.neuron.2019.01.014

Mi, H., Huang, X., Muruganujan, A., Tang, H., Mills, C., Kang, D., & Thomas, P. D. (2017). PANTHER version 11: expanded annotation data from Gene Ontology and Reactome pathways, and data analysis tool enhancements. *Nucleic Acids Res, 45*(D1), D183-D189. doi:10.1093/nar/gkw1138

Muffat, J., Li, Y., Omer, A., Durbin, A., Bosch, I., Bakiasi, G., . . . Jaenisch, R. (2018). Human induced pluripotent stem cell-derived glial cells and neural progenitors display divergent responses to Zika and dengue infections. *Proc Natl Acad Sci U S A, 115*(27), 7117-7122. doi:10.1073/pnas.1719266115

Muffat, J., Li, Y., Yuan, B., Mitalipova, M., Omer, A., Corcoran, S., . . . Jaenisch, R. (2016). Efficient derivation of microglia-like cells from human pluripotent stem cells. *Nat Med, 22*(11), 1358-1367. doi:10.1038/nm.4189

Nguyen, Q. H., Pervolarakis, N., Nee, K., & Kessenbrock, K. (2018). Experimental Considerations for Single-Cell RNA Sequencing Approaches. *Front Cell Dev Biol, 6*, 108. doi:10.3389/fcell.2018.00108

Nimmerjahn, A., Kirchhoff, F., & Helmchen, F. (2005). Resting microglial cells are highly dynamic surveillants of brain parenchyma in vivo. *Science, 308*(5726), 1314-1318. doi:10.1126/science.1110647

Oakley, H., Cole, S. L., Logan, S., Maus, E., Shao, P., Craft, J., . . . Vassar, R. (2006). Intraneuronal beta-amyloid aggregates, neurodegeneration, and neuron loss in transgenic mice with five familial

Alzheimer's disease mutations: potential factors in amyloid plaque formation. *J Neurosci, 26*(40), 10129-10140. doi:10.1523/JNEUROSCI.1202-06.2006

Ormel, P. R., Vieira de Sa, R., van Bodegraven, E. J., Karst, H., Harschnitz, O., Sneeboer, M. A. M., . . . Pasterkamp, R. J. (2018). Microglia innately develop within cerebral organoids. *Nat Commun, 9*(1), 4167. doi:10.1038/s41467-018-06684-2

Paloneva, J., Autti, T., Hakola, P., & Haltia, M. J. (1993). Polycystic Lipomembranous Osteodysplasia with Sclerosing Leukoencephalopathy (PLOSL). In M. P. Adam, H. H. Ardinger, R. A. Pagon, S. E. Wallace, L. J. H. Bean, K. Stephens, & A. Amemiya (Eds.), *GeneReviews((R))*. Seattle (WA).

Pandya, H., Shen, M. J., Ichikawa, D. M., Sedlock, A. B., Choi, Y., Johnson, K. R., . . . Park, J. K. (2017). Differentiation of human and murine induced pluripotent stem cells to microglia-like cells. *Nat Neurosci, 20*(5), 753-759. doi:10.1038/nn.4534

Paresce, D. M., Chung, H., & Maxfield, F. R. (1997). Slow degradation of aggregates of the Alzheimer's disease amyloid beta-protein by microglial cells. *J Biol Chem, 272*(46), 29390-29397. doi:10.1074/jbc.272.46.29390

Pasca, A. M., Sloan, S. A., Clarke, L. E., Tian, Y., Makinson, C. D., Huber, N., . . . Pasca, S. P. (2015). Functional cortical neurons and astrocytes from human pluripotent stem cells in 3D culture. *Nat Methods, 12*(7), 671-678. doi:10.1038/nmeth.3415

Perry, V. H., & Holmes, C. (2014). Microglial priming in neurodegenerative disease. *Nat Rev Neurol, 10*(4), 217-224. doi:10.1038/nrneurol.2014.38

Pocock, J. M., & Piers, T. M. (2018). Modelling microglial function with induced pluripotent stem cells: an update. *Nat Rev Neurosci, 19*(8), 445-452. doi:10.1038/s41583-018-0030-3

Pogenberg, V., Ogmundsdottir, M. H., Bergsteinsdottir, K., Schepsky, A., Phung, B., Deineko, V., . . . Wilmanns, M. (2012). Restricted leucine zipper dimerization and specificity of DNA recognition of the melanocyte master regulator MITF. *Genes Dev, 26*(23), 2647-2658. doi:10.1101/gad.198192.112

Prinz, M., Erny, D., & Hagemeyer, N. (2017). Ontogeny and homeostasis of CNS myeloid cells. *Nat Immunol, 18*(4), 385-392. doi:10.1038/ni.3703

Pulido-Salgado, M., Vidal-Taboada, J. M., Barriga, G. G., Sola, C., & Saura, J. (2018). RNA-Seq transcriptomic profiling of primary murine microglia treated with LPS or LPS + IFNgamma. *Sci Rep, 8*(1), 16096. doi:10.1038/s41598-018-34412-9

Quadrato, G., Nguyen, T., Macosko, E. Z., Sherwood, J. L., Min Yang, S., Berger, D. R., . . . Arlotta, P. (2017). Cell diversity and network dynamics in photosensitive human brain organoids. *Nature, 545*(7652), 48-53. doi:10.1038/nature22047

Rathinam, C., Poueymirou, W. T., Rojas, J., Murphy, A. J., Valenzuela, D. M., Yancopoulos, G. D., . . . Flavell, R. A. (2011). Efficient differentiation and function of human macrophages in humanized CSF-1 mice. *Blood, 118*(11), 3119-3128. doi:10.1182/blood-2010-12-326926

Reith, W., LeibundGut-Landmann, S., & Waldburger, J. M. (2005). Regulation of MHC class II gene expression by the class II transactivator. *Nat Rev Immunol, 5*(10), 793-806. doi:10.1038/nri1708

Río-Hortega, P. (1919a). El "tercer elemento" de los centros nerviosos: La microglia en estado normal.

Río-Hortega, P. (1919b). El "Tercer elemento" de los centros nerviosos: Naturaleza probable de la microglia.

Río-Hortega, P. (1919c). *El "Tercer elemento" de los centros nerviosos: poder fagocitario y movilidad de la microglia*.

Río-Hortega, P. (1919d). El "tercer elemento" do los centros nerviosos: Intervencion de la microglia en los procesos patologicos (celulas en bastoncito y cuerpos granulo-adiposos).

Río-Hortega, P. (1939). The Microglia. *The Lancet, 233*(6036). doi:https://doi.org/10.1016/S0140-6736(00)60571-8

Ritchie, M. E., Phipson, B., Wu, D., Hu, Y., Law, C. W., Shi, W., & Smyth, G. K. (2015). limma powers differential expression analyses for RNA-sequencing and microarray studies. *Nucleic Acids Res, 43*(7), e47. doi:10.1093/nar/gkv007

Rojo, R., Raper, A., Ozdemir, D. D., Lefevre, L., Grabert, K., Wollscheid-Lengeling, E., . . . Pridans, C. (2019). Deletion of a Csf1r enhancer selectively impacts CSF1R expression and development of tissue macrophage populations. *Nat Commun, 10*(1), 3215. doi:10.1038/s41467-019-11053-8

Rongvaux, A., Willinger, T., Martinek, J., Strowig, T., Gearty, S. V., Teichmann, L. L., . . . Flavell, R. A. (2014). Development and function of human innate immune cells in a humanized mouse model. *Nat Biotechnol, 32*(4), 364-372. doi:10.1038/nbt.2858

Rozemuller, J. M., Eikelenboom, P., Pals, S. T., & Stam, F. C. (1989). Microglial cells around amyloid plaques in Alzheimer's disease express leucocyte adhesion molecules of the LFA-1 family. *Neurosci Lett, 101*(3), 288-292. doi:10.1016/0304-3940(89)90547-8

Salter, M. W., & Stevens, B. (2017). Microglia emerge as central players in brain disease. *Nat Med, 23*(9), 1018-1027. doi:10.1038/nm.4397

Savchenko, V. L., McKanna, J. A., Nikonenko, I. R., & Skibo, G. G. (2000). Microglia and astrocytes in the adult rat brain: comparative immunocytochemical analysis demonstrates the efficacy of lipocortin 1 immunoreactivity. *Neuroscience, 96*(1), 195-203. Retrieved from https://www.ncbi.nlm.nih.gov/pubmed/10683423

Schafer, D. P., Lehrman, E. K., Kautzman, A. G., Koyama, R., Mardinly, A. R., Yamasaki, R., . . . Stevens, B. (2012). Microglia sculpt postnatal neural circuits in an activity and complement-dependent manner. *Neuron, 74*(4), 691-705. doi:10.1016/j.neuron.2012.03.026

Schneider, V. A., Graves-Lindsay, T., Howe, K., Bouk, N., Chen, H. C., Kitts, P. A., . . . Church, D. M. (2017). Evaluation of GRCh38 and de novo haploid genome assemblies demonstrates the enduring quality of the reference assembly. *Genome Res, 27*(5), 849-864. doi:10.1101/gr.213611.116

Schulz, C., Gomez Perdiguero, E., Chorro, L., Szabo-Rogers, H., Cagnard, N., Kierdorf, K., . . . Geissmann, F. (2012). A lineage of myeloid cells independent of Myb and hematopoietic stem cells. *Science, 336*(6077), 86-90. doi:10.1126/science.1219179

Shannon, P., Markiel, A., Ozier, O., Baliga, N. S., Wang, J. T., Ramage, D., . . . Ideker, T. (2003). Cytoscape: a software environment for integrated models of biomolecular interaction networks. *Genome Res, 13*(11), 2498-2504. doi:10.1101/gr.1239303

Shapiro, L. A., Perez, Z. D., Foresti, M. L., Arisi, G. M., & Ribak, C. E. (2009). Morphological and ultrastructural features of Iba1-immunolabeled microglial cells in the hippocampal dentate gyrus. *Brain Res, 1266*, 29-36. doi:10.1016/j.brainres.2009.02.031

Sheridan, G. K., & Murphy, K. J. (2013). Neuron-glia crosstalk in health and disease: fractalkine and CX3CR1 take centre stage. *Open Biol, 3*(12), 130181. doi:10.1098/rsob.130181

Shitaka, Y., Tran, H. T., Bennett, R. E., Sanchez, L., Levy, M. A., Dikranian, K., & Brody, D. L. (2011). Repetitive closed-skull traumatic brain injury in mice causes persistent multifocal axonal injury and microglial reactivity. *J Neuropathol Exp Neurol, 70*(7), 551-567. doi:10.1097/NEN.0b013e31821f891f

Sieff, C. A. (1987). Hematopoietic growth factors. *J Clin Invest, 79*(6), 1549-1557. doi:10.1172/JCI112988

Sims, R., van der Lee, S. J., Naj, A. C., Bellenguez, C., Badarinarayan, N., Jakobsdottir, J., . . . Schellenberg, G. D. (2017). Rare coding variants in PLCG2, ABI3, and TREM2 implicate microglial-mediated innate immunity in Alzheimer's disease. *Nat Genet, 49*(9), 1373-1384. doi:10.1038/ng.3916

Slattery, C. F., Beck, J. A., Harper, L., Adamson, G., Abdi, Z., Uphill, J., . . . Mead, S. (2014). R47H TREM2 variant increases risk of typical early-onset Alzheimer's disease but not of prion or frontotemporal dementia. *Alzheimers Dement, 10*(6), 602-608 e604. doi:10.1016/j.jalz.2014.05.1751

Soneson, C., Love, M. I., & Robinson, M. D. (2015). Differential analyses for RNA-seq: transcript-level estimates improve gene-level inferences. *F1000Res, 4*, 1521. doi:10.12688/f1000research.7563.2

Song, W. M., Joshita, S., Zhou, Y., Ulland, T. K., Gilfillan, S., & Colonna, M. (2018). Humanized TREM2 mice reveal microglia-intrinsic and -extrinsic effects of R47H polymorphism. *J Exp Med, 215*(3), 745-760. doi:10.1084/jem.20171529

Stevens, B., Allen, N. J., Vazquez, L. E., Howell, G. R., Christopherson, K. S., Nouri, N., . . . Barres, B. A. (2007). The classical complement cascade mediates CNS synapse elimination. *Cell, 131*(6), 1164-1178. doi:10.1016/j.cell.2007.10.036

Stewart, W. F., Kawas, C., Corrada, M., & Metter, E. J. (1997). Risk of Alzheimer's disease and duration of NSAID use. *Neurology, 48*(3), 626-632. doi:10.1212/wnl.48.3.626

Subramanian, A., Tamayo, P., Mootha, V. K., Mukherjee, S., Ebert, B. L., Gillette, M. A., . . . Mesirov, J. P. (2005). Gene set enrichment analysis: a knowledge-based approach for interpreting genome-wide expression profiles. *Proc Natl Acad Sci U S A, 102*(43), 15545-15550. doi:10.1073/pnas.0506580102

Takata, K., Kozaki, T., Lee, C. Z. W., Thion, M. S., Otsuka, M., Lim, S., . . . Ginhoux, F. (2017). Induced-Pluripotent-Stem-Cell-Derived Primitive Macrophages Provide a Platform for Modeling Tissue-Resident Macrophage Differentiation and Function. *Immunity, 47*(1), 183-198 e186. doi:10.1016/j.immuni.2017.06.017

The Gene Ontology, C. (2017). Expansion of the Gene Ontology knowledgebase and resources. *Nucleic Acids Res, 45*(D1), D331-D338. doi:10.1093/nar/gkw1108

Tremblay, M. E., Lecours, C., Samson, L., Sanchez-Zafra, V., & Sierra, A. (2015). From the Cajal alumni Achucarro and Rio-Hortega to the rediscovery of never-resting microglia. *Front Neuroanat, 9*, 45. doi:10.3389/fnana.2015.00045

Tsuchiya, T., Park, K. C., Toyonaga, S., Yamada, S. M., Nakabayashi, H., Nakai, E., . . . Shimizu, K. (2005). Characterization of microglia induced from mouse embryonic stem cells and their migration into the brain parenchyma. *J Neuroimmunol, 160*(1-2), 210-218. doi:10.1016/j.jneuroim.2004.10.025

Ueda, Y., Gullipalli, D., & Song, W. C. (2016). Modeling complement-driven diseases in transgenic mice: Values and limitations. *Immunobiology, 221*(10), 1080-1090. doi:10.1016/j.imbio.2016.06.007

Ulrich, J. D., Finn, M. B., Wang, Y., Shen, A., Mahan, T. E., Jiang, H., . . . Holtzman, D. M. (2014). Altered microglial response to Abeta plaques in APPPS1-21 mice heterozygous for TREM2. *Mol Neurodegener, 9*, 20. doi:10.1186/1750-1326-9-20

Varley, A. W., Coulthard, M. G., Meidell, R. S., Gerard, R. D., & Munford, R. S. (1995). Inflammation-induced recombinant protein expression in vivo using promoters from acute-phase protein genes. *Proc Natl Acad Sci U S A, 92*(12), 5346-5350. Retrieved from https://www.ncbi.nlm.nih.gov/pubmed/7539915

Velasco, S., Kedaigle, A. J., Simmons, S. K., Nash, A., Rocha, M., Quadrato, G., . . . Arlotta, P. (2019). Individual brain organoids reproducibly form cell diversity of the human cerebral cortex. *Nature*. doi:10.1038/s41586-019-1289-x

Walker, D. G., Tang, T. M., Mendsaikhan, A., Tooyama, I., Serrano, G. E., Sue, L. I., . . . Lue, L. F. (2020). Patterns of Expression of Purinergic Receptor P2RY12, a Putative Marker for Non-Activated Microglia, in Aged and Alzheimer's Disease Brains. *Int J Mol Sci, 21*(2). doi:10.3390/ijms21020678

Wang, P., Mokhtari, R., Pedrosa, E., Kirschenbaum, M., Bayrak, C., Zheng, D., & Lachman, H. M. (2017). CRISPR/Cas9-mediated heterozygous knockout of the autism gene CHD8 and characterization of its transcriptional networks in cerebral organoids derived from iPS cells. *Mol Autism, 8*, 11. doi:10.1186/s13229-017-0124-1

Wang, Y., Cella, M., Mallinson, K., Ulrich, J. D., Young, K. L., Robinette, M. L., . . . Colonna, M. (2015). TREM2 lipid sensing sustains the microglial response in an Alzheimer's disease model. *Cell, 160*(6), 1061-1071. doi:10.1016/j.cell.2015.01.049

Wang, Y., Szretter, K. J., Vermi, W., Gilfillan, S., Rossini, C., Cella, M., . . . Colonna, M. (2012). IL-34 is a tissue-restricted ligand of CSF1R required for the development of Langerhans cells and microglia. *Nat Immunol, 13*(8), 753-760. doi:10.1038/ni.2360

Webster, D. E. (2013). FOCIS (Version 1.2). Retrieved from https://sourceforge.net/projects/focis/

Webster, S. D., Yang, A. J., Margol, L., Garzon-Rodriguez, W., Glabe, C. G., & Tenner, A. J. (2000). Complement component C1q modulates the phagocytosis of Abeta by microglia. *Exp Neurol, 161*(1), 127-138. doi:10.1006/exnr.1999.7260

Weinhard, L., di Bartolomei, G., Bolasco, G., Machado, P., Schieber, N. L., Neniskyte, U., . . . Gross, C. T. (2018). Microglia remodel synapses by presynaptic trogocytosis and spine head filopodia induction. *Nat Commun, 9*(1), 1228. doi:10.1038/s41467-018-03566-5

Wickham, H. (2016). *ggplot2: Elegant Graphics for Data* (2nd ed.): Springer Nature.

Wolf, S. A., Boddeke, H. W., & Kettenmann, H. (2017). Microglia in Physiology and Disease. *Annu Rev Physiol, 79*, 619-643. doi:10.1146/annurev-physiol-022516-034406

Wu, Y., Dissing-Olesen, L., MacVicar, B. A., & Stevens, B. (2015). Microglia: Dynamic Mediators of Synapse Development and Plasticity. *Trends Immunol, 36*(10), 605-613. doi:10.1016/j.it.2015.08.008

Xiang, X., Piers, T. M., Wefers, B., Zhu, K., Mallach, A., Brunner, B., . . . Haass, C. (2018). The Trem2 R47H Alzheimer's risk variant impairs splicing and reduces Trem2 mRNA and protein in mice but not in humans. *Mol Neurodegener, 13*(1), 49. doi:10.1186/s13024-018-0280-6

Yates, A. D., Achuthan, P., Akanni, W., Allen, J., Allen, J., Alvarez-Jarreta, J., . . . Flicek, P. (2020). Ensembl 2020. *Nucleic Acids Res, 48*(D1), D682-D688. doi:10.1093/nar/gkz966

Ye, F., Kang, E., Yu, C., Qian, X., Jacob, F., Yu, C., . . . Zhang, M. (2017). DISC1 Regulates Neurogenesis via Modulating Kinetochore Attachment of Ndel1/Nde1 during Mitosis. *Neuron, 96*(5), 1041-1054 e1045. doi:10.1016/j.neuron.2017.10.010

Yin, Z., Raj, D., Saiepour, N., Van Dam, D., Brouwer, N., Holtman, I. R., . . . Boddeke, E. (2017). Immune hyperreactivity of Abeta plaque-associated microglia in Alzheimer's disease. *Neurobiol Aging, 55*, 115-122. doi:10.1016/j.neurobiolaging.2017.03.021

Yousef, H., Czupalla, C. J., Lee, D., Chen, M. B., Burke, A. N., Zera, K. A., . . . Wyss-Coray, T. (2019). Aged blood impairs hippocampal neural precursor activity and activates microglia via brain endothelial cell VCAM1. *Nat Med, 25*(6), 988-1000. doi:10.1038/s41591-019-0440-4

Yuan, P., Condello, C., Keene, C. D., Wang, Y., Bird, T. D., Paul, S. M., . . . Grutzendler, J. (2016a). TREM2 Haplodeficiency in Mice and Humans Impairs the Microglia Barrier Function Leading to Decreased Amyloid Compaction and Severe Axonal Dystrophy. *Neuron, 92*(1), 252-264. doi:10.1016/j.neuron.2016.09.016

Yuan, P., Condello, C., Keene, C. D., Wang, Y., Bird, T. D., Paul, S. M., . . . Grutzendler, J. (2016b). TREM2 Haplodeficiency in Mice and Humans Impairs the Microglia Barrier Function Leading to Decreased Amyloid Compaction and Severe Axonal Dystrophy. *Neuron, 90*(4), 724-739. doi:10.1016/j.neuron.2016.05.003

Zanjani, H., Finch, C. E., Kemper, C., Atkinson, J., McKeel, D., Morris, J. C., & Price, J. L. (2005). Complement activation in very early Alzheimer disease. *Alzheimer Dis Assoc Disord, 19*(2), 55-66. doi:10.1097/01.wad.0000165506.60370.94

Zerbino, D. R., Achuthan, P., Akanni, W., Amode, M. R., Barrell, D., Bhai, J., . . . Flicek, P. (2018). Ensembl 2018. *Nucleic Acids Res, 46*(D1), D754-D761. doi:10.1093/nar/gkx1098

Zhou, Y., Song, W. M., Andhey, P. S., Swain, A., Levy, T., Miller, K. R., . . . Colonna, M. (2020). Human and mouse single-nucleus transcriptomics reveal TREM2-dependent and TREM2-independent cellular responses in Alzheimer's disease. *Nat Med, 26*(1), 131-142. doi:10.1038/s41591-019-0695-9